

Technical University of Crete

School of Electrical and Computer Engineering

Digital Image and Signal Processing Laboratory

Non-linear functional connectivity of resting-state fMRI data from patients with brain insults: A time-varying analysis

A Thesis submitted in partial fulfillment of the requirements for the diploma
degree of Electrical and Computer Engineering

THESIS COMMITTEE:

Professor Zervakis Michalis, Thesis Supervisor, School of Electrical and Computer
Engineering Technical University of Crete

Professor Liavas Athanasios, School of Electrical and Computer Engineering
Technical University of Crete

Professor Stamatakis Emmanuel, Division of Anaesthesia, Queens' College,
Cambridge, United Kingdom

Nikolaos Ioannis Simos

October 2021

ABSTRACT

Mild Traumatic Brain Injury (mTBI) is a frequently occurring condition, with approximately 90% of TBI being classified as mild. However, diagnostic criteria for mTBI fail to reveal a positive outcome due to the ineffectiveness of current diagnostic procedures including conventional neuroimaging techniques and the necessity for improvements is more than essential. In this regard, rs-fMRI has shown great research potential and promising diagnostic capabilities in multiple clinical scenarios and it is being explored in this thesis. To this end, a novel combination of rs-fMRI functional connectivity (FC) metrics is utilized for the classification of chronic mTBI patients and healthy controls that has never been assessed to the best of our knowledge. Static (SFC) and dynamic (DFC) indices are computed using linear and non-linear connectivity estimation measures. A state-based DFC approach is used attempting to characterize time-resolved networks as predominately integrated or segregated based on network topology. Network reduction via Orthogonal Minimum Spanning Trees is used, maximizing efficient information flow. Graph metrics are employed in both SFC and DFC cases, describing various topological and functional network characteristics. Several types of features are combined in the final step in order to produce a more robust model. A decision-fusion Machine Learning scheme is evaluated against more traditional approaches. A consensus-based nested cross validation pipeline is used combined with a feature-importance based feature selection method. Classification accuracies of up to 80% were achieved using an XGBoost classification and selection model and a logistic regression meta-estimator. Significant brain regions detected are consistent with previous mTBI work with the addition of some novel findings. These regions lead to interesting interpretations in relation with trauma characteristics. This proof-of-concept combination of techniques certainly paves the way of further investigation using similar approaches.

ACKNOWLEDGMENTS

I would like to thank my supervisor, Professor Michalis Zervakis for all the help and constructive critique he has offered on the current thesis. Furthermore, I would like to thank Professor Emmanuel Stamatakis, Dr. Andrea I. Luppi, Dr. Stavros Dimitriadis and Dr. Marios Antonakakis for all their help and support in the conceptualization and implementation of the work presented here. I would also like to express my appreciation towards Dr. Efrosini Papadaki, Dr. Thomas G. Maris, Dr. Kostas Marias and Dr. Georgios C. Manikis who have also offered me so much in previous research attempts leading up to this work. I would also like to thank Professor Athanasios Liavas, a member of the thesis committee for reviewing the manuscript. The gratitude I would like to express toward my parents is immeasurable, firstly for their continuous and unwavering support, encouragement, reassurance and trust in me and secondarily for the introduction to this complicated and exciting academic research world. Lastly, I would like to thank my close friends, some old and some met during college. This thesis (and degree) definitely wouldn't be possible without their encouragement and support.

CONTENTS

Abstract.....	1
Acknowledgments.....	2
List of Abbreviations	7
1. Introduction.....	9
1.1 Aim of The Present Study.....	9
1.2 Study Novelty	9
1.3 Thesis Outline	10
2. Background.....	11
2.1 Mild Traumatic Brain Injury.....	11
2.2 Functional Magnetic Resonance Imaging.....	12
2.2.1 Introduction to Functional Brain Imaging	12
2.2.2 BOLD Contrast Mechanism: The Basis of fMRI	13
2.2.3 rs-fMRI Spontaneous Neural Activity and Connectivity.....	14
2.2.4 fMRI Nomenclature and Acquisition Basics	18
2.2.5 Sources of Noise and Artifacts: Preprocessing Basics	19
Temporal and Spectral	19
Spatial	22
2.3 Graph Theory and Functional Networks.....	23
2.3.1 Complex Networks	23
2.3.2 Functional Connectivity Graphs	24
Graph Node Definition	24
Connectivity Estimation.....	26
2.3.3 Functional and Topological Graph Characteristics.....	28
Graph Metrics	29

Assignment of Nodes to Modules: Louvain	37
2.3.4 Graph Reduction Techniques.....	41
Surrogate Testing for Data-Driven Statistical Filtering.....	41
MST and OMST: Data-Driven Topological Filtering	42
2.4 rs-fMRI Functional Connectivity: Dynamic and Static	44
2.4.1 Dynamic FC	44
State-Based DFC Analysis.....	46
2.4.2 <i>k</i> -Means Clustering in rs-fMRI DFC	47
2.5 Supervised Machine Learning	48
2.5.1 Classification.....	48
Boosted Trees: XGBOOST.....	49
2.5.2 Feature Selection.....	51
2.5.3 Cross Validation, Error Estimation.....	51
Nested Cross Validation	52
Classification Performance Metrics	53
2.5.4 ML Model Combination: Decision Fusion	54
3. rs-fMRI FC Research Applications	56
3.1 rs-fMRI Static FC Approaches	56
3.2 rs-fMRI Dynamic FC Approaches.....	57
Temporal State – Based Analyses.....	59
Cartographic Profiling	61
3.3 Combination of Static and Dynamic Indices	63
3.4 rs-fMRI Functional Connectivity in mTBI.....	64
Static FC In Chronic mTBI.....	65
Dynamic FC In mTBI.....	66

Goal of the Present Study	67
4. Methodology	69
4.1 Data	69
4.1.1 Subjects	69
4.1.2 MRI Acquisition Details	69
4.1.3 Data Preprocessing	70
Denoising	71
Regional Timeseries – Segmentation	72
4.2 Functional Connectivity Measures	73
4.2.1 Static Functional Connectivity	73
4.2.2 Dynamic Functional Connectivity States	75
Cartographic Profiles	76
4.3 Machine Learning Model Architecture	79
4.3.1 Individual Model Classification	79
4.3.2 Model Combination – Decision Fusion	81
4.4 Statistical Comparisons	83
4.5 Software and code	84
5. Results	85
5.1 ML Classification Results	85
Significant features	87
Feature-Level Fusion – FM1	88
Decision-Level Fusion – FM2	90
6. Discussion	93
General Remarks	93
Discussion Of Results – Significant Regions	94

Approach Usability and Generalizability.....	98
Study Limitations.....	98
Future Work.....	99
7. Conclusion.....	101
8. Appendix.....	103
Supplementary Results.....	103
9. References.....	111
10. Scientific Contributions.....	119
Peer Reviewed Proceedings.....	119

LIST OF ABBREVIATIONS

fMRI	functional Magnetic Resonance Imaging
rs-fMRI	resting state functional Magnetic Resonance Imaging
CT	Computerized Tomography
mTBI	mild Traumatic Brain Injury
GCS	Glasgow Comma Scale
EEG	Electroencephalography
MEG	Magnetoencephalography
PET	Positron Emission Tomography
BOLD	Blood Oxygen Level Dependent
DTI	Diffusion Tensor Imaging
DMN	Default Mode Network
DAN	Dorsal Attention Network
HRF	Hemodynamic Response Function
TR	Repetition Time
LFO	Low Frequency Oscillations
sLFO	systemic Low Frequency Oscillations
RSN	Resting-state Network
GSR	Global Signal Regression
SNR	Signal to Noise Ratio
FCG	Functional Connectivity Graph
PCC	Pearson Correlation Coefficient
MI	Mutual Information
SFCG	Static Functional Connectivity Graph
DFCG	Dynamic Functional Connectivity Graph
(O)MST	(Orthogonal) Minimum Spanning Trees
GE	Global Efficiency
LE	Local Efficiency
BC	Betweenness Centrality
EC	Eigenvector Centrality

PC	Participation Coefficient
SWP	Small World propensity
ML	Machine Learning
RF	Random Forest
SVM	Support Vector Machine
CV	Cross Validation

1. INTRODUCTION

1.1 AIM OF THE PRESENT STUDY

Mild Traumatic Brain Injury patient classification through rs-fMRI-derived connectivity indices is the main diagnostic challenge addressed by the present study. mTBI is a highly prevalent condition which is characterized by one or more signs and symptoms that significantly affect quality-of-life. The further understanding of the underlying mechanisms causing these encumbrances on mTBI patients' lives is the main goal of the research presented in this thesis. Data-driven or exploratory analyses are utilized including static and dynamic-based functional connectivity approaches as well as linear and non-linear regional interdependence metrics. Importantly, metrics derived from different, complementary techniques are combined, rather than simply compared, in order to produce a more robust and well-performing model. Graph theoretical approaches are applied on brain networks in order to derive the core underlying network structure as well as for the extraction of useful measures. State-of-the-art Machine Learning classification techniques are evaluated for this challenging diagnostic task.

1.2 STUDY NOVELTY

Several studies have examined rs-fMRI functional connectivity in mTBI patients and compared their findings to those obtained from healthy control subjects. The novelty of the current work lies in the coupling of the dataset with the selected approach. To our knowledge, there are no chronic mTBI studies that have utilized a combination of static and time-varying connectivity measures with the goal of mTBI vs healthy control classification. The presented approach includes a robust and cutting-edge Machine Learning classification scheme where only a few classification studies exist, only in acute mTBI. Additionally, non-linear region interdependence measures have not been studied in the current research setting.

1.3 THESIS OUTLINE

Initially, in 2.2 *Functional Magnetic Resonance* Imaging an overview of the fMRI functional neuroimaging modality is presented, including details on the nature of the obtained signal and noise as well as the main preprocessing steps. The notion of connectivity and brain networks is next introduced and analyzed in 2.3 *Graph Theory and Functional* Networks. The graph theoretical methods for estimating functional associations and obtaining useful results are presented next. Following, several functional connectivity approaches that utilize these graph theoretical notions are analyzed in 2.4 *rs-fMRI Functional Connectivity: Dynamic and Static*. In 2.5 *Supervised Machine Learning*, Supervised Machine Learning classification methods specifics are discussed, culminating in Machine Learning fusion that is implemented in the present work. Following is a thorough analysis of significant rs-fMRI functional connectivity approaches. Methodological counterparts of various aspects of the selected analysis pipeline are presented throughout the *rs-fMRI FC Research Applications* section. In 3.4 *rs-fMRI Functional Connectivity in mTBI*, related work on mTBI is presented with analytical review of relevant methodology as well as reported findings. Next, is the methodological part (section 4) containing all the details of the analysis. Subject and acquisition details are presented first followed by functional connectivity calculation and derivation of various indices. Method evaluation methods are described in 4.3 *Machine Learning Model Architecture* 4.4 *Statistical Comparisons*. Results are presented next, in the form of 5.1 *ML Classification Results and Significant features* indicating regions of increased importance. Next, the obtained results are discussed for their implications alongside several *Study Limitations* and *Future Work* ideas. After the *Conclusion*, *Supplementary Results* are given in the *Appendix*. Finally, after the bibliography section, a recent scientific contribution related to parts of this work is included.

2. BACKGROUND

2.1 MILD TRAUMATIC BRAIN INJURY

Mild Traumatic Brain Injury (mTBI) is a frequently occurring condition, with an approximate percentage of 2% of the population of the U.S. dealing with some degree of disability due to TBI (Ruff et al., 2009). Sport-related or motor vehicle accidents tend to be the most frequent causes of mTBI in addition to blast-related accidents. Symptoms associated with mTBI, especially cognitive recovery might resolve within a three-month period, though it is not uncommon for some to persist into chronic status (Levin & Diaz-Arrastia, 2015). Some examples of chronic symptoms associated with mTBI, include headaches, dizziness, vertigo, depression, fatigue, impulsiveness, irritability as well as cognitive and memory deficits. Depression specifically has been the main research interest of several studies in the field (Moreno-López et al., 2016).

Approximately 90% of TBIs are classified as mild (Len & Neary, 2011), however diagnostic criteria for mild TBI are in need of improvement (Ruff et al., 2009). An important issue in this potential ineffectiveness of current diagnostic procedures is that conventional neuroimaging techniques often do not reveal cues able to aid a correct diagnosis. Building on the last point, cases with an absence of Computerized Tomography (CT) intracranial pathology detections are characterized as “uncomplicated mTBI”. Whereas cases with findings such as parenchymal lesions, intracerebral and extra-axial hemorrhage, brain swelling and shear injury within the first 24 hours after the injury are characterized as complicated mTBI. Complicated mTBI cases, which also typically score poorer on the Glasgow Comma Scale (GCS) have been shown to correlate with worse clinical outcomes (Levin & Diaz-Arrastia, 2015). Diffuse axonal injury is considered one of the main pathological mechanisms in mTBI, while additional pathologies include microhemorrhages as well as abnormalities in cerebral blood flow.

For the reasons mentioned above, alternative approaches utilizing functional imaging techniques are currently being explored as a helpful tool in more effective mTBI diagnosis. Some examples include (Vergara et al., 2016, 2018) where Machine Learning classification techniques have been

employed in conjunction with resting state fMRI (rs-fMRI) dynamic or static functional connectivity or fractional anisotropy in order to effectively distinguish between mTBI patients and healthy controls. Good classification performance is achieved in these studies with functional scans acquired during the acute phase of trauma, i.e., a small number of days after the accident. Only few significant findings refer to disturbances captured by similar imaging modalities later than the sub-acute phase. The study of chronic mTBI, exploring the functional deficits or irregularities captured several months after the accident are of increased interest. Such studies could shed light into the mechanisms responsible for the chronic symptoms discussed, weighing significantly on the quality of life for several sufferers. In addition to aiding in the understanding of mTBI pathophysiology, functional neuroimaging modalities allow for the effective monitoring of mTBI patients with the simultaneous tracking of their symptoms. The latter also constitutes the main goal of the present work.

2.2 FUNCTIONAL MAGNETIC RESONANCE IMAGING

2.2.1 INTRODUCTION TO FUNCTIONAL BRAIN IMAGING

Functional brain imaging modalities vary greatly depending on the type of brain process they aim to record. Magnetoencephalography (MEG) aims at recording neuronal signaling while Positron Emission Tomography (PET) measures metabolic activity rates of neurons. fMRI (and PET) image brain activity by measuring the blood flow provided to sets of neurons. It is easily understood that the phenomena measured by these different modalities are closely related, elevated spontaneous or induced neuronal signaling requires increased rates of glucose and oxygen, contained within blood. Additionally, Diffusion Tensor Imaging (DTI) aims to quantify the functional integrity of neuronal axon bundles. This is achieved by measuring the ease of diffusion of water molecules along neuronal axons.

Imaging data obtained via all neuroimaging modalities except from MEG are considered to be inherently valid, in terms of temporal and spatial representation validity of the measured quantity or phenomenon (Papanicolaou, 2017). This relates to the need of solving the inverse problem,

often without unique solutions. Furthermore, the temporal resolution of these methods varies greatly, from milliseconds between samples recorded using MEG, to seconds for fMRI or PET and minutes for metabolic PET. The substantially lower temporal resolution of fMRI compared to MEG, further worsened by blood flow related delays (discussed below) is partially compensated by the substantially better spatial resolution, a typical voxel (3D space element) is 3 x 3 x 3 mm and does not require further analysis in order to calculate the probable signal source. These details, as well as the fact that MRI acquisition devices are massively more commonplace than MEG systems, typically located in every hospital as well as many research centers/Universities, lead fMRI to be the most frequently used functional neuroimaging modality. This statement can be easily quantified as fMRI accounts for most of the neuroimaging literature.

Electroencephalography (EEG) measures the electrical signal generated by groups of brain cells, action potentials, as they are electrically conducted through the skull and skin. EEG, similar to MEG offers outstanding temporal resolution but suffers from the same spatial localization problems, requiring a solution of the inverse problem in order to pinpoint the multiple sources that produce the final measured signal. However, this has nowadays become very accurate through the Finite Element Method or FEM (Antonakakis et al., 2019). All neuroscience tools have limitations and strong suits, each informing in more detail about certain aspects of neural computation. An additional important point to be made is that in a healthy brain, brain activity images recorded by means of quantifying signaling, metabolism or blood flow, recorded under similar conditions are expected to be very close (Papanicolaou, 2017).

2.2.2 BOLD CONTRAST MECHANISM: THE BASIS OF FMRI

As stated previously, fMRI is based on the measurement of blood oxygen, present in a specific brain region. Oxygen consumption in the brain being mostly neuronal, the neuron metabolic rate closely relates to rate of neuronal activation. Neural activation leads to an increase in deoxyhemoglobin (non-oxygenated blood), followed by an overcompensation due to the decrease in oxygen (due to increased metabolic rates) via an increase in oxygenated blood.

The mechanism connecting increased blood flow to sets of neurons and increased neuronal activation is relatively straightforward yet not entirely understood. Adding to the complexity, neuronal oxygen consumption and oxygen supply processes are probably not entirely connected by a linear relationship (Logothetis & Wandell, 2004).

Although some uncertainty remains regarding the specifics of these underlying mechanisms, it is generally accepted that the strength of neuronal signaling is reflected by the magnitude of recorded fMRI signals. Synaptic potentials being the main cause of the observed signal response. The measured signal driven by the mechanism described above is called a **Blood-Oxygen Level Dependent** signal or BOLD contrast response. Figures 1 through 4 are all examples of fMRI data. *Figure 3* is an example of an actual regional BOLD timeseries.

Although the validity of the relationship between neuronal activation, metabolic rates and increased blood flow have been accepted, the calculation of the duration of this process, posed an additional challenge to fMRI researchers. Without diving too deep into the entire biological chain of events, the vascular system response delay to local oxygen demands leads to an observable surplus of oxygenated blood in an activated area around 4-6 seconds following neuronal activation. Due to this delay in measurable blood flow compared to local demands, the fMRI signal measured captures activation with an analogous delay of 4-6 seconds, compared to the immediate response in action potentials captured by MEG or EEG. The Hemodynamic Response Function (HRF) describes the response to stimuli expected in a certain region's BOLD signal (Papanicolaou, 2017).

2.2.3 RS-fMRI SPONTANEOUS NEURAL ACTIVITY AND CONNECTIVITY

“Resting-state” brain activity can be defined as the set of processes present when the brain is not explicitly engaged or performing a specific task. This activity includes basic functions of awareness and consciousness as well as maintaining various biological processes necessary for maintaining life. The mental processes that exist in these low-frequency fluctuations measured by rs-fMRI can also be characterized as self-referential and introspective.

The measured BOLD signal response is significantly slower than neuronal firing, thus fMRI cannot reflect rapid changes in neuronal activity (Logothetis et al., 2001). The BOLD signal

consists of rapid neuronal activity convolved with much slower hemodynamic response functions, similar to the HRF used in task-based activation calculations. Typical fMRI BOLD LFOs exist in the $\sim 0.01 - 0.15$ Hz frequency range. However, as is thoroughly discussed in (Tong et al., 2019), a substantial amount of total BOLD signal variance, probably $>30\%$, is caused by systemic Low Frequency Oscillations (sLFOs) travelling through the vasculature, intertwining with neuronal-based hemodynamic activity, thus adding to noise and diminishing overall signal clarity. Methods for mitigating the effect sLFO on the voxel BOLD time-courses are discussed in section 1.2.4.

Resting-state network or RSN is the name given to any group of brain regions that exhibit similar BOLD activation patterns during a resting-state acquisition. In typical task-based experimental setups, resting-state activation is sometimes considered as the control state against which regional activation values are compared. This “noise” against which task activation is usually compared, accounts for around 20% of the body’s energy, while the increases in neuronal metabolism that are task-related account for less than 5% (Fox & Raichle, 2007). This fact combined with many positive signs of the modality’s significance have led many researchers to delve deeper into the study of resting-state brain activation and connectivity measured through fMRI.

Resting-state related activations are not evenly distributed throughout the cortex. The posterior cingulate cortex (PCC), ventral anterior cingulate cortex (vACC) and bilateral inferior parietal cortex are some of the significantly active regions at rest (Mazoyer et al., 2001). These regions exhibit stronger activations (and connections/associations) when no specific task is being completed compared to when a specific mental task is underway. Activation or co-activation of several regions leads to the formation of “resting-state networks”. One of the significantly active sets of regions at rest (and attenuated during task) is the Default Mode Network (DMN). Many studies have been reporting results including the DMN, but several details concerning its exact function still remain unanswered. Regions comprising the DMN include the precuneus, posterior cingulate cortex (PCC), inferior parietal lobule, lateral temporal cortex and medial prefrontal cortex. DMN regions are depicted in *Figure 1*.

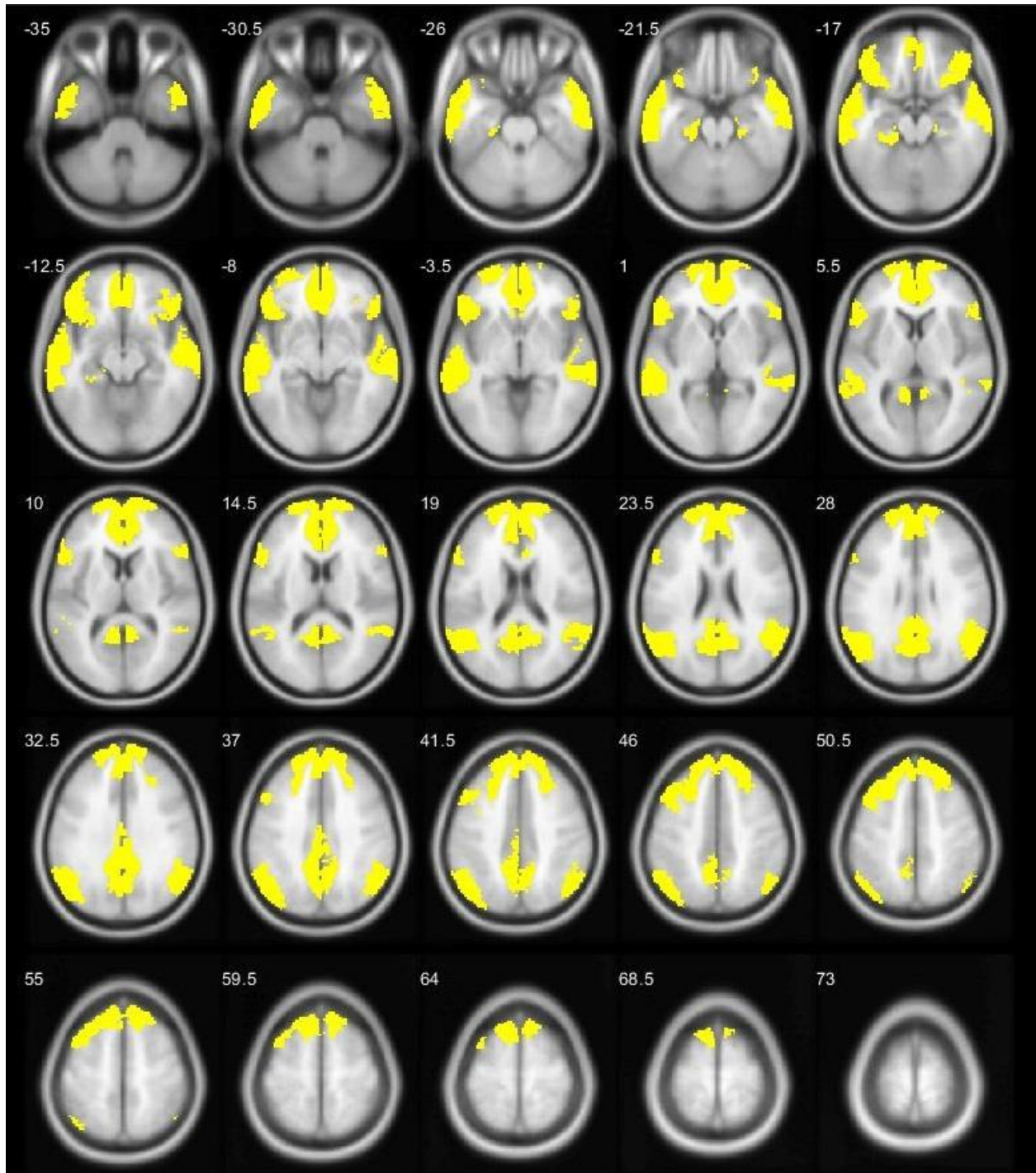


FIGURE 1 – THE DEFAULT MODE NETWORK

The Dorsal Attention Network (DAN) is also of increased importance in rs-fMRI studies, typically exhibiting increased co-activation in goal-oriented scenarios. It is also often referred to as the “Task Positive Network” or TPN as it typically exhibits increased activation in heightened mental loads and decreased presence at rest. The DAN consists of the insula, supplementary motor area, dorsolateral prefrontal cortex, frontal eye fields and inferior parietal cortex (Bijsterbosch et al., 2017). The main regions of the DAN are visually depicted in *Figure 2*. Both *Figure 1* and 2 were created by overlaying each network’s regions on a healthy participant’s MRI data.

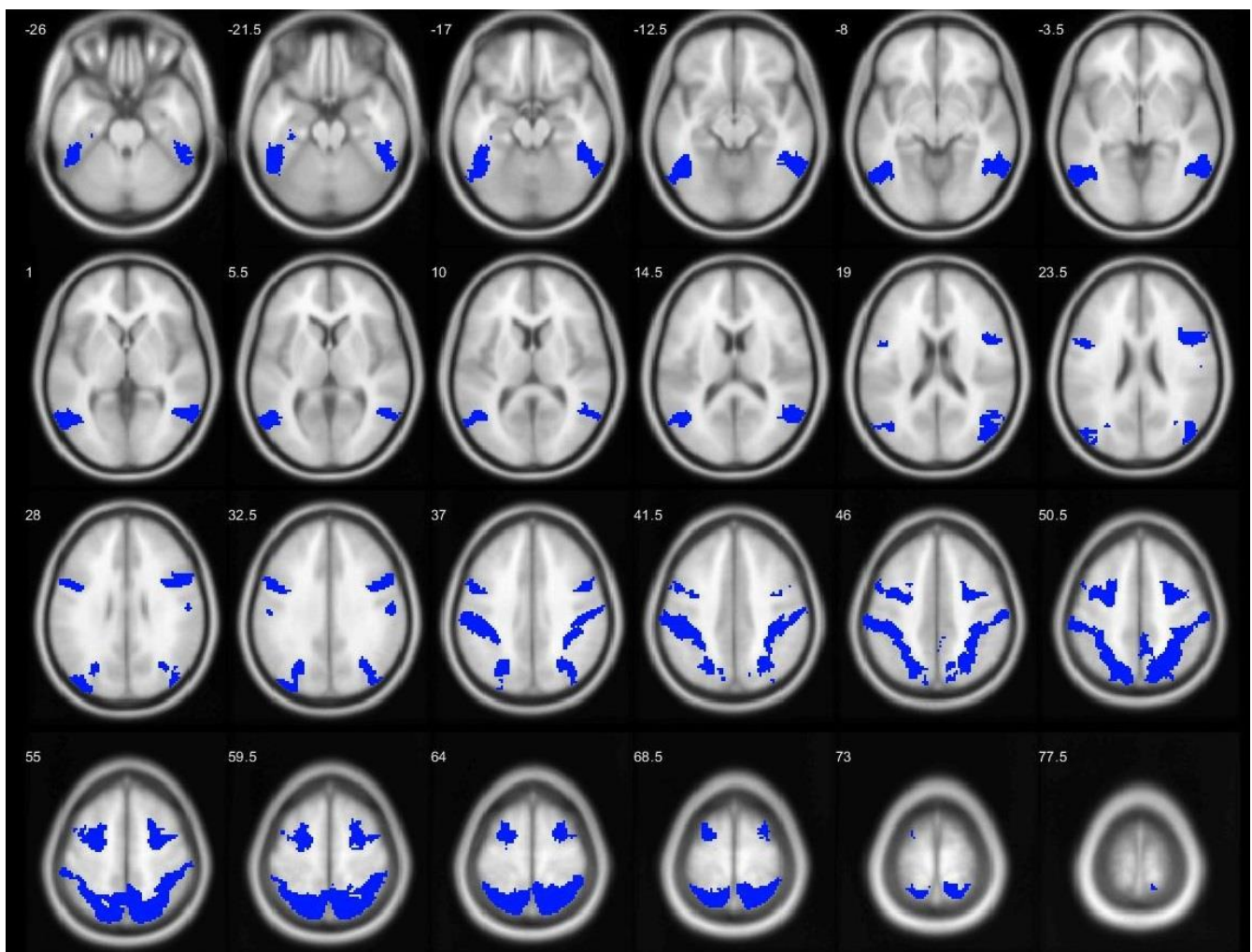


FIGURE 2 - THE DORSAL ATTENTION NETWORK

The notion of functionally connected regions is different to that of simply activated or activated to a similar degree. While traditional activation-based analyses study the relative “strength” of activation of different brain regions (via the BOLD signal) be that at rest or in a task-based experiment, connectivity aims at quantifying the interconnection of different brain regions of various sizes (single voxels up to several hundred voxels).

Rs-fMRI is a non-invasive modality that can be performed in most hospitals and many research centers. It has gained significantly in popularity and research interest in the past years. It has demonstrated an impressive potential in aiding disease diagnosis as well as providing new insight in the understanding of various diseases, conditions or processes and their underlying neural mechanisms. Gaining a better understanding of the intrinsic neural architecture by studying various communication characteristics during rest is a strong motivation alone. Some good examples that support the last statements are: (Arbabshirani et al., 2013; Basile et al., 2014; Kavroulakis et al., 2021; Khazaei et al., 2017; Pappas et al., 2019).

2.2.4 FMRI NOMENCLATURE AND ACQUISITION BASICS

In order to avoid confusion with several existent terminologies referring to the same aspects of fMRI recoding, next, some basics terms and their definitions are presented. ‘BOLD signal’ or ‘BOLD signal response’ or ‘BOLD contrast response’ refers to each brain point’s (voxel’s) relative activation value, measured based on the principles explained in 2.1.2. The term ‘voxel’ refers to the spatial object recorded in fMRI, similar to an image’s pixels but in 3D space. A voxel has a specific size in 3D space, depending on the acquisition system and specifications, a typical size can be 3 x 3 x 3 mm, which would be referred to as 3mm isotropic as it has the same size in each dimension. Repetition time or ‘TR’ refers to the time interval between successive functional image acquisitions, typical values being around 2 seconds. In this example, every 2 seconds, an entire 3D image is recorded consisting of a few hundred thousand voxels. The 3D image is scanned in axial slices (in the direction of the top of the head towards the body), each slice having the thickness of a single voxel. Each slice is often scanned in an interleaved fashion, meaning the slices are not scanned sequentially towards one direction. The entirety of slices scanned in one TR constitute a

single ‘volume’, a single 3D BOLD contrast image recorded on a specific timepoint. A whole fMRI scan, be that resting-state or task-based, is comprised of tens or even hundreds of volumes. For example, a ten-minute scan, with a repetition time of 2 seconds, will contain 300 volumes, often referred to as ‘timepoints’, as they represent the entire brain’s BOLD activation information at that timepoint. A single subject’s fMRI data is as a result 4D, three spatial dimensions and one temporal, e.g., voxels x voxels x voxels x TRs.

2.2.5 SOURCES OF NOISE AND ARTIFACTS: PREPROCESSING BASICS

SPM, FSL, AFNI and Brain Voyager are some of the most popular packages for fMRI preprocessing and further analysis. Other analysis packages such as CONN (Whitfield-Gabrieli & Nieto-Castanon, 2012) and DPARSF (Chao-Gan & Yu-Feng, 2010), incorporate many preprocessing steps from SPM, and provide an entire analysis pipeline, from raw data to subject or group level statistical results (connectivity or voxel level metrics). All above mentioned packages are able to perform most of the preprocessing steps analyzed below. Some studies following most of the mentioned preprocessing steps include (Antypa et al., 2021; Moreno-López et al., 2016; Price et al., 2014; Rashid et al., 2016; Saccà et al., 2019).

TEMPORAL AND SPECTRAL

Resting-state fMRI is typically recorded in a frequency band lower than 0.1Hz and thus should be free from prominent cardiac and respiratory artifacts as well as eye movement and other muscle induced artifacts, which pose a substantial problem in other neural recordings such as EEG and MEG.

sLFOs have recently been discussed by several fMRI research teams around the world, as a portion (around 30%) of the BOLD frequency spectrum seems to be dominated with this (initially apparent) “noise”. As shown by (Tong et al., 2019), the sLFO signal travels through the vasculature and its source is probably non-neuronal, though common RSNs exhibit similar patterns if delayed

versions of this signal are measured. Fortunately, supporting the validity of the majority of rs-fMRI RSN findings, regions that exhibit very similar activation patterns are likely to have developed temporally similar vascular supplies. An initial attempt to mitigate the sLFO effect on any results based on the BOLD response, was the application of Global Signal Regression (GSR). The mean global signal exhibits the characteristics of the sLFO quite prominently and thus regressing out the global signal will somewhat mitigate its effect on voxel time-series. An important drawback though, is that the use of GSR mathematically mandates the creation of a large amount of, previously non-existent and artifactual, anticorrelations between regions. CompCor (Behzadi Y et al., 2007) avoids these drawbacks significantly, while removing the effect of sLFO to a certain degree. The most frequent use of CompCor entails regressing out the first five components of the white matter and cerebrospinal fluid signals as well as their first order derivatives. The removal of these nuisance variables from voxel time courses is considered to aid significantly in overall signal denoising.

Adding to the time course aspect of preprocessing, in the majority of studies, linear detrending is applied to all voxel's BOLD timeseries in combination with bandpass filtering. Detrending aims at mitigating very slow fluctuations or trends often present while bandpass filtering attempts to remove (MRI acquisition related) low frequency drifts and "high frequency" noise, a typical band retained is around 0.01 and 0.1. In the following figure, a visual depiction of the effect of these preprocessing steps is provided. The voxel timeseries visualized is for a healthy control volunteer. The bandpass filtering frequency band used was 0.008-0.09 Hz, in the lower graph, White matter and Cerebrospinal Fluid (CSF) signals were regressed out. The timecourses presented in *Figure 3* show BOLD signal power (y axis) through scan time in TRs (0-150).

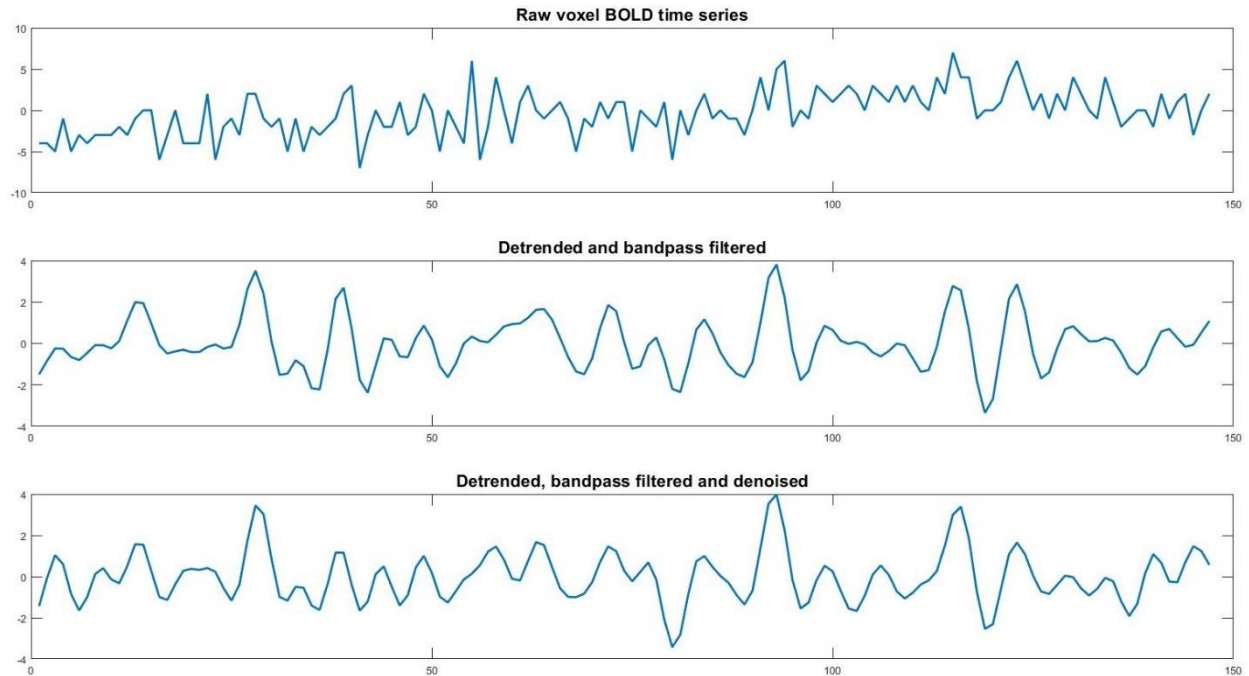


FIGURE 3 – RAW, BANDPASS FILTERED, FILTERED & DENOISED VOXEL BOLD TIMESERIES

In most fMRI studies, the first few volumes are discarded in order to allow for the magnetization from the acquisition equipment to stabilize. A typical number of initial discarded volumes is between 3 and 6, although in long acquisition time studies, more than ten may be not included in the analysis. Slice-timing correction is often performed in order to correct for the difference in exact acquisition times of each volume's slices. A single volume is scanned within the window of one TR (~2s), entailing the scan of tens of axial slices, slice-timing correction aims at adjusting the BOLD signal of each slice while considering the pattern of scanning.

SPATIAL

It is logical to assume that in a 5–15-minute scan, some at the least slight head movement has occurred. This automatically means that a particular voxel in 3D space, corresponds to a different brain region in timepoints before and after any movement more than a millimeter or so. For this reason, motion correction is typically one of the first preprocessing steps performed on raw fMRI data. This within subject correction step is also referred to as realignment as it involves realigning all volumes to the first or to a mean of all volumes. This is completed using linear transformations in each of the three spatial axes.

An important point concerning the interpretability through visualization of recorded fMRI images entails the need of capturing the subject's anatomical images alongside the functional results. Functional images are not “clear” enough for identification of the main anatomical landmarks, as can be seen in *Figure 4*. Thus, in order to visually analyze any results and examine detailed anatomical proximity of activated regions, the functional data must be superimposed on the subject's structural data or normalized to a standard space/template, the most used being MNI or Talairach. Typically, in studies with multiple subjects, the researchers utilize the second option for easier comparison of findings among subjects. The process of transforming (warping) the subjects' images to a standard space is called spatial normalization. An additional spatial preprocessing step often utilized is spatial smoothing. Smoothing aims at slightly improving the signal-to-noise ratio of each scan while also correcting potential anatomical variability that was not rectified by the spatial normalization step. A Full Width at Half Maximum (FWHM) gaussian filter is typically used, while its size is determined by the smallest brain region that will be studied in the following analysis steps, 6-8mm kernel sizes are often selected.

Regarding the images presented in Figures 1-4, all structural (MRI) and fMRI images and timeseries (*Figure 3*) are from the present dataset's healthy population and are used as typical examples.

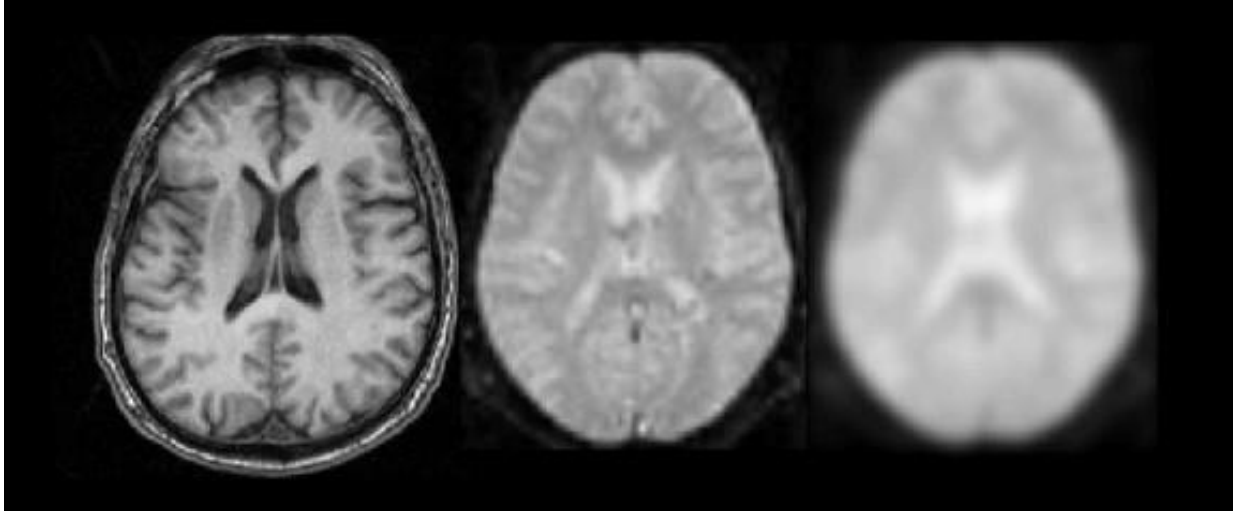


FIGURE 4 - LEFT TO RIGHT: STRUCTURAL MRI IMAGE (T1), FMRI IMAGE, SMOOTH FMRI IMAGE

2.3 GRAPH THEORY AND FUNCTIONAL NETWORKS

2.3.1 COMPLEX NETWORKS

Network science is the study of a large variety of networks, such as social, telecommunication, computer, biological, cognitive and neural. A network is simply a set of objects or elements, usually referred to as ‘nodes’ that are “connected” by edges. An edge between two nodes can simply indicate the present or not of some sort of communication or similarity between the nodes or the degree/weight/extent of the connection that exists between them. The first is called a binary network while the latter, a weighted network. The value corresponding to a specific edge is analogous to the relationship between the nodes. For example, in a social network, a strong edge would indicate that the two individuals connected by it, maintain a strong social bond, meet frequently, exchanging many messages etc. Additionally, a network can be directed or undirected, referring to the symmetry of connection between nodes. A frequent interpretation of directed networks is for indicating information flow. In a directed network, a node A may provide more to

B than B provides to A, demanding the existence of two edges between each pair of nodes, whereas in an undirected network all connections are symmetric. A network, also referred to as a graph is usually represented in matrix form for storage and analysis purposes. In an adjacency matrix, the value of $A_{i,j}$ represents the connection information between nodes i and j . If the graph is binary, $A_{i,j} = 0$ or 1 , while for weighted graphs, $A_{i,j} \in [0, 1]$, or any other continuous range.

Neuronal networks, describing the relationships between different brain regions, are considered to be (some of) the most complex networks, thus borrowing many sophisticated network analysis techniques from network science or graph theory. The first step of any functional connectivity study, estimated e.g., through rs-fMRI, would be the construction of a functional brain connectivity network. Depending on the size of brain regions used in the definition of the graph's nodes, two main directions exist for this process, node or voxel-based techniques.

2.3.2 FUNCTIONAL CONNECTIVITY GRAPHS

GRAPH NODE DEFINITION

In voxel-based approaches, the connectivity strength of single voxels is estimated with several or all other voxels in the brain. Seed-based correlation analysis is an example of this type of approach, where the connection strengths are calculated between a predefined region (or voxel) and all other regions in the brain. Another example can be found in (Martuzzi et al., 2011; Vatansever et al., 2016) that used a type of connectivity called ICC or Intrinsic Connectivity Contrast, calculating the average connection of each voxel to all others, this can be considered a global connectivity measure.

In node-based connectivity studies, the graph nodes represent larger brain regions (groups of tens to hundreds of voxels), usually called Regions of Interest (ROIs) or simply nodes. Anatomical or functional atlases are frequently used in order to parcellate the brain into many distinct regions whose functional relationships are under study. In this case, ROI-ROI pairwise connectivity is estimated. In the case of larger brain regions, the question arises of how to calculate the entire

ROI's representative BOLD timeseries in order to estimate its connections with other regions. In the majority of studies, this is completed by using the mean timecourse of all voxel timecourses within that region. Other approaches such as the application of Principal Component Analysis (PCA) on voxel timeseries and using the first component (with the highest amount of variance explained) as the representative timeseries have also been proposed (Sato et al., 2010). Regardless of the regional timeseries extraction method, depending on the number of regions defined by the selected parcellation method, a fixed number of regional timeseries will be produced and used for connectivity analysis.

A node-based functional connectivity approach was followed in the current study. The functional characteristics under study did not require the finer spatial detail obtained by voxel-based approaches. In order to maintain enough anatomical specificity, a relatively finer-detail functional atlas was used containing 200 cortical (Schaefer et al., 2018) and 32 subcortical (Tian et al., 2020) regions. The “Schaefer” and “Melbourne” atlases both provide multiple different numbers of regions, leading to an atlas of varying detail in ROI specificity. The specific “resolution” and combination of atlases was selected based on (Andrea I. Luppi and Emmanuel A. Stamatakis, 2020; Luppi, Gellersen, et al., 2021). In the following figure (*Figure 5*), a node-based FC approach is visualized with colored lines between regions representing their connections. Thicker lines indicate a stronger association. This is also an example of ROI segmentation with spheres representing region centers.

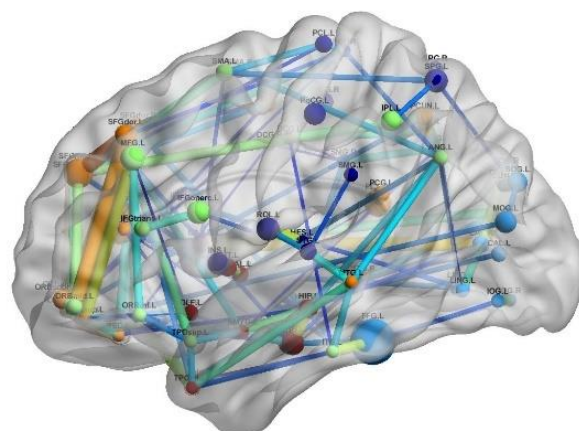


FIGURE 5 – NODE-BASED FC APPROACH

CONNECTIVITY ESTIMATION

With the popular example on node-based FC in mind, two often utilized connectivity estimation methods are discussed below, the Pearson Correlation Coefficient (PCC) and Mutual Information (MI). The former describing strictly linear relationships between region activations and the latter both linear and non-linear.

PEARSON CORRELATION COEFFICIENT

The Pearson correlation coefficient is most frequently used in order to estimate functional connectivity between regions. PCC is calculated for pairs of BOLD timeseries, be that the timeseries of two voxels, one seed region and a voxel or two regions. The PCC lies in the -1 to 1 range, 1 dignifying very high similarity, i.e., when one signal rises the other rises as well or when one falls the other follows. Negative values indicate anticorrelated signals, exhibiting opposite tendencies. Zero or close to zero PCC values indicate no resemblance or common linear patterns present in the two timeseries. PCC is closely related to the covariance of two random variables, “normalized”/divided by the product of their individual standard deviations.

$$PCC_{X,Y} = \frac{E[(X - \mu_X)(Y - \mu_Y)]}{\sigma_X \sigma_Y}$$

$$cov(X, Y) = E[(X - \mu_X)(Y - \mu_Y)]$$

$$PCC_{X,Y} = \frac{cov(X, Y)}{\sigma_X \sigma_Y}$$

σ_X : standard deviation of X , σ_Y : standard deviation of Y

μ_X : mean of X , μ_Y : mean of Y , E denotes the expected value of a random variable

In the case of the application of PCC to actual recorded data (sample), the sample PCC is computed as follows:

$$PCC_{(sample)xy} = \frac{n \sum x_i y_i - \sum x_i \sum y_i}{\sqrt{n \sum x_i^2 - (\sum x_i)^2} \sqrt{n \sum y_i^2 - (\sum y_i)^2}}$$

n : number of samples (time points/length of timeseries)

x, y : sample points of length n , indexed with i (timeseries of two ROIs)

MUTUAL INFORMATION

In its essence, Mutual Information between X and Y , estimates how well X can be predicted (e.g., a BOLD timecourse) once Y is known or vice versa. Thus, quantifying the “mutual information” between two random variables. In its calculation the initial statement is depicted inversely, i.e., what is the reduction in uncertainty of one variable when the other is known.

$$MI(X; Y) = H(X) + H(Y) - H(X, Y) = H(X) - H(X|Y) = H(Y) - H(Y|X)$$

$H(X)$ represents the Shannon Entropy of the variable X .

$H(X|Y)$ and $H(Y|X)$ are the conditional entropies, $H(X, Y)$ is the joint entropy of variables X, Y

Also, $MI(X, Y) = MI(Y, X)$

The PCC is by definition, a linear similarity measure. Mutual Information is able to capture both linear and non-linear interdependencies that exist between two sets of observations. MI, similar to the PCC is not directional and in addition, only produces positive values between 0 and 1. In the

present study, both connectivity metrics were utilized in order to examine the effect of the methodological differences in network identification and significance.

2.3.3 FUNCTIONAL AND TOPOLOGICAL GRAPH CHARACTERISTICS

In node-based connectivity studies, estimated by PCC or MI, a symmetrical matrix is produced containing all the ROI-ROI pairwise associations. For example, an $n \times n$ (n : number of ROIs) square matrix $FCG_{i,j}$ (Functional Connectivity Graph) contains in the position 2, 3, the estimated connection strength between regions 2 and 3. For undirected metrics such as PCC and MI, undirected graphs-matrices are produced. This leads the FCG to be symmetric around the first diagonal ($i=j$) and thus values are duplicated in the upper and lower triangular portion of the matrix. For example, the connection strength between 2 and 3 is the same as between 3 and 2 or, $FCG_{2,3} = FCG_{3,2}$. This also means that the “unique” values contained in an FCG are less than half of the entire matrix entries. For instance, with 100 regions an $FCG_{100 \times 100}$ contains 10000 total entries, the 100 diagonal entries are all 1 as each region’s association with itself is always full and are therefore useless information. Dividing these remaining values by two because of the symmetry, $(10000 - 100) / 2 = 4950$ connections. This can also be calculated using the binomial coefficient (n over k), calculating the possible pairs ($k=2$) of 100 objects ($n=100$), without including transverse pairs.

$$\binom{n}{k} = \binom{100}{2} = 4950$$

These unique/useful values extracted can be vectorized for more efficient storage and compared between subjects-groups (referred to as a vectorized FCG). This representation however does not take into account any topological characteristics of the original network.

An additional important point that must be made is in regard to the “type” of graph weighting. The FCGs described are formed with the notion of a similarity measure describing the association between nodes. More “traditional” graphs such as geographical networks, where the nodes represent cities, towns etc. and the edges portray the physical distances between them. The latter is usually called distance weighting, a simple transformation is needed in order to convert one type

of weighting to the other, such as taking the multiplicative inverse ($1/FCG$). This is often needed as many graph measures (several are described later) require distance weighting for graphs instead of association/similarity.

GRAPH METRICS

Various measures have been developed in order to examine different functional and topological aspects of complex networks. Graph measures may examine network characteristics at a global, or local (nodal) level. Global metrics refer to a tendency exhibited by the network as a whole, while local/nodal measures examine patterns in local neighborhoods, the surroundings of each node.

Some main notions often studied in depth are the efficiency of communication or information flow, the formation of network hubs that control the communication among several other nodes as well as the tendency of a network to form strongly connected subnetworks. These basic ideas as well as some more sophisticated, are analyzed and discussed below. In the current study, weighted-undirected networks were used in all analysis steps. The connectivity measures used are by nature undirected. Binary graphs were deemed not able to capture the complex network characteristics able to distinguish the groups in question. Therefore, the graph measure formulas for weighted-undirected networks are provided below, additional information and calculation details for other types of networks can be found in (Rubinov & Sporns, 2010).

Some basic notation used for the calculation of several graph metrics below:

- N : all the nodes of the network
- n : the number of nodes
- v : sum of the network's connections, $v = \sum_{i,j \in N} w_{ij}$
- w_{ij} : the edge weight between nodes i and j .
- $a_{ij} = 1$ when a connection exists between i, j , 0 otherwise.
- The **shortest path** d_{ij} between nodes i, j is the path connecting the two nodes with the least sum of distances (maximum sum of strengths).

As mentioned above, two types of graph weighting exist, most metrics operate on distance weighted networks, thus all formulas and discussion of graph metrics refers to distance weighting. Brain networks created using PCC or MI are similarity weighted. A transformation of $1./FCG$ is used in all cases where this is needed, taking the edge-wise multiplicative inverse.

CHARACTERISTIC PATH LENGTH

The characteristic path length of a given graph is the average shortest path between all pairs of nodes. High values of this measure indicate a global trend of connections/paths with low cost (short length). It is thus a global measure of functional integration. In general, integrated networks exhibit globally strong connectedness that is controlled by hub nodes. A more diffuse connectedness is expected in such networks.

$$L = \frac{1}{n} \sum_{i \in N} \frac{\sum_{j \neq i} d_{ij}}{n - 1}$$

GLOBAL EFFICIENCY

Global Efficiency (GE) is calculated as the average inverse shortest path length, it is inversely related to the characteristic path length. The interpretations and uses of global efficiency are very similar to those of characteristic path length but with inverse value ranges. Lower values of characteristic path length indicate more efficient communication overall, high values of global efficiency indicate the same. Additionally, the characteristic path length is mostly influenced by longer paths while the opposite is true for global efficiency, this also makes global efficiency better fitted for judging the communication structure in disconnected graphs. In these cases, the calculated efficiency value is zero.

$$E = \frac{1}{n} \sum_{i \in N} \frac{\sum_{j \in N, j \neq i} 1/d_{ij}}{n-1}$$

LOCAL EFFICIENCY

Higher values of Local Efficiency (LE) (or clustering coefficient) indicate better communication efficiency among the nodes of an immediate local community. Local efficiency is equivalent to global efficiency calculated on the neighborhood of a node. It is also quite similar to the clustering coefficient as it is described below, for this reason typically one of the two measures is used per application.

The inverse shortest path length calculated on the subgraph of all immediate neighbors of a particular node is then normalized by the possible connections that could exist among those nodes.

In general terms, it encapsulates whether a system is more immune to faults by quantifying the efficiency of communication between a node and its neighbors if it were removed from the network.

$$E_{Loc} = \frac{1}{n} \sum_{i \in N} \frac{\sum_{j \in N, j \neq i} (w_{ij} w_{ih} \frac{1}{d_{ij(N_i)}})^{1/3}}{k_i(k_i - 1)}$$

CLUSTERING COEFFICIENT

The quantification of segregation via increased clustering in complex networks usually revolves around the prevalence of triangles. The ratio of neighbors around a particular node that are also neighbors with each other, calculated through a fraction of triangles, is known as the binary clustering coefficient (Watts & Strogatz, 1998). In the weighted graph case, conceptually and computationally similar to local efficiency, the clustering coefficient measures the degree of

information segregation at a given node's neighborhood. Segregated networks are typically characterized by more clearly formed local communities, disconnected from each other and with strong internal associations.

$$C = \frac{1}{n} \sum_{i \in N} \frac{2t_i}{k_i(k_i - 1)}$$

(Onnela et al., 2005)

$$t_i = \frac{1}{2} \sum_{j,h \in N} (w_{ij}w_{ih}w_{jh})^{\frac{1}{3}}$$

t_i : Geometric mean of triangles around the node i

SMALL-WORLDNESS

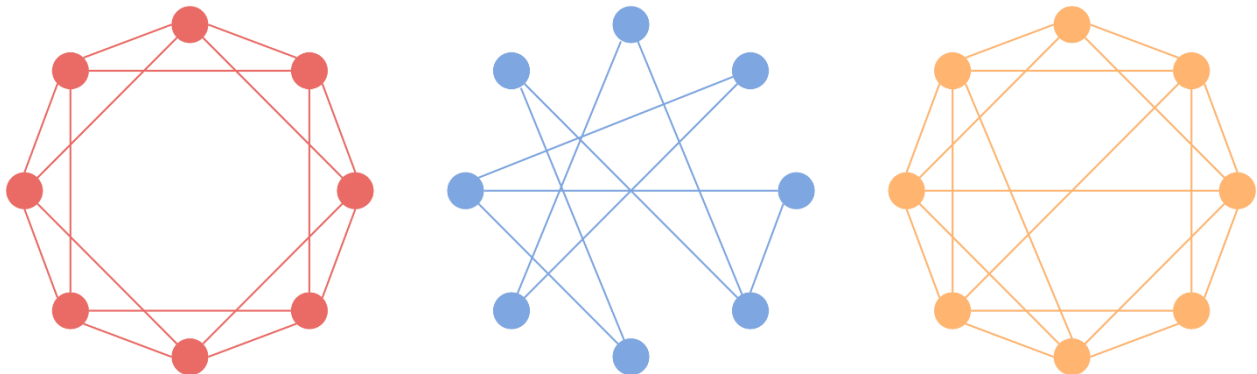


FIGURE 6 – LATTICE NETWORK - RANDOM NETWORK - SMALL WORLD NETWORK

Networks that exhibit increased local clustering combined with short links that connect these local communities with distinct parts of the network are referred to as ‘small world’ networks. Small-world networks manage to maintain good overall connectedness (relatively high Global

Efficiency) without most nodes having an increased number of connections. They represent a balance between the high global efficiency of Random networks and the high local efficiency found in Lattice networks. This can be clearly seen in the examples provided for each type of network. The above statement easily leads to the formulation of a measure quantifying this network behavior. As can be seen below, the straightforward approach to calculate small-worldness is to obtain the ratio of the standardized clustering coefficient to standardized characteristic path length. The weighted clustering coefficient strongly resembles the weighted local efficiency, while global efficiency is the inverse of the characteristic path length. Standardization can be achieved by dividing each metric by the mean values of those obtained from “random” networks. The random networks can be derived from random rewirings of the initial network. Small-worldness values obtained from the given formula are often much greater than one.

$$SW = \frac{C/C_{rand}}{L/L_{rand}}$$

C: Clustering coefficient, *C_{rand}*: Clustering coefficient of random network

L: Characteristic path length, *L_{rand}*: Characteristic path length of random network

Conceptually, small-world networks can be considered as a balance between local and global processing (Bassett & Bullmore, 2017). Additionally, more prominent small-world characteristics tend to indicate efficiency-optimality of information capacity (Barttfelda et al., 2015).

SMALL-WORLD PROPENSITY

The small-worldness measure defined above has a few inherent drawbacks. Namely, it is dependent on a network’s density while not taking into account the edge weights. Both these points significantly limit the measure’s ability to be compared across different network topologies of varying densities and overall wiring weights. This disadvantage is particularly obstructive in the comparison of brain networks from different individuals, conditions, repeated scans etc. For these

reasons, an improved metric was formulated by (Muldoon et al., 2016), namely, small-world propensity (SWP). Small-world propensity was developed in order to overcome the significant drawbacks of the small-worldness measure by quantifying the exhibited small-world characteristics of a given network while taking into account the potentially different density. A brief examination of the SWP's formula can reveal the potential improvements. The deviation of the given network's clustering coefficient and characteristic path length is measured against those calculated on lattice and random networks. The random and lattice networks created for these comparisons retain the same degree distributions as the original. Finally, the SWP produces values ranging for 0 to 1.

$$SWP = 1 - \sqrt{\frac{\Delta_c^2 + \Delta_L^2}{2}}$$

$$\Delta_c = \frac{C_{latt} - C_{obs}}{C_{latt} - C_{rand}}$$

$$\Delta_L = \frac{L_{obs} - L_{rand}}{L_{latt} - L_{rand}}$$

C_{obs} : Observed clustering coefficient, L_{obs} : Observed characteristic path length

C_{rand} : Random network clustering coefficient, L_{rand} : Random network characteristic path length

C_{latt} : Lattice network clustering coefficient, L_{latt} : Lattice network characteristic path length

Δ_c , Δ_L are calculated as the fractional deviation of the network's actual clustering coefficient, characteristic path length against those of a lattice and random network

SWP's sensitivity and strength has also been corroborated by (Luppi, Carhart-Harris, et al., 2021), whose direction of analyses is very similar to the present study.

DEGREE

Functional centrality metrics attempt to encapsulate node importance in a single nodal graph measure. A node predominately acting as a network hub, interacting with many other nodes and facilitating integrative network behavior should correspond to increased values of centrality. Node degree (DEG) is the simplest measure of centrality, revealing the number of nodes that a given node interacts with (or overall strength of interactions). Binary node degree (k^b) simply counts a particular node's connections, while weighted degree (k^w) sums over that node's connection weights towards all other nodes.

$$k_i^b = \sum_{j \in N} a_{ij} , \quad k_i^w = \sum_{j \in N} w_{ij}$$

BETWEENNESS CENTRALITY

The appropriately named metric of Betweenness Centrality (BC) attempts to measure node importance based on the number of strong connections a given node is located between and thus helps mediate. It is formally calculated as the number of shortest paths passing through a particular node divided by the total number of shortest paths of the network.

$$BC_i = \frac{1}{(n-1)(n-2)} \sum_{\substack{h,j \in N \\ h \neq j, h \neq i, j \neq i}} \frac{sp_{hj}(i)}{sp_{hj}}$$

sp : The number of shortest paths

sp_{hj} : The number of shortest paths between nodes h and j

$sp_{hj}(i)$: Shortest paths between nodes h and j that cross over i .

EIGENVECTOR CENTRALITY

Eigenvector Centrality (EC) is a self-referential measure of centrality i.e., a node with high values of EC must be connected to other nodes with increased EC. This nodal centrality measure's values are computed as eigenvector elements, corresponding to the highest eigenvalue of the adjacency matrix. Quite differently from node degree, EC (and BC), do not rely on the mere number of connections a node possesses but the 'importance' of its connections which in turn lead to higher values of centrality and importance. BC accomplishes this by incorporating the number of important connections in the calculated measure, while EC attempts to quantify node importance, i.e., relationships with more 'important' nodes increases that particular node's importance/centrality.

FUNCTIONAL MODULES – MODULARITY

In order to define the measure of modularity, the idea of functional modules must be first introduced. Often in networks, groups of strongly connected regions often emerge, exhibiting only weak associations with other nodes or groups. These strongly interconnected subcomponents of the original network are usually referred to as 'modules' or 'communities' (Newman, 2004). As will be discussed later in the Louvain algorithm details, the "weak connections" of modules towards other modules can also be negative correlations in the case of the PCC that provides signed values. The detection of such clusters in complex brain networks provides important insight of the inner workings of the network. Additionally, the quantification of decomposability or 'modularity' can also be a significant condition or disease-related biomarker indicating a generalized dysfunction in connectedness. Modularity can be included in the category of functional segregation measures, as exhibiting a prevalence of isolated communities is predominately segregated behavior.

$$Q = \frac{1}{v} \sum_{ij \in N} (w_{ij} - \frac{k_i k_j}{v}) \delta_{M_i M_j}$$

This modularity calculation can be interpreted as the average difference of actual within module connections, represented by w_{ij} and within module connections expected to be present by chance.

ASSIGNMENT OF NODES TO MODULES: LOUVAIN

Building upon the notion of functional modules discussed previously, methods have been developed for the detection of such structure in networks. Contradictory to all other network measures discussed here, the assignment of nodes to modules utilizes optimization and is therefore not computed directly. In the implementation used, the Louvain greedy algorithm, different possible partitions are evaluated and the “optimal” is chosen by maximizing the modularity function Q . When working with strictly positive-weighted networks as in the case of MI FCGs, the modularity calculation described above is used. Furthermore, as previously mentioned, connection sign can be utilized in the module assignment process, based on the notion that modules can exhibit anticorrelations among each other. Most algorithms treat negative and positive weights symmetrically, something problematic in practice and in conceptualization. Initially, regarding the underlying neuronal network, negative connections are not of as high importance as positive. The main structures under study, the modules themselves, should be mainly defined by the strength of the positive connections existing between their nodes. Negative correlations should affect the network’s modular characterization more than simply weak connections but definitely not as importantly as (strong) positive connections. This is also emphasized in (Rubinov & Sporns, 2011), where partitions obtained with high Q^- are found less optimal than high Q^+ partitions, $Q^{+/-}$ referring to the modularity function for positive and negative weights accordingly.

The asymmetric treatment of positive and negative weights in the Q^* function proposed by (Rubinov & Sporns, 2011), leads to desirable behavior in terms of Q^* ’s output. Firstly, an increase in positive connections reduces the effect of negative connections, while an increase in negative connections does not lessen the effect of positive connections on the partition’s computed modularity value. Finally, in a network with an equiprobable distribution of positive and negative weights, negative connections will affect the modularity value only half as much as the positive.

$$Q^* = Q^+ + \frac{v^-}{v^+ + v^-} Q^- = \frac{1}{v^+} \sum_{ij} (w_{ij}^+ - e_{ij}^+) \delta_{M_i M_j} - \frac{1}{v^+ + v^-} (w_{ij}^- - e_{ij}^-) \delta_{M_i M_j}$$

Q^* , Q^+ , Q^- : Modularity values for asymmetric treatment of positive & negative, positive, negative weighted networks accordingly.

$\delta_{M_i M_j}$: 1 when i and j are in the same module or 0 otherwise.

e_{ij}^\pm : The weight of an edge divided by the graphs total weight v^\pm :

$$e_{ij}^\pm = \frac{k_i^\pm k_j^\pm}{v^\pm}$$

Although many implementations make claims of reproducibility, in practice, a significant amount of stochasticity seems to exist in the results, demanding additional steps to ensure stability. A much needed step towards this direction is proposed by Rubinov, co-creator of the Brain Connectivity Toolbox (BCT), which includes the implementation of Louvain's algorithm (Rubinov & Sporns, 2011). This entails continuously calculating new module partitions while the modularity increases, stopping only when the change in modularity is minuscule (e.g., less than 0.00001). Furthermore, in (Shine et al., 2016), a similar iteration procedure is proposed, repeating the module assignments 500 times and retaining the consensus assignment. A combination of both was implemented in the current study, externally iterated 100 times and internally until the modularity no longer increases. Externally, the assignment with maximized modularity is selected as the optimal partition. This simply ensures that the assignments are repeated at least one hundred times and the most modular selected, somewhat balancing the substantial stochasticity observed in consecutive runs.

A potential source of inconsistencies in the results of earlier studies is discussed by (Rubinov & Sporns, 2011), who stress the importance of so called "degenerate" partitions: partitions with similar (high) values of modularity, which may seem to "alternate" in appearance during calculation. An argument is made that in some cases degeneracy may be able to provide insightful results when multiple partitions are studied. This optional analytic step was not possible in the present study as it was not compatible with other parts of analysis.

PARTICIPATION COEFFICIENT

The Participation Coefficient (PC) aims at measuring a node's intermodular connections. In this manner, it reveals whether a particular node acts as a connector hub mediating global integration. This concept can be better understood via the visual aid provided below. The colored, intermodular edges are the main point under study by the PC. Its calculation includes the ratio of degree values towards other modules by that of connections towards all nodes.

$$PC_i = 1 - \sum_{m \in M} \left(\frac{k_i^w(m)}{k_i^w} \right)^2$$

M : the set of modules identified using the Louvain algorithm discussed above

$k_i(m)$: the number of links between the node i and all the nodes of module m .

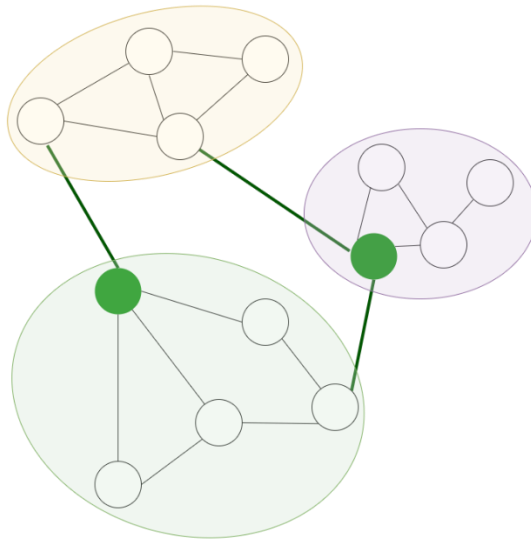


FIGURE 7 – PARTICIPATION COEFFICIENT

WITHIN-MODULE DEGREE Z-SCORE

Within-module degree z-score attempts to describe a nodes intramodular degree of connectedness. It does so by normalizing weighted degree metric by means of the well-known z-score, subtracting the mean and dividing by the standard deviation. In this manner, the measure captures the strength of membership of a given node to its assigned module.

$$z_i = \frac{k_i^w(m_i) - \bar{k}_i^w(m_i)}{\sigma^{k^w(m_i)}}$$

m_i : The module containing node i

$k_i(m_i)$: The within-module degree of i

k bar represents the mean of the within-module degree distribution, while σ the standard deviation

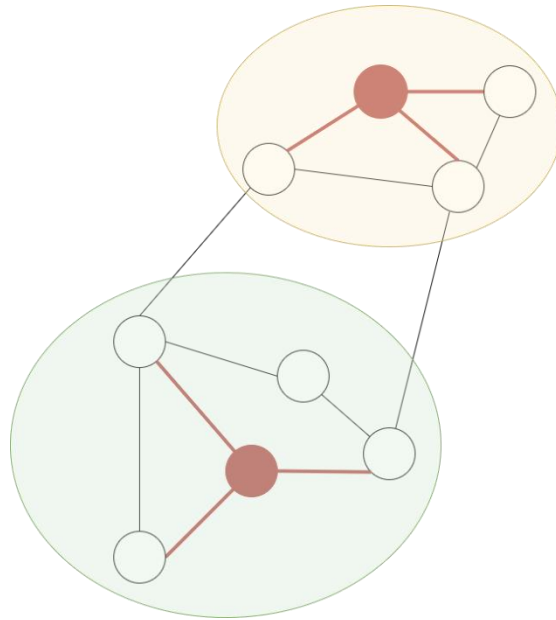


FIGURE 8 - WITHIN-MODULE DEGREE Z-SCORE

2.3.4 GRAPH REDUCTION TECHNIQUES

Typically, a fully connected weighted FCG (i.e., with all possible edges present), will contain anywhere from a few hundred to tens of thousands of connections between regions. For instance, if a study utilizes the very frequently used AAL atlas (Tzourio-Mazoyer et al., 2002), which includes 90 cortical regions, 4005 connections will be calculated (upper triangular of the 90x90 matrix of pairwise ROI-ROI connectivity values). In the case of a more “detailed” atlas, such as the one developed by (Schaefer et al., 2018), containing 100 to 1000 regions, up to 499500 connections will be calculated between regions. A method capable of identifying the “strongest” or “most significant” connections is therefore needed either in order to perform statistical comparisons on a lower number of variables or in order to obtain the region’s edges that tend to exhibit interesting patterns and form significant subnetworks of varying sizes. Many methods have been utilized in order to achieve this graph sparcification or filtering, the simplest being, maintaining only connections above a certain predefined threshold (Hojjati et al., 2017; Khazaei et al., 2017) or in a specific percentile of all connections, e.g., only top 10%. Also, an often-seen procedure is maintaining only nodes that are connected to the same number of other nodes, i.e., have the same degree values (Milo et al., 2002).

SURROGATE TESTING FOR DATA-DRIVEN STATISTICAL FILTERING

Approaches based on statistical filtering of node edges have been proposed as a more data-driven graph reduction technique. In (Nicholas J. Simos et al., 2020) 1000 surrogate timeseries were created for each actual ROI timeseries with their accompanying FCGs, 1000 connections were produced for each real edge. Edges were maintained or excluded after comparing their value to the distribution of surrogate connections. Each edge was deemed significant if it was significantly higher than the surrogate-derived edges. By counting the number of surrogate connections greater than the true connections, one-sided p-values were obtained and corrected for multiple comparisons using FDR. The resulting graph with only significant connections maintained was significantly reduced and lead to interesting results after further analysis steps.

MST AND OMST: DATA-DRIVEN TOPOLOGICAL FILTERING

Topological graph filtering schemes have been implemented, based on the optimal detection of significant subnetworks and maintaining relevant structure rather than focusing on connectivity strength alone. An example of this methodological direction is the application of Minimum Spanning Trees (MST) (Saba et al., 2019), a well-known graph theory technique aimed at maintaining all network nodes with the “optimal” path between them. The ‘tree’ in minimum spanning tree refers to the acyclic form of the paths created, meaning there are no loops in the final network. The absence of loops also leads the tree to include $n-1$ edges exactly, where n the number of nodes. The ‘minimum’ referring to the minimization of total edge weight. MST guarantees uniqueness of the solution in addition to the tree representing the minimum-cost subgraph of the original graph. Kruskal’s or Prim’s/Dijkstra’s algorithms are often used for such computations. In Prim’s implementation, the tree is “grown” one edge at a time, starting from a random node and the cheapest edge is selected at each step in classic greedy algorithm fashion. The main drawback of MST is that in some instances the tree includes weak connections in order to satisfy the main criteria. Additionally, the solutions can often be considered too sparse, including only $n-1$ edges/connections, too few for capturing complex interactions between brain regions (Antonakakis et al., 2016).

An improvement to classic MST, namely OMST, has been proposed and its effectiveness proven (Dimitriadis et al., 2018; Dimitriadis, Antonakakis, et al., 2017; Dimitriadis, Salis, et al., 2017; Luppi, Gellersen, et al., 2021). The ‘O’ in OMST refers to the orthogonality between trees, a differentiating aspect from MST being, the creation of multiple trees that do not share common edges, instead of a single tree connecting all graph nodes. Multiple MSTs are formed, and the trees characterized by the most efficient information transfer are retained. The graph measure of Global efficiency is utilized for quantifying this aspect of each MST, while overall wiring cost is also minimized. Cost refers to the ratio of the total edge weight divided by the total edge weight of the unreduced fully weighted graph. Multiple orthogonal (without overlapping edges) MSTs are combined, and the formed network ranked according to Global Efficiency minus Cost over cost (Dimitriadis, Salis, et al., 2017). This is repeated for a range of sequentially derived OMSTs, while connections are aggregated to the main network and the objective function J computed. The

network that maximizes the GE – Cost over Cost value is considered optimal and used as the final reduced network.

$$J_{GCE}^{OMSTs} = GE - Cost$$

An example of the use of OMST can be seen in *Figure 9*, where the original unreduced network is presented next to the reduced network. OMST was utilized for graph reduction purposes in the present analysis, providing the desired sparsity in individual subject’s FCGs. Statistical filtering through surrogate time series has also been implemented prior to OMST (Dimitriadis, Salis, et al., 2017). However, preliminary analyses on the current rs-fMRI dataset using this method resulted in excessively sparse networks with insufficient connections to assess, and interpret, potential group differences. Finally, it must be noted that as a standalone graph reduction / network extraction technique, OMST significantly prevails over surrogate-based methods in terms of speed, an important point especially in studies where MI is used, as its computation is very time consuming.

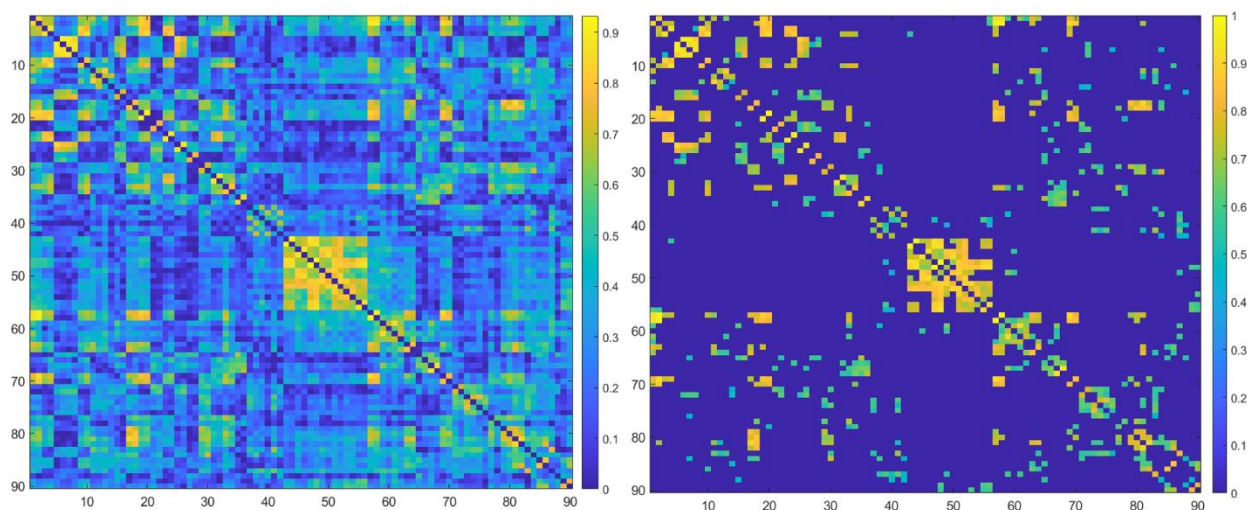


FIGURE 9 – LEFT: PCC-DERIVED FCG, RIGHT: SAME FCG AFTER OMST REDUCTION

2.4 RS-FMRI FUNCTIONAL CONNECTIVITY: DYNAMIC AND STATIC

The main framework for calculating functional connectivity described above, mostly centered on ROI-ROI pairwise functional connectivity using regional BOLD timecourses. Thus, it refers to regional associations that are fixed throughout the entire scan length, meaning that a pair of brain regions must exhibit similar activation behavior for the entirety of the rs-fMRI acquisition (typically 4-15 minutes) in order to produce high connectivity values. Several studies that follow a static functional connectivity approach are discussed below in the related work section, including some of our team's previous attempts. This hypothesis has clearly produced captivating results in a plethora of studies over the past several years, but alternatives definitely exist and require investigation.

2.4.1 DYNAMIC FC

Surely, in such an immensely complex network such as the human brain, temporal dynamics and characteristics must be studied besides topological and functional. The answer in terms of functional connectivity studies is often called dynamic or time-varying functional connectivity, as opposed to static. The importance of rs-fMRI DFC and the need for more and robust studies in the subfield are emphasized by well-established pioneers in the area (Calhoun et al., 2014). The validity of rs-fMRI DFC is extensively discussed in (Preti et al., 2017), with an impressive amount of positive examples provided. DFC also provides bright implications for clinical applications, correlations with several demographic characteristics as well as cognition and consciousness related studies. The latter is the main focus of studies carried out by *The Cognition and Consciousness Imaging Group*, headed by Dr Emmanuel A. Stamatakis, where rs-fMRI DFC related metrics were examined under various states of consciousness and/or under the influence of drugs (Luppi et al., 2019; Luppi, Carhart-Harris, et al., 2021). The association of rs-fMRI DFC-related measures and electrophysiological findings were extensively studied in (Tagliazucchi et al., 2012) producing very interesting findings. Increased EEG gamma band power was beneficial

for longer range connection of brain regions recorded by rs-fMRI. Alpha and beta band power correlated negatively with functional connectivity. More examples of studies following various DFC approach directions are discussed in the related work section, while some basic DFC techniques are analyzed next.

One way to explore dynamic functional connectivity, is to estimate the associations between regions in several successive portions of the scan. The timeseries may be cut into smaller sections or “windows” as they are usually called. In the “sliding-window” approach, as it is referred to, windows often overlap by a certain number of TRs. Functional connectivity is then estimated within each timeframe using reduced portions of the original timeseries, producing one FCG for each window, multiple time-resolved FCGs can be referred to as DFCGs. The selection of window size/length in such approaches is of high importance. Elongating the window size will potentially decrease the effect of noise on the connectivity estimate but will eventually defeat the purpose of DFC by not being able to detect more rapid temporal changes of the neural connectome. A generally accepted range for window length is around 30 – 60 seconds (Bijsterbosch et al., 2017). In the present study, a window length of ~53 seconds (23 TRs), overlapping by a single TR was selected in order to be able to effectively identify temporal dynamics and avoid creating spurious connections due to short noisy timeseries. Because of the arbitrary dissection of the entire timeseries into smaller portions, the danger of splitting the signal at the wrong time regarding the waveform of the BOLD fluctuation is present. This can potentially have effects similar to aliasing and have a negative effect on connectivity estimation. For this purpose, several studies chose to taper each window’s timecourse, thus lessening the effect of edge values. This is achieved by convolving the e.g., 22 TR window with a gaussian kernel of 3 TRs (Allen et al., 2012). A diagram of the sliding-window DFC approach is presented in *Figure 10*.

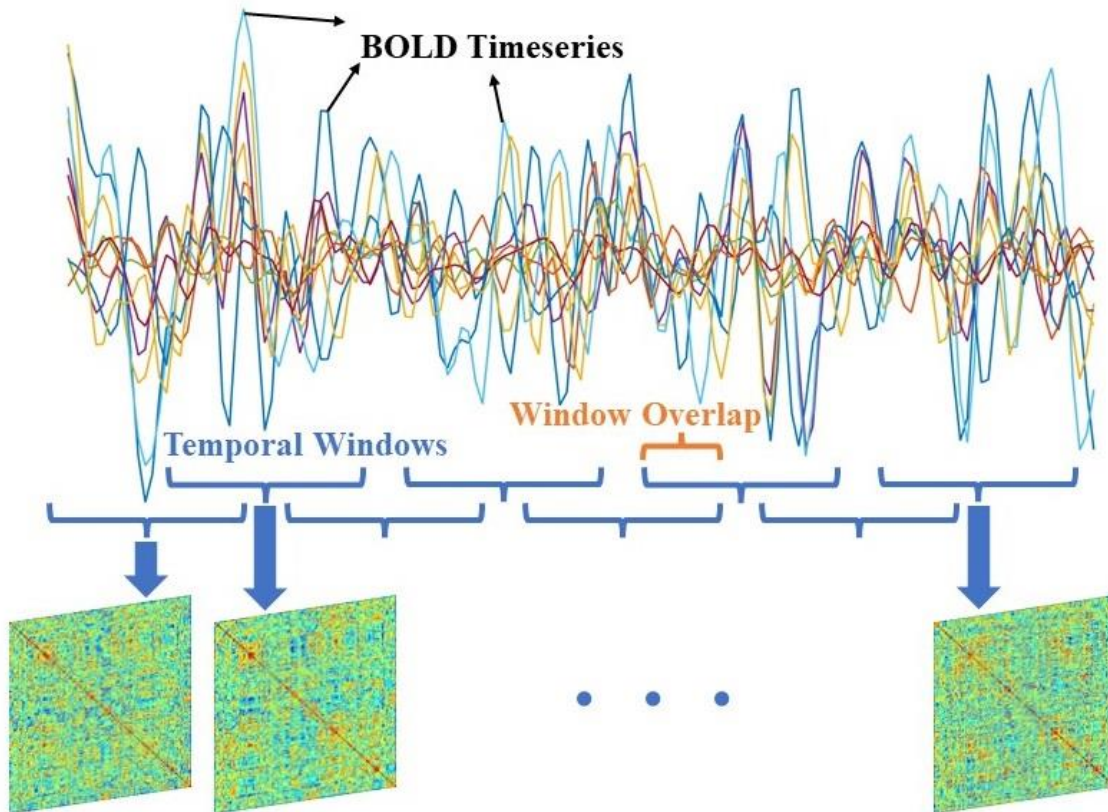


FIGURE 10 - OVERLAPPING SLIDING-WINDOW DFC

The raw amount of connectivity information in DFC methods is much greater than in static FC analyses, requiring different approaches to further analyze this data. Some straightforward solutions are to examine the averaged (through time) DFCGs or the edge variability over time calculated by standard deviation. More sophisticated DFC-based approaches are discussed later.

STATE-BASED DFC ANALYSIS

Rs-fMRI DFC paves the way for the study of more advanced spatio-temporal patterns. The reoccurrence of specific connectomic behaviors throughout the scan is the base of several such analyses. One hypothesis is that DFC alternates between discrete network “states”, the temporal characteristics of this fluctuation as well as the functional and topological properties of these

distinct states being the main points under study. Alternative approaches are based on the assumption that any time-resolved network can be described by the combination of latent states. The first usually entails some form of clustering (unsupervised learning, discussed later on), while the latter is often based on decomposition techniques for the extraction of latent components-states. Part of the analysis described in later parts of this thesis follow the first approach's direction, including measures that characterize each state's network properties as well as the fluctuation patterns of these states. Returning to the study of the states' temporal characteristics, a straightforward measure related to the dynamic connectome's behavior, observed through state transitions, is dwell time or occupancy, quantifying the time each individual spent in a specific state. This measure has shown promising results in several studies (Allen et al., 2012; Damaraju et al., 2014; Rashid et al., 2014) and was thus included in the analyses discussed later.

2.4.2 K-MEANS CLUSTERING IN RS-FMRI DFC

The main purpose of clustering techniques is partitioning the available data into disjoint groups. This is done without any a-priori information on groupings or class memberships. Clustering techniques are of increased interest in the rs-fMRI and especially DFC as they are often used for the identification of two or more characteristic states that are repeated throughout the scan and thus warrant further investigation. *K*-means clustering is a frequently used tool in these types of approaches (Allen et al., 2012; Damaraju et al., 2014; Shine et al., 2016). An initial estimate of possible cluster centroids is set and refined iteratively as datapoints are assigned to the centroids. Centroids are updated as new datapoints are assigned to them. *K*-means attempts to minimize within cluster variances calculated using some form of distance metric, squared Euclidian, one minus cosine similarity or correlation are some examples. Correlation distance was utilized for similar input data as in the present study in (Fukushima, Betzel, He, van den Heuvel, et al., 2018; Shine et al., 2016) and is therefore selected as the preferred distance metric for forming clusters. Many re-initializations of the entire *k*-means clustering algorithm are also suggested by these studies (500 times). This was followed in the current analysis as well, with 2000 random restarts in order to highly reduce the probability of the outputs being driven by unpredictable initial conditions.

2.5 SUPERVISED MACHINE LEARNING

2.5.1 CLASSIFICATION

In supervised learning problems, the set of available samples is split in training and testing data, a simple 80/20 split can be imagined. A model is then “trained” using the training data, containing multiple features/variables, in order to predict the target variable. In the case of classification, the target variable is categorical, denoting class or category association, for binary classification this is a simple 0 or 1 prediction. The term “model” refers to some form of mathematical structure that acting solely on a specific set of input variables can produce accurate predictions, even (especially!) when the specific instance or sample has not been previously seen by the model. Abstractly, a classification model is typically employed when the problem aims at distinguishing between two populations or groups using several input variables to do so.

The simplest example of a supervised Machine Learning (ML) model is linear regression, it is used for predicting a continuous dependent variable with independent variables as input. This entails the (linear) weighted combination of input features:

$$\hat{y}_i = \sum_j \theta_j x_{ij} \quad , \quad i \in [1, [0.8N]], \quad N: \text{number of samples}, \quad j \in [1, M], \quad M: \text{number of features}$$

Where \hat{y}_i denotes the prediction for a sample i , x_{ij} the input feature j for the sample i , θ_j the coefficients according to each feature x_j . In terms of symbology, \hat{g} denotes the prediction of variable g .

The learning process needed in this case entails tuning the coefficients using the training data, attainable through a loss function. This is achieved in the simplest case by minimizing the mean squared error between prediction and actual values of y from the training data. Additionally, linear regression usually includes an additive error term, that encapsulates variance in the data that cannot be explained by the input features. Finally, an important remark is in regard of regularization, closely related to the bias-variance tradeoff in ML. The regularization term should also be optimized similarly to the loss function as it pushes towards the direction of a more generalizable model, meaning its performance will be similar with completely new samples. The opposite

direction entails “overfitting” the data, by learning even the smallest patterns too well. Regularization aims at balancing the tradeoff between few misclassified samples and a more flexible and generalizable model, completed by adding a penalty parameter to the loss function. This penalty increases as the magnitude of coefficients and error term increase. Ridge or Lasso are two examples of regularized regression.

The output \hat{y}_i is continuous by default, in order to produce a categorical value, it can be logistic transformed, the weighted sum of inputs, i.e., \hat{y} can be passed through an activation function called logistic or sigmoid function (‘s’ shaped curve) and then thresholded after the transformation. Before thresholding, the transformed prediction can be thought as the probability of that sample belonging to a specific class, after thresholding, the output is categorical and fit for classification applications. This extended version is called logistic regression. Although simple, it has been applied to many problems as well as the present and is therefore discussed further in later sections.

BOOSTED TREES: XGBOOST

The gradient boosting decision tree algorithm (also referred to as gradient boosting, stochastic gradient boosting, or multiple additive regression trees), is an ensemble Machine Learning technique that utilizes gradient descent in order to minimize overall model loss. Ensemble or averaging ML methods combine multiple “weak” learners, often decision trees and average their predictions in order to produce the final class estimate. Individual decision trees are characterized by high variance in their estimate and do not perform well, by combining multiple complimentary simple estimators a substantially better prediction machine is created. Decision trees get their name from the tree-like structure of the set of rules that defines them. They consist of multiple splits, nodes and leaves (terminal nodes), which produce the output variables. Ensemble techniques are utilized for increased prediction accuracy and control of model overfitting. One such approach is bagging utilized by Random Forests (Breiman, 2001). Boosting entails adding new models (decision trees) to the main model in order to correct current model error. This is performed sequentially until no further improvements are possible. In gradient boosting, the new models added are aimed at predicting the residuals/errors of the existent model. New learners are

formulated in order to be highly correlated with the negative gradient of the loss function of the entire model. More abstractly, these types of models focus on the more problematic parts of the existing model or ensemble and formulate new additions in order to correct them.

XGBoost (Chen & Guestrin, 2016) is a library that implements the gradient boosting decision tree algorithm discussed above. XGBoost has been previously used in an fMRI setting for classification of patient populations (Torlay et al., 2017). It is available in multiple programming languages and environments; the python version was utilized in the current experiments. A significant strongpoint of the XGBoost package regards the inclusion of parallelized execution. Speeds achieved in model training and testing are massively reduced from those observed in other ensemble techniques. In order for this execution speed increase, XGBoost utilizes close to 100% of processor resources in all available cores.

An important point that is fortunately taken care of by the XGBoost implementation regards regularization. Due to the additive approach followed in boosted trees for adding new learners, it is potentially easier to keep adding learners until the data is completely overfitted. Overfitting or bias is a very serious problem in Machine Learning. When a model overfits the data, it has gone too far in describing the patterns present in the specific sample set and has traded off generalization for increased model accuracy. In this situation, the model learns to predict the training data itself instead of the pattern between input and response variables. An additional regularization term has been added to the objective function compared to traditional boosted trees in order to smooth the final weights learned thus avoiding overfitting. The regularized objective function will lead the model to be simpler and more generalizable.

Random Forests are a somewhat similar algorithm to gradient boosted trees, both being ensemble techniques. The main difference lies in the fact that RF estimators/learners are independent whilst in boosting subsequent learners are very much related, as every new addition focuses its “learning” on the loss of its predecessors, who it will next join.

Due to the reasons discussed above gradient boosting machine such as XGBoost are considered highly accurate, generalizable and scalable, while able to deal with missing or sparse data. Additionally, decision tree ensembles in general perform well even when dealing with combination of different types of data, e.g., categorical and continuous.

2.5.2 FEATURE SELECTION

In a large number of studies that utilize ML methods, some modality of feature selection is often also employed. With a large number of input variables or features, ML models tend to perform sub-optimally and even overfit. A general rule of thumb regarding an acceptable number of input features is to always stay below the number of samples (Guyon & Elisseeff, 2003). Feature selection methods vary vastly among studies, the main categories being supervised and unsupervised approaches. Unsupervised feature selection methods typically operate on the entirety of the available samples. An example of such a method is the collinearity test, entailing the elimination of features that tend to contribute highly similar information. Supervised or labeled feature selection operates on subsamples of the data, namely the training data, inside the Cross Validation loop. For example, Recursive Feature Elimination (RFE) in conjunction with a classification model able to produce feature importance values (e.g., SVM, RF or XGBoost) recursively eliminates features with low relative importance until a criterion is met or the desired number of final features is reached. Feature importance-based feature selection methods are quite popular and have been utilized in prior ML schemes by our team (N. J. Simos et al., 2019; Nicholas J. Simos et al., 2020) where RFE or RF importance-based selection techniques were implemented accordingly. Similar to the latter, a feature importance rank approach was utilized in the current work, with more details presented in the methodological section. The importance-based ranking is an integral part of the cross-validation methodology.

The “gain” type feature importance provided by XGBoost describes the average gain across all splits the particular feature is used in. The relative contribution of a feature is quantified by calculating the improvement in accuracy after the addition of this new split to its branch.

2.5.3 CROSS VALIDATION, ERROR ESTIMATION

Cross validation (CV) is an integral part of most ML-based pipelines. CV’s main goal is an effective estimation of a model’s prediction accuracy capabilities. Proper CV setup is a very important task, directly affecting the generalizability and relationship between reported prediction

metrics and real-world performance of a given model. Model overfitting and bias or high variance are two issues that must be appropriately addressed by the error estimation method.

Leave-one-out cross validation (LOOCV) and k-fold cross-validation are the most often used CV methods (Khazaee et al., 2017; Saccà et al., 2019; X. H. Wang et al., 2018). The main difference between them lies in the number of testing samples left out in each iteration. In k-fold, for example in a 5-fold CV, the data is split in 80% training set plus 20% testing set and this is repeated 5 times in order to include all samples in the test and train set once. In LOOCV the train set is the entire sample minus one, while the test sample is a single sample. This is repeated as many times as the number of initial data samples. In each iteration the model is trained on the training subsample, utilizing class labels, and predictions are made using the test samples. The averaged prediction accuracy is typically the metric presented in classification-related studies. In methodologies that employ some type of supervised feature selection, this is performed on the training subset and the selected feature indices are chosen during the testing phase. In studies where interpretability based on selected features is of paramount importance, this approach can be questionable. Because, in order to obtain the final or most significant feature set, the features selected most often in all CV iterations are ranked and presented. This can be somewhat problematic as the selected features vary between iterations, due to the extracted subset of features being subsample-related, and no “final” model has been trained and tested on these features.

NESTED CROSS VALIDATION

Nested Cross Validation has been formulated in order to address several drawbacks of traditional CV. In one type of nested CV, two CV iterations are used, one internal and one external, the role of the internal loop is feature selection (over multiple subsamples) as well as model tuning. In this manner, more stable, “consensus” features can be selected in the internal CV loop, which operates only on the training subset of the external, and the outer (often optimized/tuned) model is trained and evaluated using the reduced feature set. Hyperparameter tuning is often incorporated in nested CV, the best performing classifier-specific parameters are selected using the internal CV loop and then used in the external model.

Regarding feature selection and its incorporation in the nested CV design, two main directions exist, classification-based and consensus or ranking-based. This difference is excellently explained, analyzed, and compared in (Parvande et al., 2020), where a consensus nested CV is proposed. In standard nested CV, the best performing feature set is selected internally based on best classification accuracy and is subsequently used in the external model. In consensus or ranking based nested CV, features that are more frequently selected internally are retained in the final model. This method improves in speed (as classification/prediction is not needed internally) and feature/model stability externally (Parvande et al., 2020). This approach was utilized in previous work of our team in (Nicholas J. Simos et al., 2020) in order to obtain stable and reliably reproducible final features of importance to the particular clinical comparison. These notions are also discussed in (Zhong et al., 2020) where a similar consensus-based nested CV pipeline is proposed utilizing ensemble learners as in the present study.

CLASSIFICATION PERFORMANCE METRICS

Several metrics are often utilized in ML classification studies for the performance evaluation of the proposed Model. Firstly, some basic measures must be introduced: tp : true positive, tn : true negative, fp : false positive, fn : false negative. True or false characterization refers to correct or mistaken classification while positive and negative refer to the predicted label, positive (logical '1') is typically the patient class while negative, (logical '0') is the control group.

The most straightforward, **Accuracy**, is computed as the ratio of correctly classified samples by the total number of samples. It measures the overall accuracy or correctness of predictions.

$$Accuracy = \frac{tp + tn}{tp + tn + fp + fn}$$

Precision or positive predictive value, measure the ability of the model not to label a negative sample as positive. It is calculated as:

$$PPV = \frac{tp}{tp + fp}$$

Sensitivity/Recall or true positive rate quantifies the ability of classifying the positive (e.g., patient) class correctly. High sensitivity indicates a lower possibility of making a false negative prediction, i.e., diagnosing a patient as healthy.

$$TPR = \frac{tp}{tp + fn}$$

Specificity or true negative rate describes the ability of determining the negative (control) cases correctly. Correspondingly to sensitivity, increased specificity indicates lower possibilities of false positives or misclassifying healthy individuals.

$$TNR = \frac{tn}{tn + fp}$$

F1 score is a combination of Sensitivity and precision. It has been formulated as the harmonic average of the individual metrics. It is sometimes used in ML studies as a single metric for classification performance.

$$F1 = 2 \times \frac{PPV \times TPR}{PPV + TPR} = \frac{2tp}{tp + fp + fn}$$

2.5.4 ML MODEL COMBINATION: DECISION FUSION

The ability to combine features obtained with different modalities or approaches has been often desired in ML studies. When features are of the same “type” (e.g., continuous or categorical), this can be achieved by simply concatenating/combining multiple feature groups. This feature-level fusion is a relatively commonplace practice and has also been included in the current thesis (see also (Rashid et al., 2016) for an application of this method in similar context). However, this approach can pose possible issues as the dimensionality can increase drastically leading to overfitting problems or very time-consuming or unstable feature selection performance. Additionally, features from different sources or computation directions may be more optimally treated separately. This may also be for interpretation reasons, where the contribution of different types of features should be assessed separately.

Classifier combination methods (Tulyakov et al., 2008) have been proposed for these cases. Several such approaches use multiple classifiers trained on the same data in order to “enrich” the prediction ability of a model by averaging or taking a consensus prediction from different types of estimators. This is based on the notion that different types of models, e.g., linear, probabilistic or ensemble have different strongpoints, and their combined prediction can produce more robust results. Staying on the direction discussed previously, decision-level fusion can utilize several estimators, one for each different feature type and perform the fusion on the decision of these models (Waske & Benediktsson, 2015). A simple and somewhat lacking approach for this model fusion entails the (weighted) averaging or consensus prediction in order to utilize individual predictions. Alternatively, an additional “generic” model, often call a meta-estimator, is used for the combination of the individual model’s predictions in order to produce the final prediction. In decision fusion setups, the individual models are hypothesized as relative “experts” on the specific feature set they are individually trained on. These specialized classifier opinions are then combined in a more robust, informed decision. Such a methodology is implemented in (Bigdeli et al., 2014), where input features from different sources are fed into individual estimators whose predictions are input to a final predictor. In decision fusion cases such as the latter, the meta-estimator is trained only on the predictions of the upper learners in the form of predicted class membership probabilities or simply predicted class labels. As such, the meta-estimator learns the relative strengths and weaknesses of the upper-level learners and can develop some sort of “trust” for each model. In the testing phase, the meta-estimator predicts each sample’s class using the predictions of the upper-level models using previously untouched samples. This “trust” developed by the meta-estimator can be quantified in the form of weights, such as those of a logistic regression model. Logistic regression has been proposed for the role of meta-estimator role in (Ho et al., 1994) as well as being the proposed meta-estimator by *sklearn*, one of the most well-known ML packages available (Pedregosa et al., 2011).

3. RS-FMRI FC RESEARCH APPLICATIONS

3.1 RS-FMRI STATIC FC APPROACHES

Static FC methods are most prevalent in rs-fMRI studies and have shown promising results in several clinical populations. Small-world organization in patients with Alzheimer's disease was compared to healthy brains (Supekar et al., 2008), while similar patterns were examined in children with Attention Deficit Hyperactivity Disorder (ADHD; (L. Wang et al., 2009)). A similar approach using rs-fMRI SFC and graph measures for the study of ADHD-related network alterations is presented in (Dos Santos Siqueira et al., 2014).

Classification-based approaches are of increased interest as they can be more easily incorporated in diagnostic practices, given that the proposed ML model is accurate and robust. Rs-fMRI SFC-derived graph measures have been used for the classification of patients with Mild Cognitive Impairment (MCI) and Alzheimer's disease from cognitively non-impaired elders (Khazaei et al., 2017). Individuals with alcohol dependence and healthy controls also have been effectively classified using similar rs-fMRI SFC approaches paired with ensemble-type ML models (RF; (Kamarajan et al., 2020; Xi Zhu et al., 2019)). Finally, various ML models, such as RF, SVM and Artificial Neural Networks, have been examined for their classification ability of Multiple Sclerosis (MS) patients from healthy controls (Saccà et al., 2019).

Static FC has the clear advantage of substantially fewer initial computed metrics (i.e., edges or graph metrics). These can both be directly used as features, especially in cases where only specific networks are studied such as the DMN. This is true in some of the studies mentioned above as well as in a previous attempt by our team (N. J. Simos et al., 2019), where within-network connectivity edges of DMN, Sensorimotor and Frontoparietal networks were used as features in an ML model. In a more recent report (Nicholas J. Simos et al., 2020), a more data-driven, atlas-based approach was utilized. Parcellation of the brain into 90 anatomical regions was achieved with the AAL atlas

and connections between ROIs were statistically filtered using surrogate data created from each region's timeseries. Graph metrics computed on reduced graphs were then used for the classification of patients with Neuropsychiatric Systemic Lupus Erythematosus (NPSLE) and Healthy Controls. In dynamic-based approaches several challenges arise, for instance, the volume of data produced by the core analysis is substantially larger and additional feature extraction methods are typically employed before comparisons or classification attempts can be made.

3.2 RS-FMRI DYNAMIC FC APPROACHES

Apart from calculating a straightforward mean of the time-resolved connectivity values, temporal variability of connectivity has been studied extensively, mainly in the context of DFC. The variability or instability of connectedness of brain regions has been utilized as a biomarker of differences between populations. For instance, (Zhang et al., 2016), explored the dynamic reconfiguration properties in rs-fMRI as reflected in the variability of connectivity of a particular region in the form of the average difference of a region's connections across non-overlapping, successive time-windows. This difference was measured as one minus the Pearson correlation of all of a region's connections over successive windows according to the following formula:

$$FCV_k = 1 - \overline{PCC(F_{i,k}, F_{j,k})}, \quad i, j = 1, 2, 3, \dots, w, \quad i \neq j$$

FCV_k represents the connectivity variability of node k

i, j are different time-windows, w is the number of non-overlapping time-windows

$F_{i,k}$ is the vector of length n containing all of region k 's connections for time-window k (i.e., the k^{th} row of the $n \times n$ DFCG, where n is the number of regions)

Findings of (Zhang et al., 2016) include negative correlation of variability with BOLD amplitude, low frequency BOLD signal energy and node degree. Low variability was observed in several

primary sensory regions as well as DMN regions, such as medial frontal gyrus, posterior cingulate, and precuneus. Similar procedures for connectivity variability estimation through DFC were utilized elsewhere (Jie et al., 2018; Rolls et al., 2021). In all three studies, variability was calculated over several window lengths and averaged. Jie et al. (2018) calculated an additional measure to assess the spatial variability of a region's DFC, reporting promising results in discriminating persons with MCI vs cognitively non-impaired controls. Rolls et al. (2021) reported increased variability of DFC in the gyrus rectus, ventromedial prefrontal cortex and posterior cingulate cortex among persons with ADHD, and in early visual cortical and temporal lobe areas among chronic schizophrenia patients.

In (Huang et al., 2021), the temporal changes in module assignments are studied as a measure of a region's community-related stability. Modularity maximization-based module assignments were performed in each overlapping sliding time-window using the Louvain algorithm (see Section 2.2.3). The temporal evolution of module assignments (i.e., region module switching) was then quantified as the ratio of module changes by the maximum possible number of changes. The researchers found increased switching rates among persons with a history of childhood trauma compared to controls. These differences were more prominent in DMN cortical regions (posterior cingulate gyrus and precuneus), frontoparietal occipital and cinguloopercular regions. In another relevant work, temporal variability in inter-RSN connectivity was explored as a biomarker of ADHD using machine learning classification (X. H. Wang et al., 2018).

DFC measures were also used for prediction of increased cognitive loads (Liu et al., 2018). Three measures were evaluated in this study, DFC strength, stability and variability. DFC strength refers to the mean connectivity strength observed throughout the scan, stability is somewhat similar in calculation to the variability measures discussed above, while the variability metric is a modified version of sample standard deviation. DMN, DAN and frontoparietal networks emerged as the strongest predictors of cognitive load. Autism spectrum disorder subjects have also been classified effectively from healthy controls using DFC derived indices in an ML framework (Price et al., 2014). Mean and variance values of sliding-window DFCGs were utilized, achieving classification accuracy of 90%. The central executive network produced the best results among all the individual ICA-derived RSNs (ICA: Independent Component Analysis), while the combination of indices from multiple networks produced the best results overall.

Finally, DFC has been applied to the study of consciousness states. For instance, (Barttfelda et al., 2015) compared anesthetized and awake monkeys on dynamic measures. “Duller”, anatomically-inspired network configurations were observed during sedation, characterized mainly by positive correlations and reduced small-world characteristics. In the awake state, positive and negative correlations were observed with much “richer” network structure, deviating from structural networks. A more optimal communication structure, indexed by a small-world metric, was observed in the awake condition¹. An additional study is discussed later, exploring, among others, the dynamic connectome in conscious, unconscious and subjects with disorders of consciousness, using an approach very similar to the one applied to the present dataset.

TEMPORAL STATE – BASED ANALYSES

The notion of temporal connectivity ‘states’ was introduced above, followed by a brief discussion of how the state identification process operates with the help of k -means clustering. In (Allen et al., 2012; Damaraju et al., 2014), a frequently used approach for state identification is utilized. DFCGs (multiple time-resolved FCGs) are given as input to the k -means algorithm to derive a number of centroids constituting the representative states observed in the total group comprising of healthy or schizophrenic and healthy persons accordingly. A range of k values is tested, while the elbow criterion (i.e., ratio of within over between centroid distances), is used to determine the optimal value of k . Finally, for a fixed number of clusters, e.g., $k=5$, the state FCGs (cluster centroids) are obtained and examined. State representative FCGs are also calculated as the median of all DFCGs belonging to each state. DFCGs are considered to belong to the state with which they showed the highest similarity as indexed by the shortest distance between DFCG and state FCG. Findings include network-based differences between groups, in terms of more prominent presence of well-known RSNs in state FCG as well as temporal-related differences such as dwell time in each state.

¹ For a more recent application of DFC to the study of consciousness states in humans using a method similar to the one employed in the present study see Luppi et al. (2019), described in more detail in the next section on Cartographic Profiles.

In (Allen et al., 2012; Damaraju et al., 2014; Menon & Krishnamurthy, 2019), group ICA was employed instead of atlas-based brain segmentation to derive the set of regions which were subsequently subjected to the DFC analysis. Modular organization was observed within sensory areas and DMN which were negatively correlated with each other (Allen et al., 2012). Language areas exhibited strong relationships with DMN areas, possibly reflecting silent speech during the scan. Moreover, connectivity variability was lowest among DMN areas, and higher among visual areas. Regarding the identified states, the first state accounting for more than 30% of acquisition time, resembled the SFCG quite closely. Differences between states presented as deviations in DMN organization, with e.g., more segregated characteristics in posterior DMN in some states. Hyperconnectivity was observed between thalamus and sensory RSNs in schizophrenia patients (Damaraju et al., 2014). Significantly increased state dwell times were found in patients compared to controls in the sparsely connected state.

An alternative to the well-established state-based approaches mentioned above is proposed in (Saha et al., 2021). Typically, the elbow criterion (explained previously) is used for selecting the number of states present in the data, in this study, a classification-based approach is utilized for this purpose. The cluster model order is optimized using an exhaustive search, with the optimization criterion being classification performance using an SVM classifier on a subset of the data. A different model order is found by this method ($k=4$) compared to the typical method ($k=5$), for the particular dataset.

An interesting comparison is performed by (Fukushima, Betzel, He, de Reus, et al., 2018), between state representative (centroid) FCGs and FCGs derived from periods of low and high modularity. Timeframes of increased or decreased modularity are initially detected by comparing DFCG modularity values to the median values across subjects. The centroid FCG is computed as the edge-wise median of the different modularity “states”/levels. Similar connectivity patterns were observed among the two different modularity level FCGs and the two k -means ($k=2$) classified temporal states. Within the same subject, DFCGs with similarly high modularity displayed increased similarity with each other while the same was not true for lower modularity networks. In terms of known network organization of these modularity “states”, the DMN exhibited higher dissociation with task-positive networks in the high modularity periods while subtler connectivity

structures were observed in the low modularity periods. These definitely warrant further investigation, especially in relation to the analytic approaches discussed next.

CARTOGRAPHIC PROFILING

Several groups have employed a hypothesis-driven approach for state-identification (Fukushima, Betzel, He, van den Heuvel, et al., 2018; Luppi et al., 2019; Luppi, Carhart-Harris, et al., 2021; Shine et al., 2016) which is based on the assumption of the presence of states with relatively well-defined functional-topological characteristics. The notion of predominately integrated or segregated states is introduced into the state identification process and a combination of graph measures is utilized for this characterization. Integrated networks exhibit globally strong connectedness that is controlled by hub nodes. On the other hand, segregated networks are characterized by more clearly formed modules, communities with strong connections between the member-nodes and weak connections between communities.

Nodal graph metrics were employed in order to quantify prevalent network tendencies, with the goal of characterizing each time-resolved FCG as predominately integrated or segregated. One of these measures is within-module degree z-score, i.e., the connection strength of a given ROI to other ROIs of the same module standardized for the connection strength of other nodes of module. Obvious from its calculation, within-module degree z-score, quantifies the overall connectivity strength of a node to its module. An additional measure is then needed in order to judge the level connectedness of a node to those from other modules. The participation coefficient does exactly that, a higher value indicates stronger connections towards nodes of other modules. Together, these two complementary measures are able to characterize these main network topologies. The joint histogram of the two metrics was aptly named “cartographic profile” by (Shine et al., 2016). The reshaped cartographic profile for each time-resolved FCG is used as the feature vector/ input to the k -means clustering algorithm ($k=2$), on a subject level. The output of k -means is then analyzed in order to determine which cluster represents the integrated and which the segregated state. The mean participation coefficient values are used for this goal, higher values indicate more diffuse connectedness, thus indicating the integrated state. At the end of this stage of the analysis, all DFCGs have been classified as belonging to one of the two states, while the temporal fluctuation

of states in the form of a binary time series is also retained for further analysis. Representative FCGs can also be calculated as the edge-wise median of each state's graphs, producing two FCGs for each subject.

(Shine et al., 2016) applied this analysis on resting-state and task-based (N-back task) data from healthy participants. In order to mitigate the chance of spurious connections due to task-related activity, the block-design time series convolved with the HRF was, first, regressed out of the voxel time series. The Multiplication of Temporal Derivatives (MTD) (Shine et al., 2015) was utilized as the connectivity measure instead of the PCC in a sliding-window based approach. The Gordon and Harvard-Oxford atlases were used for brain segmentation, producing 375 ROIs. Global efficiency and modularity measures were evaluated on weighted state FCGs. The state fluctuation timeseries describing the estimated state assignment of each timepoint was also analyzed in conjunction with the task's onset timing. Cartography findings and their association with pupil diameter, behavior as well as to the task timing are presented. In the resting-state data, the integrated state networks exhibited a generalized increase in communication among different modules. Increased values of modularity were observed in predominately segregated DFCGs while global efficiency was elevated in the integrated state networks². Finally, increased participation was observed in DMN regions during the segregated state. This particular study also performed several replication analyses, in order to assure reliability across datasets acquired by different scanners and imaging protocols, as well as across different subjects and sessions.

Finally, (Luppi et al., 2019) used a similar analysis in order to study consciousness-related temporal alterations in propofol-anesthetized healthy participants, persons with neurological conditions causing Disorders Of Consciousness (DOC) and healthy, fully conscious subjects. Apart from the temporal evolution of integrated and segregated states, small-worldness was calculated on the state representative FCGs. In both DOC and propofol groups, DMN and frontoparietal network anticorrelations were observed in the integrated state, while disconnection between the DMN and thalamus was found during the segregated state. Additionally, within-network connections of the DMN were found reduced in both states for these two groups, also the integrated state demonstrated less small-world tendencies. An interesting finding includes the

² This is relatively straightforward and expected given the basic notion of integration and segregation. Integrated networks should have by definition high global efficiency while segregation is expected to have predominately elevated modular characteristics.

comparison of DFC findings with SFC, demonstrating the importance of such approaches, as the specific network-region finding could not be reproduced by static FC measures. This analysis was also utilized in (Fukushima, Betzel, He, van den Heuvel, et al., 2018), where the integrated and segregated DFC states were compared with structural connectivity (calculated through diffusion tractography).

The cartographic profile state-related approach is generally more “fixed” or stringent regarding its detection strategy. Instead of designating the role of identifying temporally recurring network patterns to the *k*-means clustering algorithm, two a-priory defined network patterns are being searched for in the time-resolved DFCGs. In part, this approach takes away a portion of the variability and potential lack of reproducibility between studies due to differences in populations and acquisition systems/parameters that can potentially exist in the former analyzed approach of entirely data-driven state clustering.

Perhaps the most serious limitation of this approach is that the predominately integrated and segregated states are not necessarily clearly defined in each subject or population, although the *k*-means algorithm is forced to produce state-specific graphs. This is in part mitigated by repeating the re-initialization of *k*-means’ centroids hundreds or thousands of times and obtaining a consensus decision of state assignments.

3.3 COMBINATION OF STATIC AND DYNAMIC INDICES

Static and dynamic functional connectivity metrics have been compared in several studies in order to determine whether the information provided by each approach is different or the two are somewhat complementary. In (Menon & Krishnamurthy, 2019) DFC derived indices are found more capable (compared to PCC SFC) of differentiating individual subjects and performing classification based on biological sex. In (Ramos-Nuñez et al., 2017) the two “modalities” are found overall more complementary, each correlating with different aspects of behavioral and cognitive measures.

Very few research teams have grouped metrics obtained from the two methods and attempted to differentiate groups on combined feature sets. For instance, (Rashid et al., 2016) calculated a static FCG alongside a state-based DFC similar to those described previously by applying *k*-means clustering directly on the DFCGs. Classification performance was evaluated using the dynamic and static features individually as well as their combination. For the DFC model, the beta-coefficients from the temporal regression of DFCGs were used as features, indicating the presence of each detected state at each time point. In the case of SFC, the double input symmetric relevance (DISR) method was utilized in order to select the top 100 connections. Overall, the combination of static and dynamic indices outperformed the individual models in distinguishing schizophrenia and bipolar disorder patients from healthy controls using an SVM classifier.

3.4 RS-FMRI FUNCTIONAL CONNECTIVITY IN MTBI

As a very common neuropsychiatric disorder lacking detectable signs on conventional neuroimaging modalities, mTBI has attracted increased attention from fMRI groups in the past years (Iraji et al., 2014; Johnson et al., 2012; Mayer et al., 2011; Tang et al., 2011; Zhou et al., 2012). As discussed in Section 2.1 Mild Traumatic Brain Injury, mTBI cases represent approximately 90% of brain trauma cases and can have several quality-of-life affecting symptoms. However, accurate diagnosis can often pose a substantial challenge, warranting the investigation of alternative modalities for this task. Dynamic functional connectivity methods, studying the temporal variability of the connectome in mTBI patients have also been implemented (Hou et al., 2018) as well as in combination with ML in order to effectively distinguish mTBI cases from healthy controls using DFC-derived features (Vergara et al., 2018). Most studies focus on the acute or sub-acute phase of mTBI, with rs-fMRI scans completed within a few days post-injury. As discussed in the mTBI section of the introduction, many symptoms attributed to mTBI such as headaches, dizziness, vertigo, depression, fatigue, impulsiveness, irritability and even cognitive and memory deficits can remain for many months after the trauma has occurred. In order to better understand the underlying mechanisms responsible for these symptoms, there is a need for more chronic mTBI studies such as the present. In this context, it is also important to examine the course

of connectivity patterns over the first few months post-injury, to determine which changes are characteristic to the acute phase and which ones persist chronically (Palacios et al., 2016).

STATIC FC IN CHRONIC MTBI

Researchers in (Madhavan et al., 2019) applied seed-based static FC as well as fractional Amplitude of Low Frequency Fluctuations (fALFF) analysis in a longitudinal study including scans from 3 days up to 3 months after the injury. As a reminder, seed-based FC calculates connectivity between all voxels and a specific “seed” region. A single whole brain mask is produced for each selected seed region. These relatively simple analyses revealed correlations between connectivity in the salience, motor and visual networks and symptom severity.

A similar seed-based static FC approach is followed in (Champagne et al., 2020) where within and between network disturbances are studied in chronic mTBI patients. The DMN, DAN and Frontoparietal network connections were found significantly different between mTBI patients and healthy controls. More specifically, several regions of the DMN are observed to have higher connectivity strengths in mTBI subjects as well as some regions of the DAN, Visual and Ventral attention network. Several regions of the Somatomotor, DAN and frontoparietal exhibit decreased connection strengths in mTBI patients.

Decreased DMN connectivity in the left inferior temporal gyrus, right precentral gyrus, left caudate and right inferior parietal lobule was found (Nathan et al., 2014), while increased activity was found in other parts of the DMN, namely, left and right posterior cingulate (PCC), temporal regions in addition to left cerebellum lobule VII and right SMA (non-DMN). This study also examined correlations of connectivity in these regions with neuropsychological test scores. Several regions of the DMN were found correlated with reaction times on sustained attention, speed of processing, verbal generativity, emotional manifestations of mood change, irritability and anxiety. Most notably, increased connectivity in the left and right temporal regions was found correlated with measures of depression, aggressive behavior and stress.

An additional study with chronic mTBI patients is presented in (Sours et al., 2015). A seed-based static FC analysis was followed, seed regions including the posterior cingulate cortex (PCC) of

the DMN and the dorsolateral prefrontal cortex of the DAN. Increased connectivity between DMN and DAN networks was found in chronic mTBI patients while reduced within network connectivity was observed in the DMN. Within and between network connection strengths of the DMN and DAN were also calculated. Similar patterns were observed, with increased DMN-DAN connections and reduced average connectivity between DMN regions in the chronic stage.

Moreover, (Vergara et al., 2016) were able to effectively distinguish semi-acute mTBI patients from healthy controls using an SVM classifier (84% AUC). An SFC analysis was followed here as well, between network (ICA derived) connectivity strengths were utilized as features. Elevated connectivity was observed between the DMN's Left Angular Gyrus and the posterior precuneus (PCC) as well as the cerebellum and sensorimotor networks. A slightly different analysis on the same dataset using seed-based SFC is presented in (Mayer et al., 2011). Decreased connectivity in mTBI patients was discovered in the supramarginal gyrus, superior frontal gyrus (DMN), rostral anterior cingulate cortex, posterior cingulate cortex (PCC) as well as between the lateral prefrontal cortex and left medial and superior frontal gyrus. Increased connectivity was found in mTBI patients compared to controls between the anterior cingulate cortex and bilateral prefrontal cortex as well as between the lateral prefrontal cortex and bilateral medial superior parietal lobule, right frontotemporal cortex and striatum. Finally, increased connectivity in mTBI patients was observed between the inferior parietal lobule and the posterior parietal cortex.

DYNAMIC FC IN MTBI

In contrast with the previous section which discusses findings in chronic mTBI cases such as those studied in the current thesis, for an overview of approaches including DFC approaches in mTBI, acute and sub/semi acute studies must be included as there seem to be no works on chronic mTBI rs-fMRI DFC. Most of the literature on temporal connectivity dynamics in mTBI is based on one dataset (Mayer et al., 2011, 2014; Vergara et al., 2016, 2018) with a mean time of 14 days between injury and functional scans. Both works discussed below initially implement group ICA analysis in order to derive the parcellation used for FC estimation.

In (Vergara et al., 2018) a sliding window state-based DFC analysis is used, utilizing *k*-means clustering. Four states are detected in the dataset studied and a representative FCG is calculated for each subject and each state. The state of highest classification ability is evaluated by AUC scores calculated in each LOOCV iteration. In addition, two-sample t-tests are used in order to detect the specific connections of a state's representative FCG that are significantly different in the two groups (repeated for each CV train set). These rigorously selected features are tested on the single left out testing sample in each iteration. Classification accuracies of up to 87% were attained when using all estimated states and up to 92% using a singular state. The most significant connections derived from this process were between cerebellum and sensorimotor regions and were higher in mTBI patients compared to controls.

A very similar DFC approach is followed in (Mayer et al., 2014) with the addition of a more traditional SFC analysis. However, the results report no significant differences detected with the inclusion of FDR correction. Decreased (in mTBI) static connectivity was found between the posterior cingulate cortex (PCC) and anterior cingulate and middle frontal gyrus (DMN). Visual, auditory, sensorimotor and putamen network connections were found elevated in mTBI patients compared to controls. Connections between the bilateral pre-central gyrus and right inferior parietal lobule as well as between the right anterior insula and right inferior frontal gyrus were also higher in mTBI subjects. Aberrant variability was detected in DMN and visual network connections.

GOAL OF THE PRESENT STUDY

In order to address the gaps present in mTBI research, the present study utilized rs-fMRI data obtained in the chronic phase post-injury from a relatively large sample of patients with mTBI. Several network measures were selected in order to capture regional and global functional and topological characteristics of individual subject networks instead of relying on connectivity strengths (graph edges). Choice of connectivity measures was based on several previous reports (outlined in Section 2.2.3) to capture both general and localized network characteristics while keeping the number of metrics derived from each network relatively low.

A robust Machine Learning setup utilizing a relatively conservative validation strategy was selected for model error estimation that should be indicative of real-world testing results. The final features, selected by the ML process and statistically thresholded (and corrected) for the maximization of mTBI and control group differences are of paramount importance to the current study, more so than solely the classification accuracies. These steps are described in much more detail in the following section (4).

4. METHODOLOGY

4.1 DATA

4.1.1 SUBJECTS

The dataset studied in the present thesis comprises rs-fMRI scans obtained in the chronic phase from patients with mTBI (N=36), compared to healthy controls (N=39). All patients had suffered mild head trauma without detectable focal, structural lesions on CT or MRI at the time of the injury as well as the time of the rs-fMRI study. All mTBI patients were hospitalized at least one day in the Neurology clinic of the University Hospital of Heraklion, Crete, Greece, with admission Glasgow Comma Scale scores of 14-15 points. The resting-state functional acquisitions were performed at least six months post-injury. The two groups were closely matched on age (mTBI mean: 43, SD= 17.4 years, controls mean: 41.1, SD= 15.6 years), although the former group included a higher percentage of men (75%, vs. 34%). The study was approved by the University Hospital Ethics Review Board, details of the procedure was explained to all participants, volunteers and patients, while informed consent forms were signed before undergoing MRI.

4.1.2 MRI ACQUISITION DETAILS

All participants underwent brain MRI scans in the MRI Unit, University Hospital of Heraklion using identical scanning parameters. MRI scans were acquired on a clinical, upgraded 1.5T whole-body superconducting imaging system (Vision/Sonata, Siemens/Erlangen), equipped with high performance gradients (Gradient strength: 40 mT/m, Slew rate: 200 mT/m/ms) and a two-element circularly polarized head array coil (minimum voxel dimensions: $70 \mu\text{m} \times 70 \mu\text{m} \times 300 \mu\text{m}$). The main imaging protocol consisted of a 3D T1-w MPRAGE (TR/TE: 1570/1.73 ms, 1 mm/1 NEX/160 axial sections), a T2wTSE (TR/TE: 5000/98 ms, 4 mm axial sections) and a Turbo FLAIR (TR/TE/TI: 9000/120/2320 ms, 4 mm axial sections) sequence. Axial sections were

acquired parallel to the plane passing through the anterior and posterior commissures (AC–PC line). Conventional MR images were interpreted by a senior neuroradiologist (Dr Efrosini Papadaki, MD, PhD) with 20 years of experience. Rs-fMRI sequences were derived from a T2*-weighted, fat-saturated 2D-FID-EPI sequence with repetition time (TR) 2320 ms, echo time (TE) 50 ms, field of view (FOV) $192 \times 192 \times 108$ (x, y, z).

Whole brain 3D images consisted of 36 transverse slices with 3.0-mm slice thickness and no interslice gap. Voxel BOLD time series consisted of 150 dynamic volumes, while the voxel size was $3 \times 3 \times 3$ mm (3mm isotropic). Each subject's fMRI data is 4-dimensional (x, y, z, time), the 4th dimension is of length 150, as this was the number of acquired volumes. Acquisition duration lasted ~6 minutes ($150 \times 2320\text{ms} = 348\text{s} = 5.8\text{min}$)

4.1.3 DATA PREPROCESSING

The main preprocessing directions analyzed in 2.2.5 *Sources of Noise and Artifacts: Preprocessing Basics* were followed. These were in line with several rs-fMRI DFC studies such as (Luppi, Carhart-Harris, et al., 2021) including previous work of our team using data from the same MRI system (Antypa et al., 2021; Kavroulakis et al., 2021; N. J. Simos et al., 2019; Nicholas J. Simos et al., 2020).

Firstly, the first three volumes were discarded in order to allow for magnetization effects to stabilize. Slice-timing correction, re-alignment/recentering and co-registration/normalization to standard MNI space were subsequently performed (middle image in *Figure 11*). Lastly, spatial smoothing with a 6mm FWHM (Full Width at Half Maximum) gaussian kernel was applied in order to improve SNR (right image *Figure 11*). These basic preprocessing steps were carried out in SPM12.

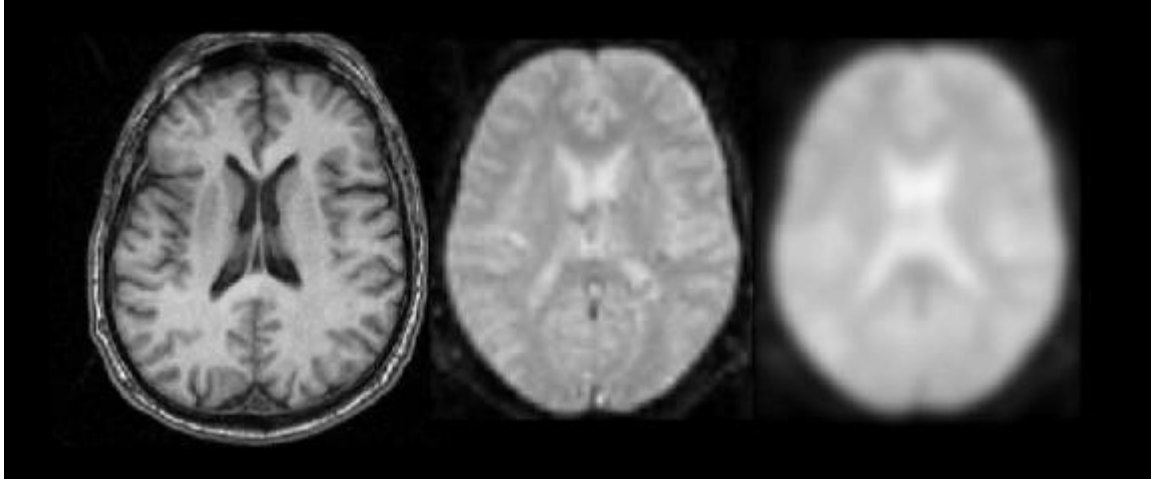


FIGURE 11 - LEFT TO RIGHT: STRUCTURAL MRI IMAGE (T1), fMRI IMAGE, SMOOTHED fMRI IMAGE

DENOISING

Next, for further noise reduction and mitigation of non-relevant signals on voxel timeseries, nuisance regression was applied as discussed in Section 2.1.5. White matter and cerebrospinal fluid (CSF) signals were regressed out of voxel time series in order to reduce their influence. The first five principal components of white matter and CSF signals were regressed out as well as their first order derivatives. These steps were carried out using CompCor (Behzadi Y et al., 2007) included in the CONN (Whitfield-Gabrieli & Nieto-Castanon, 2012) preprocessing modules controlled through MATLAB scripts.

Following denoising, voxel timeseries were detrended and bandpass filtered to 0.008-0.09 Hz in order to eliminate low frequency drift and high frequency noise. As discussed in the initial sections on rs-fMRI BOLD signal properties, this is a relatively “standard” frequency range, often used in functional connectivity studies. The effects of these preprocessing steps can be seen visually in *Figure 3*.

REGIONAL TIMESERIES – SEGMENTATION

Brain parcellation followed, which entailed the use of an atlas for region segmentation (see *Figure 12*). A relatively finer-detail functional atlas was selected containing 200 cortical (Schaefer et al., 2018) and 32 subcortical (Tian et al., 2020) regions. This resolution and combination of functional atlases was selected based on (Andrea I. Luppi and Emmanuel A. Stamatakis, 2020; Luppi, Gellersen, et al., 2021). Brain masks indicating the position of the 232 regions were overlaid on preprocessed subject data. BOLD timeseries of voxels included within a particular region were averaged in order to obtain regional timecourses. These ROI representative timeseries (232 per subject) were input to functional connectivity analysis pipeline described in the next section.

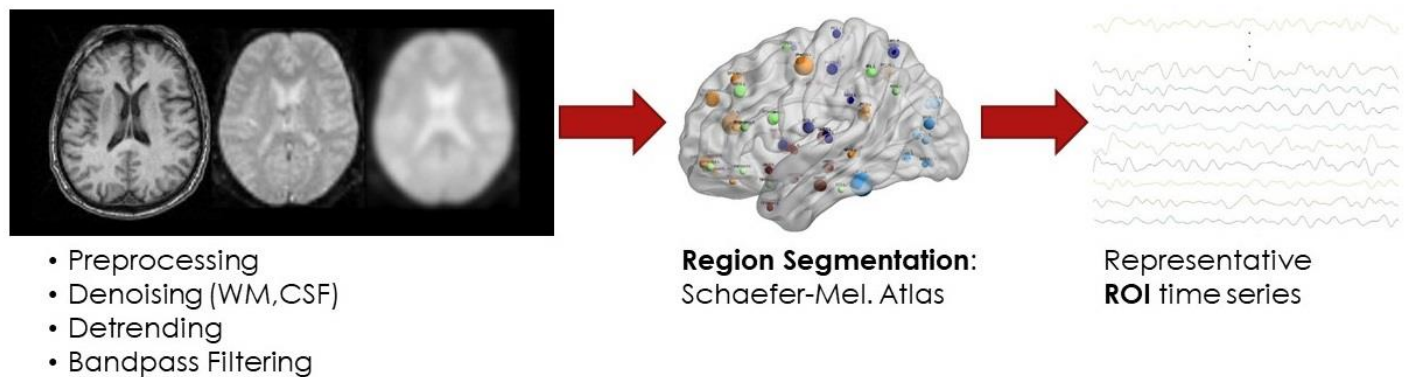


FIGURE 12 – RAW DATA TO ROI TIMESERIES

4.2 FUNCTIONAL CONNECTIVITY MEASURES

4.2.1 STATIC FUNCTIONAL CONNECTIVITY

Initially, the derivation of SFC indices is described. The input data for this analysis are the ROI timeseries as they were extracted by the region segmentation process. Pairwise ROI-ROI connectivity is thence estimated between all pairs of regions using PCC or MI, separately. Leading to the creation of two SFCGs per subject, one for each connectivity estimation method, each of size 232x232. MI-derived FCGs are strictly positive due to the nature of the metric, for the more traditional PCC, only positive connections are retained while negative edges are set two zero, similarly to (Huang et al., 2021; Long et al., 2019; Pedersen et al., 2018; Yang et al., 2020). The interpretation of negative connections is not straightforward neurobiologically and was not in the scope of the current study. Fully-weighted, fully-connected subject SFCGs were then individually reduced by OMST in order to retain only connections that enhance optimal information flow, similarly to (Dimitriadis, Salis, et al., 2017). As mentioned, graph reduction is performed on each subject's network independently, leading the final networks to vary among subjects. Details concerning the formulation and implementation of OMST are discussed in the background section. In *Figure 13* an example of the original and reduced network is displayed for the same subject's PCC-derived FCG.

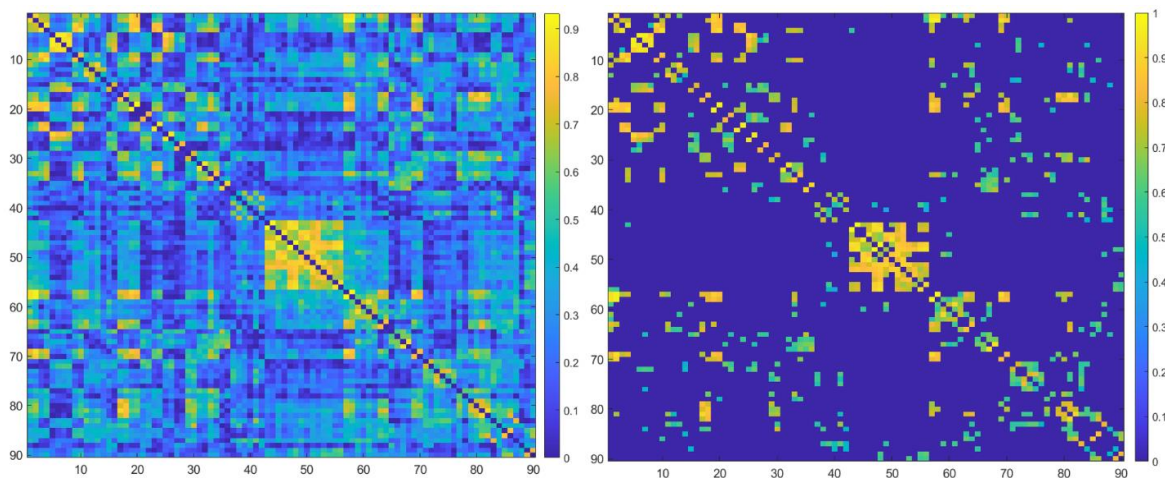


FIGURE 13 – EXAMPLE OF NETWORK REDUCTION USING OMST

Next, functional and topological properties that could characterize each group, were quantified explicitly. Global and nodal graph metrics are utilized for this task, as they enable the comparison of networks of varying density and topology. Global efficiency, Small-World propensity (both global measures), node degree, local efficiency, betweenness centrality and eigenvector centrality (four nodal measures) were computed. The various network properties measured by these metrics have been described in the *Graph Metrics* sections. Finally, the various graph metrics are combined/concatenated in order to form a feature vector describing each subject's connectomic characteristics (see *Figure 14*). This feature vector is used as input to a Machine Learning classification model in order to attempt to distinguish the two groups. The final feature vector combining 2 global and 4 nodal measures, contains a total of $2 + 4 \times 232 = 930$ features per subject. Two adjacent feature vectors are produced for the two different connectivity estimation methods, PCC and MI.

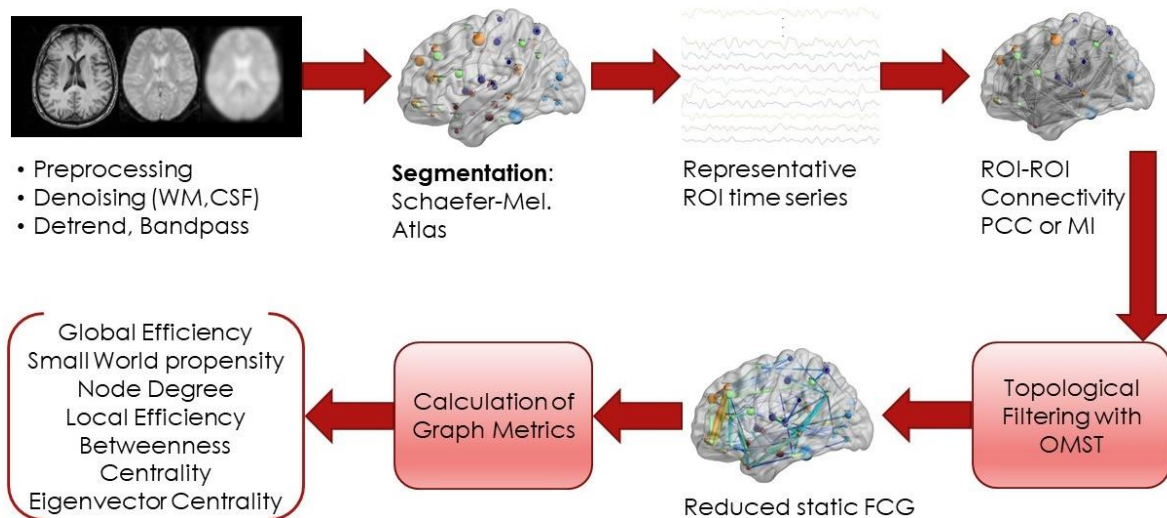


FIGURE 14 – SFC ESTIMATION PROCESS

4.2.2 DYNAMIC FUNCTIONAL CONNECTIVITY STATES

Similarly to the SFC calculation, 232 ROI timeseries are the input describing the average BOLD activity within each region. A tapered maximum overlapping sliding window approach was utilized for DFC calculation, according to (Allen et al., 2012) as described in Section 1.4.1. A window length of 23 TRs (53s) was used in line with the proposed range of 30-60s (Bijsterbosch et al., 2017) overlapping on a single TR. Tapered windows were used, achieved by convolving them with a Gaussian of $\sigma=3TRs$. In this manner, 125 windows were created, of 23TR length each. Pairwise ROI-ROI connectivity was estimated within each temporal window using the PCC or MI separately, resulting in two DFCGs (of size 232x232) computed for each temporal section, with 125 DFCGs for each connectivity estimation method. The next step involves classifying these time-resolved networks as predominately integrated or segregated based on the most prominent functional network tendencies observed. In *Figure 15* an abstract view of this process is given. The time-resolved DFCGs were given as input on the left side and a label was assigned to each window's network. In the final step, a representative network for each state as well as the temporal fluctuation of these states were computed (two graphs and one time course). The computations involved in the "Brain State Identification" step (referred to as "*cartographic profiling*" by (Shine et al., 2016) are described below and visualized in *Figure 16*.

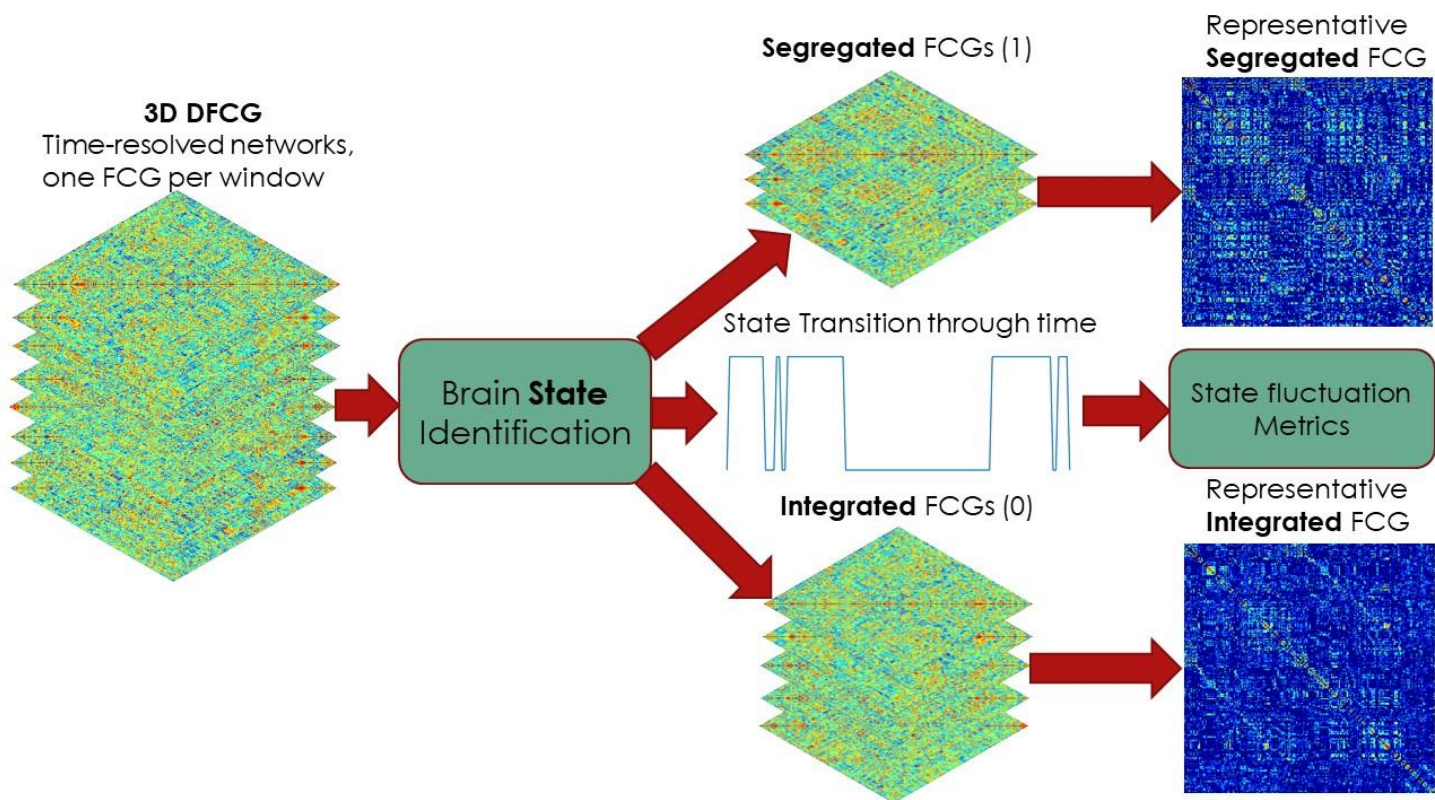


FIGURE 15 - ABSTRACT VIEW OF DFC PIPELINE

CARTOGRAPHIC PROFILES

As mentioned in the previous section, the cartographic profile approach was utilized in order to derive the predominant states present in the data and their temporal fluctuation information. An initial point that warrants clarification is that the state characterization relates to each time-resolved network/DFCG, i.e., the network computed for each temporal window. The first step in the brain state identification process is the application of the Louvain algorithm described in Section 1.3.3. Based on modularity maximization, this optimization algorithm returns the assignments of all nodes to a particular functional module, a group of nodes that are strongly connected to each other and less so (or anticorrelated) towards nodes of other modules. The asymmetric modularity function is utilized, assigning more weight to positive, as compared to negative, connections while

computing modularity (Rubinov & Sporns, 2011). In order to ensure stable and repeatable module assignments, new module partitions are computed while the modularity increases, stopping only when the change in modularity is minuscule (e.g., less than 0.00001). A similar procedure was proposed by (Shine et al., 2016) repeating the module assignments 500 times and retaining the consensus assignment. A combination of both procedures was employed in the current study, by using 100 iterations, externally and internally, until the modularity metric no longer increases. Externally, the assignment with maximized modularity is selected as the optimal partition. This approach was found to balance the substantial stochasticity observed over several consecutive runs.

Subsequently, modularity assignments were used to calculate two nodal network measures, participation coefficient and within-module degree z-score. The aim of combining the two metrics is to quantify the inter- and intra- modular connectivity of each member of the network. Briefly, nodal participation coefficient measures the connectedness of a particular node with nodes of other modules, revealing predominately integrative characteristics. Within-module degree z-score quantifies the strength a node's relationships with nodes of its own module relative to the overall connection strength between nodes of that module (for more details see Subsection entitled *Within-Module Degree Z-Score in 1.3.3*). The combination of these metrics was achieved in the form of a joint histogram or "cartographic profile" (Shine et al., 2016). The joint histograms of the two discriminative network measures (for each time-resolved network) were subsequently vectorized and used as feature input to the k -means algorithm which was then employed to classify each DFCG, into one of $k=2$ groups. Correlation distance was used as the k -means distance metric for forming clusters according to previous work (Fukushima, Betzel, He, van den Heuvel, et al., 2018; Luppi et al., 2019; Luppi, Carhart-Harris, et al., 2021; Shine et al., 2016). Multiple re-initializations of the k -means clustering algorithm (centroid reinitialization) is recommended by these studies (500 times) and implemented in the current analysis (through 2000 random restarts) in order to reduce the probability of the outputs being driven by unpredictable initial conditions. The cluster with the highest mean participation coefficient is considered as representing the integrated state, while the remaining time-resolved networks as representing the segregated state. The temporal fluctuation of the classified states is then saved in the form of a binary timeseries. This process is visually depicted in *Figure 16*.

Time-resolved networks: one **FCG** per window
Stacked: 3D DFCG

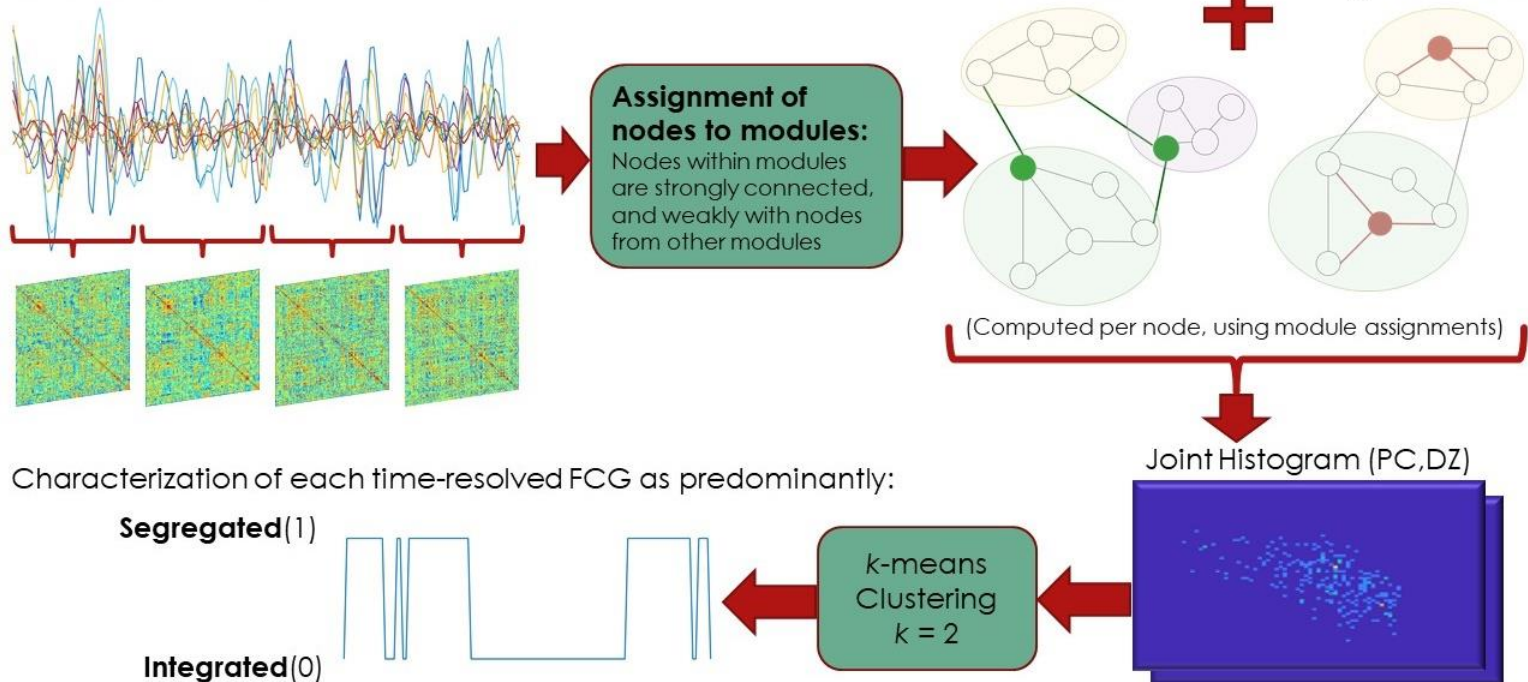


FIGURE 16 - BRAIN STATE IDENTIFICATION PROCESS

The next step after state temporal identification entails the calculation of centroid-representative networks for the integrated and segregated states, computed as the edge-wise median of each state's DFCGs for each subject. Only positive FCG values were retained from this step onward as the interpretation of negative connections are not in the scope of the current study, as discussed in the previous part regarding the SFC analysis. In the case of MI, computed values are by definition nonnegative, whereas for PCC-derived networks, negative connections were set to zero. Representative state FCGs were then reduced in order to reveal the “true” network structure using OMST (discussed in Section 1.3.4 and described in detail in (Dimitriadis, Antonakakis, et al., 2017)). This data-driven network reduction approach was selected as an alternative and potential improvement of the frequently used percentage thresholding method (e.g., (Luppi et al., 2019)).

The two reduced state networks are subsequently utilized for the calculation of several global and nodal network measures listed in Table 1. Sample entropy (Luppi et al., 2019) was computed on state fluctuation timeseries in order to quantify the randomness or predictability of the temporal state evolution. Additional “chronnectomic” features were computed on the state transition time course as in (Antonakakis et al., 2020): complexity index, percentage of time spent in each state (dwell time) as well as the ratio of state changes by the total number of possible changes (flexibility index). In addition, Modularity, Global Efficiency, Small-World Propensity (global measures) and Degree, Local Efficiency, Betweenness Centrality and Eigenvector Centrality (nodal measures) were computed on the centroid segregated-integrated FCGs and all metrics were combined into a single feature vector per subject. The total number of DFC features for each connectivity graph (correlation and MI) were 1866 as follows:

$$[4 \times 232 (\text{nodal} \times \text{nodes}) + 3 (\text{global}) + 1 (\text{dwell time})] \times 2 (\text{states}) \\ + 2 (\text{complexity, flex. index}) = 1866 \text{ features (PCC or MI)}$$

Approach	# Features
DFC Integrated/Segregated states, OMST, PCC	1866
DFC Integrated/Segregated states, MI	1866
SFC, OMST, PCC	930
SFC, OMST, MI	930
	Total: 5592 (per subject)

TABLE 1 - SUMMARY OF ALL CONNECTIVITY MEASURES COMPUTED

4.3 MACHINE LEARNING MODEL ARCHITECTURE

4.3.1 INDIVIDUAL MODEL CLASSIFICATION

For classification purposes, XGBoost (Chen & Guestrin, 2016), an implementation of regularized gradient boosted trees, was utilized as the base estimator. For comparison, results were also obtained using a Random Forest classifier (Breiman, 2001). Classification performance was found

very similar and more importantly the final selected features were virtually identical between the two models. However, XGBoost offered considerable benefits in terms of model training speed. This is due to the parallelized hardware implementation included in the former. In order to produce a more generalizable base model, less prone to overfitting, the default number of trees/estimators ($n=100$) was used, along with a maximum tree depth of 6. The recommended feature importance metric of “gain” was selected as a relatively simple and robust measure, similar to the impurity-based (using the gini metric) feature importance produced by Random Forest models. Feature importance in XGBoost models is based on the overall improvement in accuracy brought by a particular feature. It is measured as the average gain across all tree splits the feature is involved in.

As discussed in Section 1.5.3, a consensus or feature importance based ranking nested CV methodology was implemented similar to (Parvande et al., 2020; Zhong et al., 2020) and our previous work (N. J. Simos et al., 2019; Nicholas J. Simos et al., 2020). This choice was made in order to avoid overfitting and ensure a robust final model with conservative results and highly representative features to the comparison of interest. As depicted in *Figure 17*, initially an outer 80% (training) - 20% (testing) split was implemented. The outer training set was utilized for feature selection using internal CV and, subsequently, the outer model was trained on the reduced feature set. Models were trained and feature importance values were obtained, features are ranked and selected based on these values. The features selected most frequently across multiple internal CV iterations (based on feature importance ranking) were identified as significant for the external classification model.

Model testing and evaluation, using the reduced feature set, was performed on the untouched 20% portion of the data in each external iteration (>400). Classification performance metrics, namely, accuracy, precision, sensitivity, specificity, F1 score, ROC AUC, were averaged across these iterations. Final reported features were those selected most frequently across all internal (and thus all external) iterations. It is also important to mention that all CV splits were stratified by group membership (i.e., they retained an equal number of samples from each class). Additionally, for clarification purposes, each 80/20 split (internal or external) repeated multiple times (40 or 400 respectively in this case) is equivalent to a k-fold CV with $k=5$, repeated multiple times.

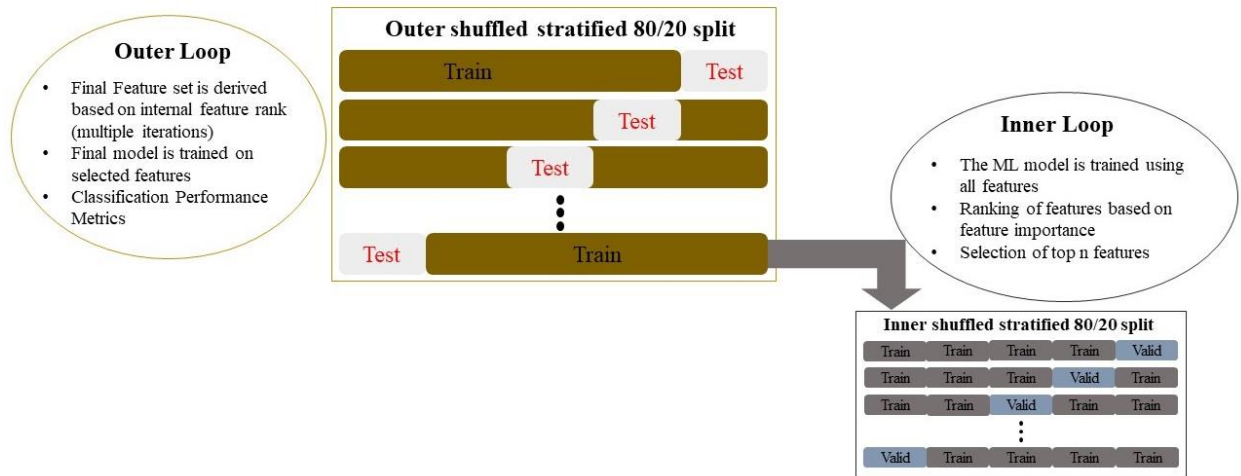


FIGURE 17 - NESTED CV DIAGRAM

4.3.2 MODEL COMBINATION – DECISION FUSION

A combination of Static and dynamic, as well as of linear and non-linear, connectivity measures was desirable in order to enhance classification robustness and compare differently obtained features utilized in the same classification grid. The most straightforward approach is to combine all the individual model features in a single feature vector. Additionally, we employed a slightly different approach, involving simple concatenation as proposed by (Rashid et al., 2016), referred to as **Fusion Model 1** or **FM1**.

The total of number of combined features was 5592 (*Table 1*). The ability of ensemble methods to handle high input dimensionality combined with the regularized boosting methodology of XGBoost and rigorous nested CV selection approach, helped to avoid overfitting and produce a well-performing model. Nevertheless, such vast number of input features could potentially lead to reduced reliability in terms of the final set of selected features. To address the issue of input dimensionality of individual models, while treating different feature types separately, we employed Decision Fusion, whereby the decisions of multiple estimators (1-4 as shown in *Figure 18*), are based, and optimized, on a single type of feature (i.e., Static or Dynamic, PCC or MI

metric). The decisions of these individual “experts” are combined by a more generic final model or Meta-Estimator, through logistic regression, as proposed by (Ho et al., 1994) and is also the proposed meta-estimator by sklearn, one of the most used ML packages (Pedregosa et al., 2011). The Meta-estimator is trained using the (training) predictions of upper models, while the testing of predictions is performed with upper model’s predictions. The outputs of Estimators 1-4 are in the form of class probability values, i.e., the estimated probability of a sample belonging to class 1. Class probabilities are produced by the model (XGBoost) and offer richer information than binary class labels. The Meta-Estimator can learn to utilize each lower model’s strengths and weaknesses. For example, if a particular model tends to misclassify most frequently samples of a particular class, the fusion model can potentially correct for this, leading to a better final result (thus the meta- prefix).

This decision fusion-based scheme also utilizes a consensus-based nested CV algorithm. Input feature vectors from each FC model are reduced individually, in each outer CV loop. The colored background of *Figure 18* represents the outer validation loop during which the features are selected by internal CV, individual models trained, and the Meta-Estimator trained. Subsequently, the Meta-Estimator is tested using Estimator 1-4 predictions and classification performance metrics obtained (accuracy, precision, sensitivity, specificity, F1, ROC AUC). The outer CV is repeated at least 400 times, while the internal (Feature Selection; Nested CV) at least 40 times. The internal selection is performed identically to the individual ML model scheme described above and a fixed numbered of 10 or 20 features are obtained. The decision fusion-based ML model combination is referred to as **Fusion Model 2** or **FM2** in subsequent sections.

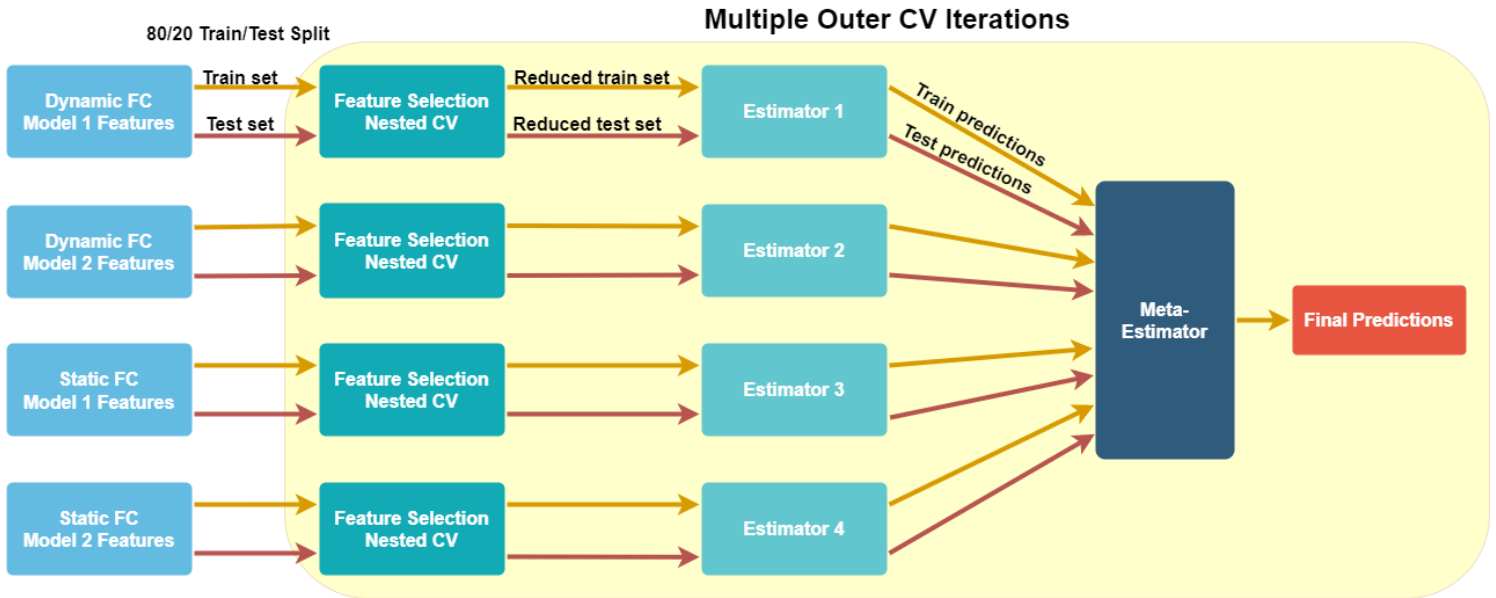


FIGURE 18 - PROPOSED DECISION FUSION SCHEME

4.4 STATISTICAL COMPARISONS

To support the interpretability of ML results, independent sample t-tests were used to assess the statistical significance of group differences on each of the final features derived by each model described in Sections 3.2.1 and 3.2.2 as well as by the combination of the four models (two dynamic and two static). Control of familywise error rate (FWER) across multiple comparisons was employed using the FDR method (Benjamini & Hochberg, 1995) with a false discovery rate $q=0.01$. All statistical comparisons were performed in MATLAB.

4.5 SOFTWARE AND CODE

Main preprocessing steps were completed in the MATLAB-based toolbox SPM12 (fil.ion.ucl.ac.uk/spm/) and denoising steps were carried out in the SPM-based toolbox CONN (web.conn-toolbox.org/). BrainNet Viewer (Xia et al., 2013) was used for brain region and connection visualization purposes (freely distributed in nitrc.org/projects/bnv/). Connectivity-related computations were performed using custom MATLAB scripts. The BCT or *Brain Connectivity Toolbox* (sites.google.com/site/bctnet/; (Rubinov & Sporns, 2010) was employed to calculate most graph measures. An implementation of the Small-World Propensity measure (Muldoon et al., 2016) can be found in (complexsystemsupenn.com). Code for topological network filtering with OMST (and several other algorithms) can be found in Dr. Stavros Dimitriadi's GitHub repository (github.com/stdimitr). Included ML experiments were set up using the python programming language. A python implementation of XGBoost can be found in (xgboost.readthedocs.io/en/latest/python/index.html). Several other ML or data transformation-related operations utilized the NumPy (numpy.org) and sklearn (scikit-learn.org) libraries (as well as pandas and SciPy).

5. RESULTS

Initially, in order to examine the soundness of the DFC state identification process based on unsupervised Learning (k -means clustering), as well as the validity of the integrated/segregated representative networks produced for each subject, a few illustrative characteristics were evaluated. Namely, modularity, mean participation coefficient and mean within-module degree z -score were calculated on the two state representative graphs of each subject. Theoretically, the integrated state should exhibit increased participation coefficient as more connections exist between a given node and nodes of other modules. Modularity and within-module degree z -score are expected to be elevated in the segregated state across subjects, quantifying the existence of more prominently distinct functional communities (measure through modularity) with strong connections between their members (quantified by within-module degree z -score). This validation step is important as the main metrics used for the state identification process (as detailed in 3.3.1) were computed on time-resolved DFCGs which were subsequently clustered and the centroid state FCGs derived as edge-wise medians. Whether these main network characteristics are retained in the state centroid/median/representative graphs is not certain.

Comparisons were performed on the data from each participant separately. All three hypotheses were confirmed (the null hypotheses rejected) using right-tailed two-sample t -tests, with mean participation coefficient being significantly higher in the integrated state ($p < 2 \times 10^{-12}$), elevated modularity in the segregated state ($p < 0.000001$) and higher mean within-module degree z -score in the segregated state found at more moderate significance ($p < 0.032$).

5.1 ML CLASSIFICATION RESULTS

Classification Performance Metrics were used to assess the capacity of a given model to distinguish between the two study groups. All classification experimental results were performed using 400 outer and 40 inner CV iterations retaining 20 best features from each model. Although, classification performance was similar by retaining 10 features from each model, the 20-feature

solutions were preferred in order to obtain richer regional information. In the case of decision fusion, 20 features were used in each internal model resulting in a total of 80 features. Results appear to stabilize at around 300-400 iterations and larger numbers resulted in virtual identical performance metrics and selected features.

Feature/Model type	Accuracy	Precision	Sensitivity	Specificity	F1 Score	ROC AUC
DFC M1: PCC, Integ. & Segr. States, multiple graph metrics	72 ± 10	72 ± 14	71 ± 16	73 ± 16	70 ± 12	72 ± 10
DFC M2: MI, Integ. & Segr. States, multiple graph metrics	65 ± 11	64 ± 15	61 ± 20	68 ± 18	61 ± 15	65 ± 12
SFC M1: PCC, multiple graph metrics	76 ± 10	76 ± 13	74 ± 16	77 ± 15	74 ± 11	76 ± 10
SFC M2: MI, multiple graph metrics	76 ± 10	77 ± 14	72 ± 17	79 ± 14	73 ± 13	75 ± 11
FM1: DFC-PCC & MI, SFC-PCC & MI Feature-level Fusion	76 ± 11	77 ± 15	72 ± 18	79 ± 15	73 ± 14	76 ± 11
FM2: DFC-PCC & MI, SFC-PCC & MI, Decision-level Fusion	80 ± 10	81 ± 13	78 ± 17	82 ± 14	78 ± 12	80 ± 11

TABLE 2 - CLASSIFICATION RESULTS – 20 FINAL FEATURES

The number of features derived from each model/approach that varied significantly between mTBI and control participants is shown in Table 3 (FDR corrected $p < .01$).

Feature type	FDR, $q = 0.01$
DFC M1: PCC	19/20
DFC M2: MI	10/20
SFC M1: PCC	18/20
SFC M2: MI	11/20
FM1: DFC-PCC&MI, SFC-PCC&MI	20/20
FM2: DFC-PCC&MI, SFC-PCC&MI	58/80

TABLE 3 - STATISTICAL SIGNIFICANCE, 10 OR 20 FINAL FEATURES

SIGNIFICANT FEATURES

An important point to mention about the significant features derived from each model, concerns the adopted feature selection approach. As analyzed in the methods section, the feature selection procedure applied to the DFC M1 (PCC), DFC M2 (MI), SFC M1 (PCC), and SFC M2 (MI) was identical to that utilized in the FM2, decision fusion-based model. As depicted in *Figure 18*, each feature set is treated individually up to the final step of fusion where the class probability results are combined by the meta-estimator. Thus, the final significant features derived by FM2 are a combination of those also selected by the individual models, although the classification results were further improved when the features were combined.

To simplify presentation of results, the entire set of features derived from FM2 are presented in Tables 5-6 with the appropriate notation regarding their origin in terms of the method they were based on and corresponding initial model (DFC/SFC, PCC/MI,). The entire set of significant regions selected as important features through nested validation and classification are presented in the Appendix.

All regional and global features included in the following tables as well as in the appendix have undergone statistical thresholding after being selected by the consensus feature importance-based ML scheme, using FDR with a false discovery rate $q=0.01$. The anatomic location of significant regions identified by each model is displayed in Figures 22-23.

FEATURE-LEVEL FUSION – FM1

Metric	FC	DFC/SFC	Hemisphere	MNI Coordinates	Region	Atlas ID #
LE	PCC	SFC	R	22,-60,8	Visual 10	110
BC	MI	SFC	R	6,-10,52	Somatomotor 11	126
LE	PCC	DFC Segr.	R	58,-46,10	Ventral Attention / Temporal-Occipito-Parietal 1	148
LE	MI	DFC Segr.	R	38,-62,48	Parietal Control 3	167
LE	PCC	DFC Integ.	R	14,-74,52	DAN Posterior 6	140
BC	PCC	SFC	L	-42,8,-18	Limbic Temporal Pole 4	60
EC	PCC	DFC Integ.	R	26,-10,-32	Limbic Temporal Pole 3	164
BC	MI	SFC	R	26,-10,-32	Limbic Temporal Pole 3	164
DEG	PCC	SFC	R	26,-10,-32	Limbic Temporal Pole 3	164
DEG	PCC	DFC Segr.	L	-22,-96,6	Visual 9	9
LE	PCC	DFC Segr.	R	6,-48,30	DMN Precuneus PCC 2	199
LE	PCC	DFC Integ.	L	-6,-54,42	DMN Precuneus PCC 4	99
LE	MI	DFC Integ.	R	52,-32,2	DMN Temporal Gyrus 5	189
DEG	PCC	DFC Segr.	R	22,-48,70	DAN Posterior 10	144
LE	PCC	SFC	R	12,-54,14	DMN Precuneus PCC 1	198
LE	PCC	SFC	R	34,-48,50	DAN Posterior 7	141
SWP	MI	DFC Segr.	-	-	Global	-
GE	MI	DFC Integ.	-	-	Global	-
LE	PCC	SFC	L	-16,-72,54	DAN Posterior 7	37
BC	PCC	DFC Segr.	L	-22,-96,6	Visual 9	9

TABLE 4 - FM1 (FEATURE FUSION) FINAL SIGNIFICANT FEATURES

Table 4 lists the graph measure utilized in the specific feature, and the connectivity estimation method (FC) and connectivity modality (SFC or DFC). For nodal metrics, the hemisphere (left or right), MNI space coordinates, and region name and numeric id according to the Schaefer (cortical) or Melbourne (subcortical) atlas are also provided, along with the name of the conventional network that a given region belongs (e.g., DMN, DAN, Limbic).

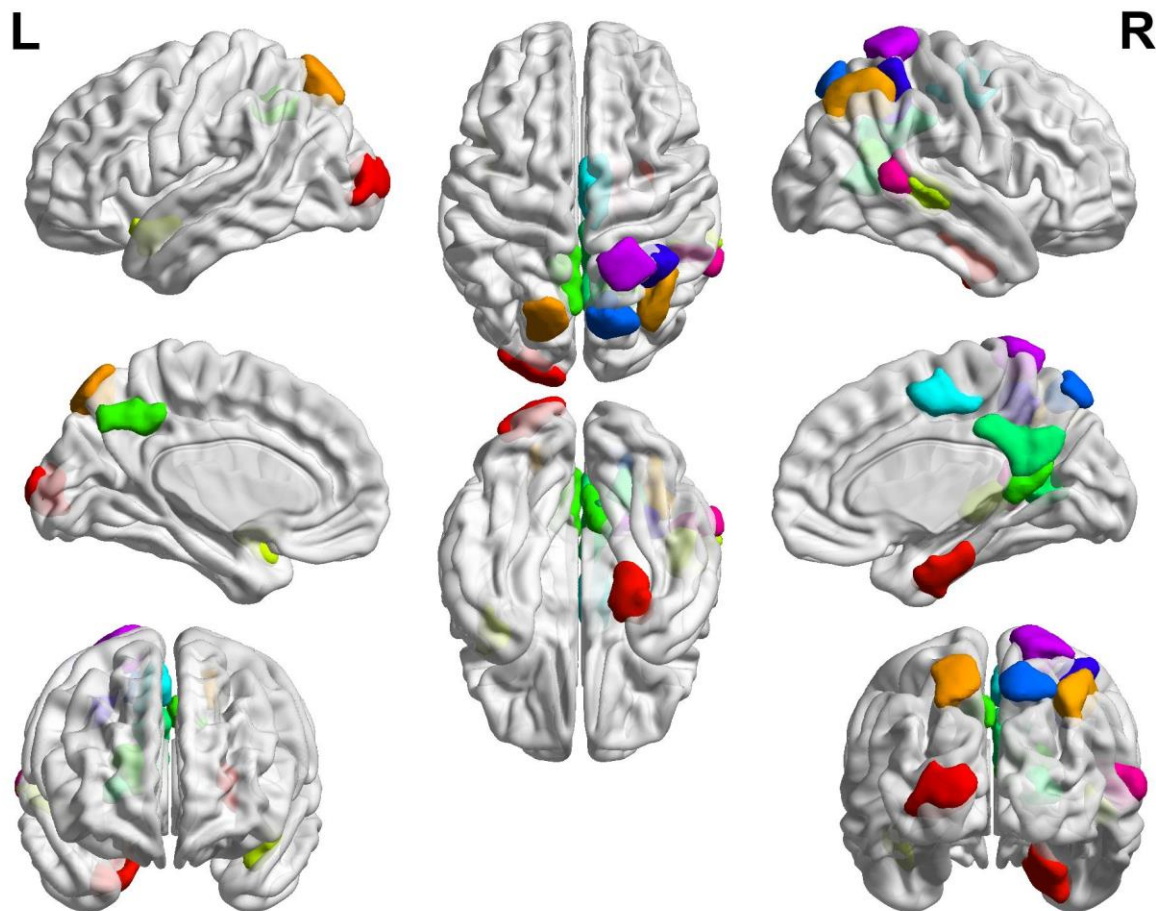


FIGURE 19 - FM1 (FEATURE FUSION): REGIONS THAT SIGNIFICANTLY DIFFERENTIATED mTBI FROM HEALTHY CONTROL PARTICIPANTS

DECISION-LEVEL FUSION – FM2

Features derived as significant from the decision-level fusion approach are presented next, in a similar fashion as the previous model's. However, separate tables are given for features with values greater in mTBI patients compared to controls and vice versa. In total, 58 out of 80 features were found significant ($q=0.01$), while 69/80 features are derived as significant at a lower threshold ($q=0.05$). The more stringent statistical threshold was selected for increased model robustness.

In Tables 5-6 each row may indicate several features that were obtained for a single brain region (e.g., Temporal Pole 3 with four features). The different metrics or connectivity estimation methods are displayed. For example, Temporal Pole 3, a region of the Limbic Network, has contributed 5 features in the right hemisphere and 4 in the left hemisphere. These contributing features are mostly all measures of centrality nodal degree, betweenness centrality and eigenvector centrality as well as one instance of local efficiency. Furthermore, the connectivity modality that contributed these features are varying between static and dynamic, linear (PCC) and linear/nonlinear measures (MI). Apart from regions contributing multiple features, regions of the same functional network (e.g., DMN, DAN etc.) according to the Schaefer functional atlas, which are also in the same hemisphere and in close anatomical proximity, are combined in a single row, for display purposes. These instances can be distinguished easily as multiple region numbers are provided in the last two columns.

Metric	FC	DFC/SFC	Hemisphere	MNI Coordinates	Region	Atlas ID #
EC, BC, DEG	PCC, MI	SFC, DFC Integ, DFC Segr	R	26,-10,-32	Limbic Temporal Pole 3	164
BC, DEG, LE	PCC, MI	SFC, DFC Integ	L	-28,10,-34	Limbic Temporal Pole 3	59
BC, LE	PCC, MI	SFC	R	30,8,-38	Limbic Temporal Pole 1	162
BC	MI	SFC	L	-30,-6,-40	Limbic Temporal Pole 1	57

BC	PCC	SFC	L	-42,8,-18	Limbic Temporal Pole 4	60
EC, BC, DEG	PCC, MI	SFC, DFC Segr	L	-22,-96,6	Visual 9	9
BC	PCC	SFC	R	22,-8,68	Somatomotor 16	131
BC	MI	SFC	R	6,-10,52	Somatomotor 11	126
DEG	PCC	DFC Segr	L	-46,8,-32	DMN Temporal 1	74
EC	MI	DFC Integ	L	-12,18,-2	Nucleus accumbens, core	226

TABLE 5 - FM2 (DECISION FUSION) FINAL SIGNIFICANT FEATURES (CONTROLS>MTBI)

Metric	FC	DFC/SFC	Hemisphere	Region	Atlas ID #
SWP	MI	DFC Integ, DFC Segr	-	Global	-
GE	MI	DFC Integ	-	Global	-
LE	PCC	SFC , DFC Segr, DFC Integ	L	DMN Precuneus PCC 1, 2, 4	96, 97, 99
LE, DEG	PCC	SFC , DFC Segr	R	DMN Precuneus PCC 1, 2	198, 199
LE	MI	DFC Integ	R	DMN Temporal 5	189
LE, EC	PCC, MI	SFC , DFC Segr, DFC Integ	L	DAN Posterior 3, 5, 7	33, 35, 37
LE, DEG	PCC, MI	SFC , DFC Segr, DFC Integ	R	DAN Posterior 5, 6, 7, 8, 10	139-142, 144
LE	PCC	DFC Segr	L	Somatomotor 4	18
LE, DEG	PCC, MI	SFC, DFC Integ	R	Somatomotor 3, 9, 12, 13	118, 124, 127, 128, 133
LE	PCC	SFC , DFC Segr	L	Limbic OFC 2	56
DEG	PCC	DFC Segr	L	Sal. Vent. Attn. Par. Oper.	45
LE	PCC	DFC Segr	R	Sal. Vent. Attn. Temp. Occ. Par.	148
LE	PCC	SFC	R	Visual 10	110
LE	MI	DFC Segr	R	Parietal Control 3	167

TABLE 6 - FM2 (DECISION FUSION) FINAL SIGNIFICANT FEATURES (MTBI>CONTROLS)

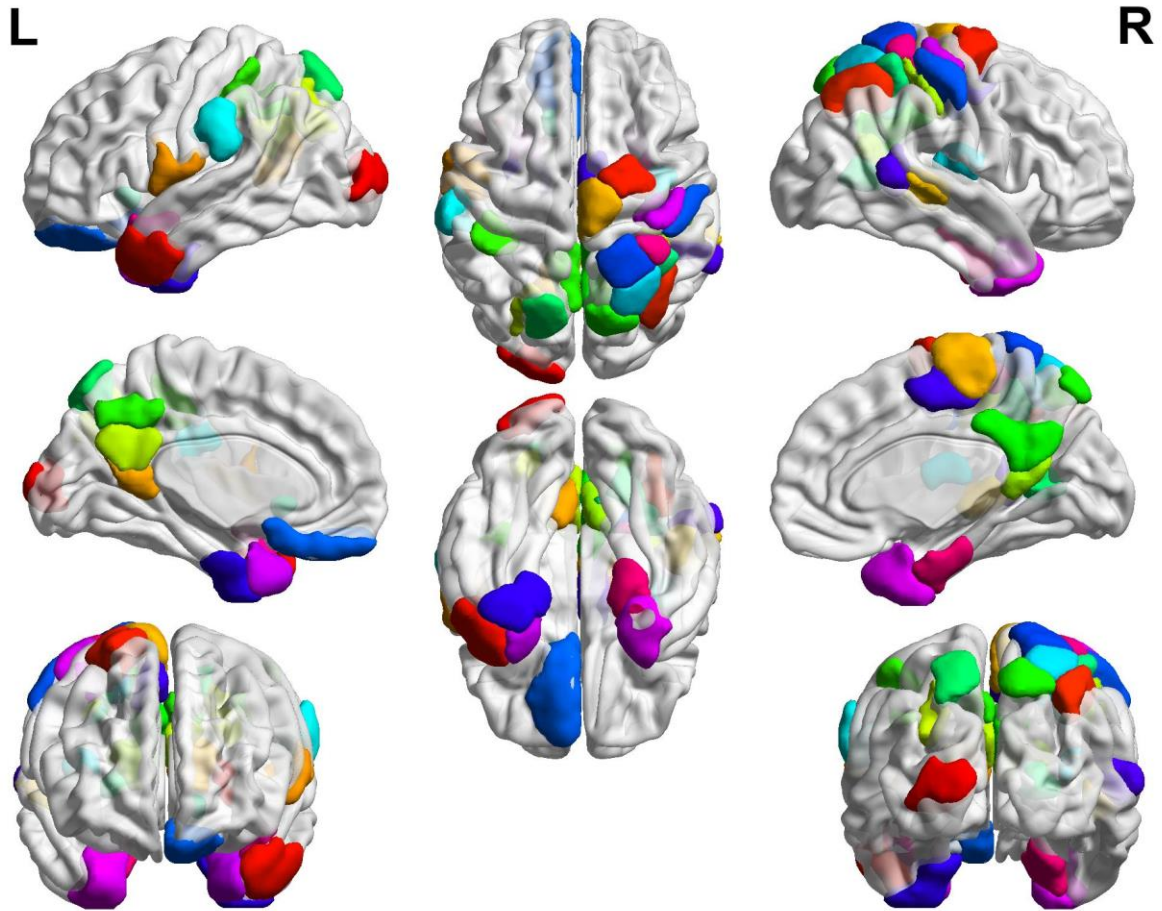


FIGURE 20 - FM2 (DECISION FUSION): REGIONS THAT SIGNIFICANTLY DIFFERENTIATED MTBI FROM HEALTHY CONTROL PARTICIPANTS

6. DISCUSSION

GENERAL REMARKS

An important initial observation concerns the general trend in types of features that have contributed most to distinguishing between the two populations. All features derived as significant by the ML validation process and the subsequent statistical testing are network measures, both nodal and global. No state fluctuation measures were identified as significant by this rigorous process, implying that they did not provide unique information that was distinct among mTBI patients.

An important point regarding the two ML model combination approaches concerns the sets of brain regions highlighted by each method. All regions included derived by the feature fusion method (FM1) were also identified by the decision fusion model (FM2) as final significant features. Additionally, in the decision fusion pipeline, each of the 4 feature sets (DFC M1, DFC M2, SFC M1, SFC M2) were independently reduced via feature selection (i.e., each group's final features are identical to the final features obtain by the individual ML models).

Concerning the often posed static versus dynamic question, the results weren't very clear cut or revealing. In FM1 12 out of 20 (60%) were DFC features, while features derived from FM2 were balanced across types (~52% SFC and 48% DFC). In terms of connectivity estimation metrics, PCC was used in 70% of FM1 and in 62% of FM2 final derived features. Additionally, among DFC features, the more conventional PCC featured more prominently when used individually compared to the MI connectivity metric. This can be attributed to the shorter timeseries associated with the sliding-window DFC method that may not be as suitable for estimating MI. Roughly half of the features in both models were Local Efficiency values, while the other half were mostly centrality measures, nodal degree, betweenness and eigenvector centrality as well as Small World Propensity and global efficiency values in both models. The segregated state contributed marginally more features relative to the predominately integrated state. In FM2, 17 features out of

28 (~60%) of DFC features were measures based on the segregated state representative networks. A similar pattern was observed in FM1 with 7 out of 12 segregated network measures.

The clearly superior model in terms of classification performance is the decision-fusion based FM2. As shown in *Table 2*, accuracy, precision, sensitivity and specificity are all higher for FM2 compared to all the individual models and the other ML fusion approach, FM1. It should be noted that specificity is valued very highly in the diagnostic problem addressed in the present study. Increased specificity indicated a lower probability of false positive diagnosis. Routine clinical practice is often faced with the problem of ascertaining whether subjective cognitive complaints attributed to alleged brain injury can be attributed to aberrant brain function. In terms of model interpretation and derivation of significant regions, FM2 encompasses all the regions selected by DFC Models 1-2 and SFC Models 1-2, as well as by FM1, and as such the entirety of the regions identified by FM2 are discussed here.

DISCUSSION OF RESULTS – SIGNIFICANT REGIONS

As mentioned in the Introduction, **this is the first study to examine changes in DFC combined with SFC in chronic mTBI**. This definitely poses a challenge in comparing the present findings with previous work. This poses a problem either due to a strictly static or dynamic approach, an acute mTBI dataset or the type of metric compared, connectivity strengths (graph edges) as opposed to graph metrics and lastly the lack of incorporation of ML classification or the type of ML classification, selection and validation pipeline. Due to the scarcity of directly relevant previous work, results are mostly discussed against studies of chronic mTBI patients using various static FC measures and studies employing DFC or SFC combined with DFC to investigate acute or subacute mTBI.

The Temporal Pole of the Limbic Network emerged as one of the most significant regions indicating functional deficiencies in mTBI patients, appearing bilaterally in more than nine of the final features. Its role is highlighted by static and dynamic connectivity from both integrated and segregated states and by connectivity networks derived by PCC and MI. All computed measures of centrality, nodal degree, betweenness centrality and eigenvector centrality all revealed similar

trends concerning the region's overall diminished functional role. Decreased values of Temporal Pole centrality (bilaterally) as well as local efficiency (only right hemisphere) were observed in mTBI patients compared to healthy controls. While this region is known to be susceptible to contusion injury following mTBI caused by direct impact on the cranium, and may present evidence of structural connectivity changes following mTBI (Van Der Horn et al., 2017) there is very limited evidence of FC abnormalities using rs-fMRI. Subtle disturbances in connectivity of this region may help explain some of the emotional manifestations of mTBI, although confirmation of the present finding and evidence of associations with emotional symptom scales are required.

Regions of the Visual and Somatomotor networks contributed significant features with decreased functional characteristics in mTBI subjects as well. Centrality of Visual and Somatomotor network regions seems to have been affected by the head trauma, highlighted by static and dynamic and both connectivity estimation methods. Decreased SFC connection strengths in chronic mTBI patients were also found by (Champagne et al., 2020). While the decreased connectivity reported by (Nathan et al., 2014) is in line with the lowered importance observed via lower nodal degree in this case.

The DMN's left and right precuneus and posterior cingulate cortex (PCC) as well as right temporal subregion showed increased values of local efficiency or nodal degree in mTBI patients compared to healthy controls. Both static and dynamic indices corroborated these trends. These findings are mostly in agreement with increased (static) connectivity observed by (Nathan et al., 2014) in left and right PCC and temporal regions which were also found correlated with measures of depression, aggressive behavior and stress. Increased DMN (static) connectivity was also observed by (Champagne et al., 2020) and (Vergara et al., 2016), between the left Angular and the PCC. However, decreased connectivity in several DMN regions, including the PCC was found by (Mayer et al., 2014), though these findings were using static indices and more importantly in sub-acute trauma patients rather than chronic.

Several posterior regions of the DAN exhibited elevated local efficiency as well as centrality (node degree or eigenvector centrality), supported by static and dynamic, PCC and MI indices. These observations are in the same direction with the findings of (Sours et al., 2015) where increased connectivity between DAN and DMN was observed in chronic mTBI patients. DAN regions also exhibited increased (static) connectivity in chronic mTBI patients (Champagne et al., 2020).

The observed general increase of functional role (local efficiency and node degree) in several regions of the somatomotor network is in line with the reported increase in connectivity between somatomotor and cerebellum regions in semi-acute mTBI patients (Mayer et al., 2014) as well as increased somatomotor connections (Vergara et al., 2016, 2018).

The heightened functional role of visual and salience ventral attention network regions is in line with increased (static) connectivity reported in chronic mTBI patients in (Champagne et al., 2020) and the elevated connectivity of visual regions in sub-acute patients through DFC in (Mayer et al., 2014). Additionally, the deficiencies observed in limbic network function can lead the subjects to be hypervigilant and overly alert of their surroundings leading to increased overall function in regions of the Salience Ventral Attention regions, such as the Parietal Operculum and Temporal Occipital Parietal that were observed here.

As can be observed by analyzing the regional features of FM2's results, overall, the deficiencies in chronic mTBI network function appear more localized and coherent in only a few key regions, in the Temporal Pole subregions bilaterally as well as regions of the Visual and Somatomotor networks. As discussed above, the significance of these regions is confirmed by the multiplicity of final features contributed by each ROI. On the other hand, the brain regions with most likely compensatory roles, producing higher centrality or connectedness efficiency values in mTBI patients are relatively more diffuse within the DMN, DAN and Somatomotor networks, most significantly. No feature/metric multiplicity was observed from any specific region in this case, but the network-specific results were quite coherent. This general pattern should be attributed to the theory of relatively specific regions having been more directly influenced by the brain injury, while compensatory phenomena in network function are on a network rather than a region level.

In terms of global metrics, both the integrated and segregated substate obtained with mutual information, exhibited increased small world characteristics, while the integrated state also had increased global efficiency. This observation is quite possibly as a result of global compensatory processes in network topology as a result of head trauma. Increased SWP indicates a balance between local and global processing and is often interpreted as increased information capacity in a given network. This occurrence is also in line with the increased global efficiency in combination with several regions with higher local efficiency values. As analyzed in *Small-World Propensity*, the normalized clustering coefficient and characteristic path length are utilized (divided) in the

SWP's calculation. Local efficiency as discussed earlier, closely parallels the weighted clustering coefficient and global efficiency is the inverse of the characteristic path length.

Overall, static and dynamic derived indices appear to be both complementary and in agreement in several cases. This leads to the conclusion that both approaches are valid and produce useful and interpretable results and should more often be used in tandem rather than individually. Furthermore, in terms of the underlying connectomic patterns being decoded by these methods, the functional behavior of some regions seems to be relatively uniform across time but likely exhibits temporally varying fluctuations not able to be fitted into the integrated or segregated motif, such as the decreased centrality in Somatomotor areas found in mTBI patients or the increases in local efficiency of visual regions. These regions' connectomic differences are only observed using SFC. Most other results, at least at a network level, seem to be more or less consistent between static and dynamic connectivity. At a region level, the information produced is much more complex and definitely richer with the combination of SFC and DFC, again highlighting the importance of this approach.

Concerning the mutual information connectivity estimation measure, several overlapping regional features were observed with those of the PCC, while only few results, especially on the network level, were derived solely through the MI index. An exception being the increased small-world characteristics indicated by SWP and MI in both DFC states in mTBI patients. This interesting finding can be also somewhat justified by the similarly elevated global efficiency in combination with several regions exhibiting heightened local efficiency in the same dynamic states. Overall, MI features did have reduced statistical significance indicated by less final features deemed significant after statistical thresholding in both static and dynamic cases. In the DFC case this is attributed to the shorter timeseries posing a challenge in MI calculation.

Regarding the participation of regions in integrated and segregated states, networks such as the DMN, exhibiting an increased functional role in mTBI compared to controls, seem to be split between the two dynamic states, indicating a DMN organization that is split between the two topologies. This is also true in the case of the DAN as well as somatomotor regions, whose increased importance indicated by elevated local efficiency or centrality measures is observed in both dynamic states. Furthermore, one of the most significant findings of the current study, the aberrant functional characteristics reported in the Temporal Pole regions of the limbic network are

corroborated by all means of computed connectivity measures. Apart from a generalized dysfunction exhibiting a plethora of topological patterns, these results could also be interpreted as a sign that a slightly different approach in the state identification method could be more suited in this diagnostic challenge. More on this is discussed in the future work section. Finally, subcortical regions did not seem to be severely affected by trauma as only a single region remained in the final set, the Nucleus accumbens, core exhibiting decreased eigenvector centrality (MI, DFC) in mTBI patients.

APPROACH USABILITY AND GENERALIZABILITY

An important point worth discussing pertains to the overall usability of the employed techniques in several different modalities and applications. Abstractly, the present is a relatively “generic” approach combining various graph theoretical parts as well as Machine Learning. This method can be easily applied on different datasets, comparisons and even modalities outside fMRI. For example, much work is carried out on mTBI using Magnetoencephalographic (MEG) recordings. With a few key changes in order to exploit different types of data, this entire pipeline can be retrofitted for MEG data. Spatially, a different atlas may be used for segmentation, while temporally, different window sizes can be used for DFC estimation given the faster updating and overall longer time series. Additionally, richer frequency information can be utilized by performing the feature extraction per band. For instance, (Antonakakis et al., 2020) is a good example of a similar analysis direction in mTBI MEG data.

STUDY LIMITATIONS

A crucial limitation of the current study pertains to the number of participants. Apart from allowing increased generalizability and more robust statistical results, the nested CV scheme implemented which splits the subjects/samples twice (externally and internally) would definitely benefit from a

larger sample size in both groups. The observed sample standard deviation of the classification performance metrics is also expected to improve.

Additionally, the length of recorded timeseries may limit the robustness of the MI algorithm (and secondarily of the PCC algorithm). Longer timecourses would allow for more stable and robust MI estimation. However, practical considerations were kept in mind when designing the experiment. Longer acquisitions are not technically difficult or immediately problematic but staying in the scanner for too long can cause other problems such as increased movement, fatigue or stress which can eventually compromise the data.

As discussed in the section entitled *Cartographic Profiling*, the notion of distinct integrated-segregated network states, although relatively straightforward, may not be truly representative of resting functional brain organization of every person and population. This analysis avoids some potential issues by moving away from the totally “undirected” alternative state-based approach using k -means directly on time-resolved graphs by using a specific combination of relevant features but can potentially suffer in this regard. Alternative measures able to capture a wider variety of network topologies can be explored (see Future Work). A related issue pertains to the suitability of the k -means algorithm to identify distinct, state-specific networks, and supported by the struggle of the algorithm to classify the states in some cases.

FUTURE WORK

An initial point of improvement is hinted in the study limitations regarding the, in some cases possibly ill-fitting, integration-segregation scheme. This can be addressed via the exploration of different state identification approaches that can possibly overcome some of the drawbacks of the current implementation. Different modularity levels have been assessed as state identifiers in (Fukushima, Betzel, He, de Reus, et al., 2018) showing promising results.

Additionally, a broader range of network configurations may be used, including states of increased small-world characteristics, elevated global and local efficiency accordingly, while maintaining the requirement that each state has a well-defined topology, as in the present approach. This set of

3 or 4 states could possibly provide a better overall “fit”, thus increasing the efficiency and accuracy of the identification through clustering (e.g. *k*-means). Alternatively, temporal networks exhibiting predominately rich-club or small-world characteristics could be searched for in a similar fashion. These topologies could potentially provide interesting results in population comparisons.

Alternative unsupervised learning techniques should also be evaluated for the task of clustering currently fulfilled by *k*-means. Hierarchical clustering, DBSCAN (Density-based spatial clustering of applications with noise) or self-organizing maps can be tested for this role.

Finally, the temporal evolution of various network measures should be further analyzed, especially regional or global metrics that emerged as significant. This can be achieved by examining the randomness or unpredictability of these measures throughout the scan (e.g. via sequence complexity or sample entropy).

The present work can be extended to assess associations of various network characteristics, such as those derived here, with patient’s neuropsychological measures. Significant correlations with the connectomic biomarkers identified in the present study process are necessary in order to establish the clinical significance of the present findings and enhance the understanding of functional neuronal changes that take place in chronic mTBI.

Finally, much more detailed investigation is still needed to examine region interactions on a network and individual ROI level. Specific region’s connections should be examined in combination with network level information in order to obtain more detailed conclusions and result interpretations. Cerebral blood flow, cerebrovascular reactivity, neuro-autonomic cardiovascular regulation and cerebral oxygenation are topics of special interest in chronic mTBI research. Cerebral autoregulatory function and its relationship with post-mTBI neurophysiological changes also constitutes one of our team’s research long-term goals.

7. CONCLUSION

In the present thesis, a novel combination of rs-fMRI functional connectivity metrics was utilized for the classification of chronic mTBI patients and healthy controls. Static and dynamic indices computed using linear and non-linear connectivity estimation measures are utilized. A state-based DFC approach is utilized attempting to detect temporal sections that are predominately segregated or integrated based on network topology. All brain networks are reduced individually in order to obtain the most significant connections. Graph metrics are employed in both SFC and DFC cases encapsulating various network characteristics. The four different feature sets derived by each approach are fused on a feature or decision level and results compared. The decision fusion approach outperformed all others in terms of classification performance and derived a superset of final features.

Overall, most regions exhibiting significantly different behaviors between the two populations are in relative agreement with previous studies in mTBI. The main exception being the Temporal Pole subregions of the limbic network. These findings have emerged with several measures and techniques making it a more robust finding. However as any novel observation, external validation/replication is needed.

The classification performance achieved is definitely acceptable and unique in the context of chronic mTBI and especially DFC-related studies. These results must be interpreted after considering the stringent and thorough validation procedure applied, aimed at avoiding overoptimistic results. Additionally, the actual diagnostic problem is not a simple one as chronic mTBI patients, examined via functional imaging more than six months after mild head trauma are not expected to exhibit very prominent connectomic disturbances in the resting-state.

This study poses in some degree a proof of concept for a novel approach in terms of the ML scheme. Decision fusion techniques haven't been tested in such scenarios for patient classification and the results are definitely promising. The combination of static and time-varying connectivity indices as well as linear and non-linear metrics has proven a rewarding attempt with interesting final outcomes. The collaborating results of the different modalities especially are of increased importance adding to overall model robustness. A definite strongpoint of ML model

fusion/combination, each with differently obtained information on the same regions is the ability to observe regions that appear with multiplicity in important features, strengthening the overall decision as well as the weight of significance allocated to the specific region and its unavoidable role in the comparison.

8. APPENDIX

SUPPLEMENTARY RESULTS

State network	Metric	Hemisphere	Coordinates	Region	#
Segr.	LE	R	58,-46,10	Temporal Occipital Parietal 1	148
Integ.	LE	R	14,-74,52	DAN Posterior 6	140
Integ.	EC	R	26,-10,-32	Limbic Temporal Pole 3	164
Integ.	LE	L	-6,-54,42	DMN Precuneus PCC 4	99
Segr.	DEG	L	-22,-96,6	Visual 9	9
Segr.	BC	L	-22,-96,6	Visual 9	9
Segr.	LE	R	6,-48,30	DMN Precuneus PCC 2	199
Integ.	BC	L	-28,10,-34	Limbic Temporal Pole 3	59
Segr.	DEG	R	22,-48,70	DAN Posterior 10	144
Segr.	LE	L	-56,-4,10	Somatomotor 4	18
Segr.	DEG	R	26,-10,-32	Limbic Temporal Pole 3	164
Segr.	LE	L	-6,-54,28	DMN Precuneus PCC 2	97
Segr.	LE	L	-26,-70,38	DAN Posterior 3	33
Segr.	LE	L	-10,-56,12	DMN Precuneus PCC 1	96
Segr.	DEG	L	-62,-26,28	Sal. Vent. Attn. Par. Oper. 2	45
Segr.	LE	L	-6,-54,42	DMN Precuneus PCC 4	99
Segr.	DEG	L	-46,8,-32	DMN Temporal 1	74
Segr.	LE	R	12,38,-22	Limbic OFC 1	159
Integ.	LE	R	46,-12,48	Somatomotor 10	125

TABLE I - DFC M1 (PCC) FINAL SIGNIFICANT FEATURES

State network	Metric	Hemisphere	Coordinates	Region	#
Segr.	SWP	-	-	Global	-
Integ.	GE	-	-	Global	-
Segr.	LE	R	38,-62,48	Parietal Control 3	167

Integ.	LE	R	52,-32,2	DMN Temporal Gyrus 5	189
Integ.	LE	R	52,-22,52	Somatomotor 9	124
Integ.	SWP	-	-	Global	-
Integ.	EC	L	-40,-36,48	DAN Posterior 5	35
Integ.	EC	L	-12,18,-2	Nucleus accumbens, core	226
Segr.	LE	L	-16,-72,54	DAN Posterior 7	37
Segr.	LE	R	22,-48,70	DAN Posterior 10	144

TABLE II - DFC M2 (MI) FINAL SIGNIFICANT FEATURES

Metric	Hemisphere	Coordinates	Region	#
LE	R	22,-60,8	Visual 10	110
LE	R	34,-48,50	DAN Posterior 7	141
DEG	R	26,-10,-32	Limbic Temporal Pole 3	164
BC	L	-42,8,-18	Limbic Temporal Pole 4	60
LE	R	12,-54,14	DMN Precuneus PCC 1	198
LE	L	-16,-72,54	DAN Posterior 7	37
LE	L	-28,10,-34	Limbic Temporal Pole 3	59
LE	R	30,8,-38	Limbic Temporal Pole 1	162
LE	R	26,-62,58	DAN Posterior 8	142
BC	R	22,-8,68	Somatomotor 16	131
DEG	R	6,-48,30	DMN Precuneus PCC 2	199
LE	L	-6,-54,28	DMN Precuneus PCC 2	97
DEG	L	-28,10,-34	Limbic Temporal Pole 3	59
LE	R	38,-14,14	Somatomotor 3	118
LE	R	26,-10,-32	Limbic Temporal Pole 3	164
EC	R	26,-10,-32	Limbic Temporal Pole 3	164
LE	R	32,-40,64	Somatomotor 13	128
LE	L	-6,-54,42	DMN Precuneus PCC 4	99

TABLE III - SFC M1 (PCC) FINAL SIGNIFICANT FEATURES

Metric	Hemisphere	Coordinates	Region	#
BC	R	6,-10,52	Somatomotor 11	126
BC	R	26,-10,-32	Limbic Temporal Pole 3	164
SWP	-	-	Global	-

LE	R	6,-22,68	Somatomotor 18	133
BC	L	-30,-6,-40	Limbic Temporal Pole 1	57
BC	L	-28,10,-34	Limbic Temporal Pole 3	59
LE	L	-16,-72,54	DAN Posterior 7	37
EC	L	-22,-96,6	Visual 9	9
BC	R	30,8,-38	Limbic Temporal Pole 1	162
DEG	R	26,-62,58	DAN Posterior 8	142
DEG	R	40,-24,58	Somatomotor 12	127

TABLE IV - SFC M2 (MI) FINAL SIGNIFICANT FEATURES

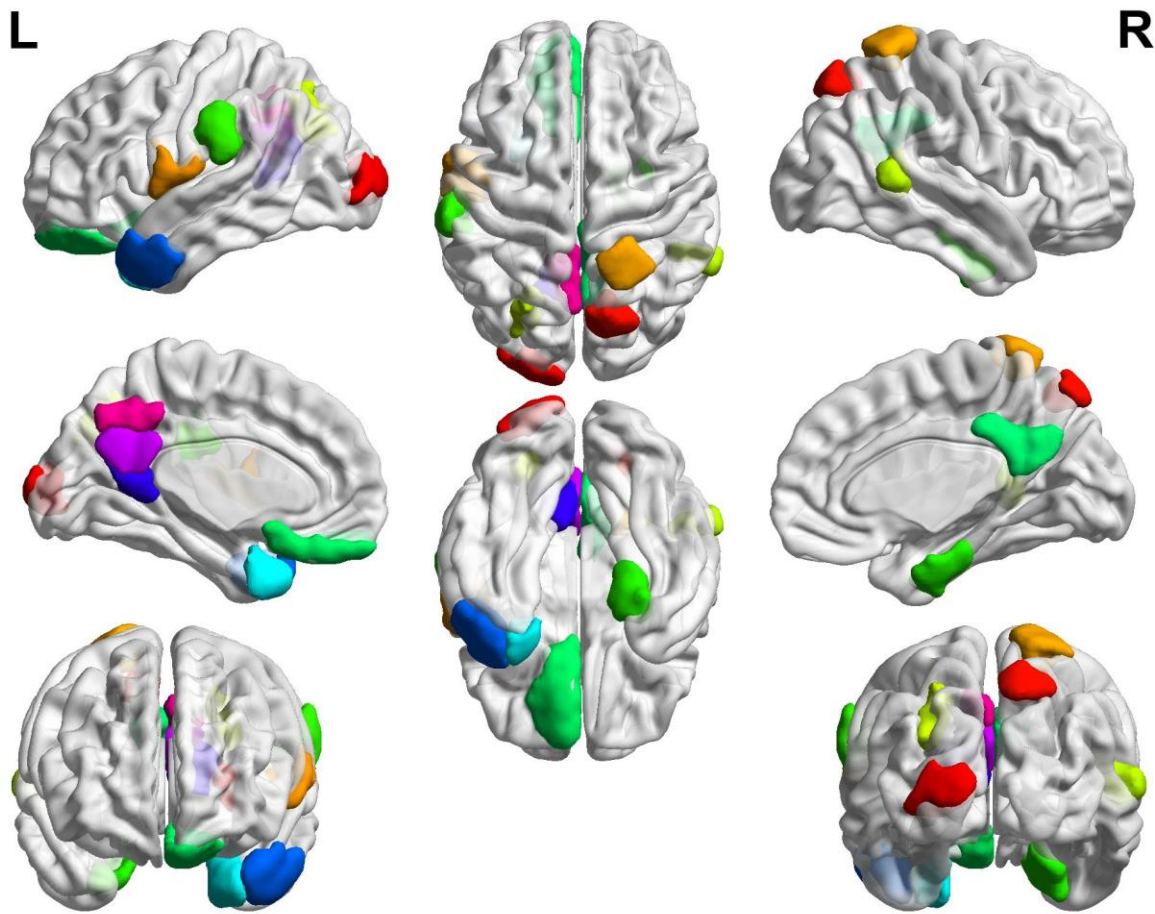


FIGURE I - DFC M1 (PCC) REGIONS OF SIGNIFICANCE

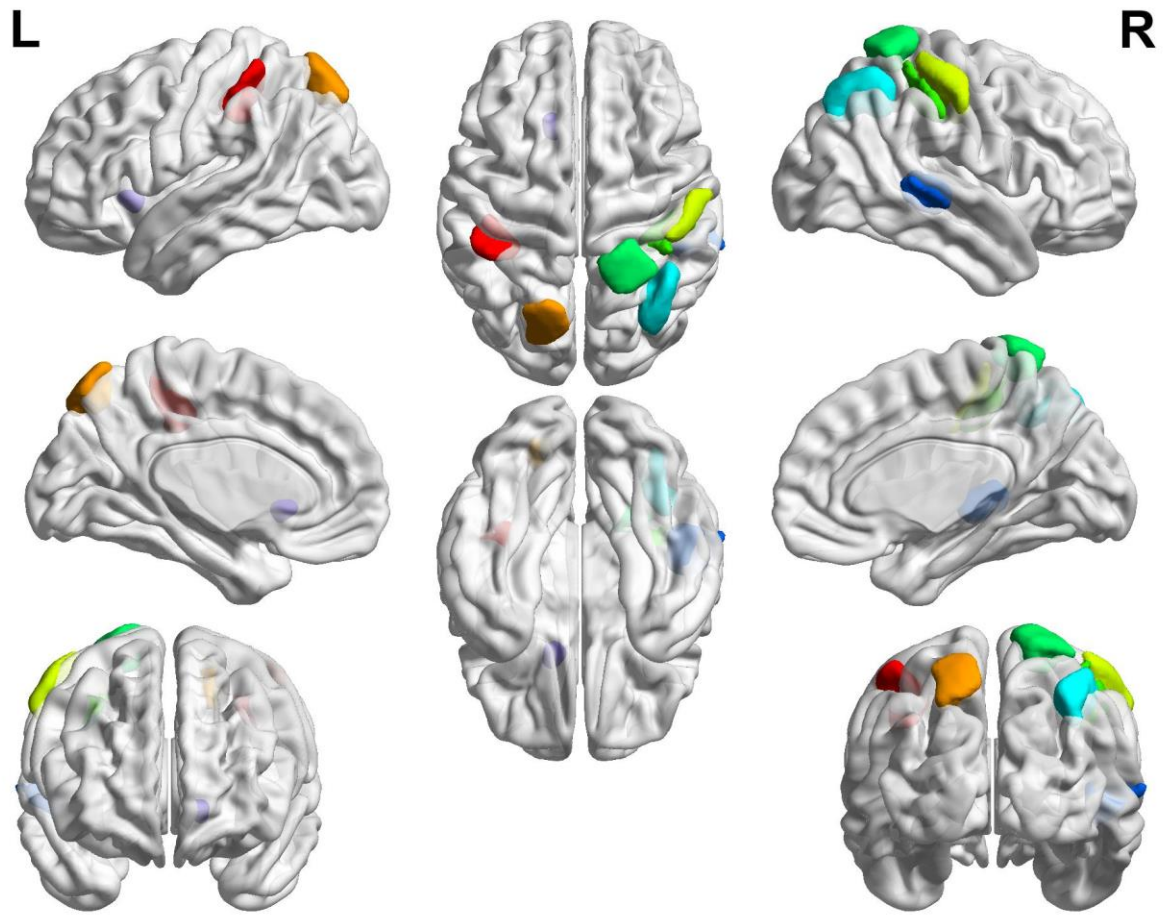


FIGURE II - DFC M2 (MI) REGIONS OF SIGNIFICANCE

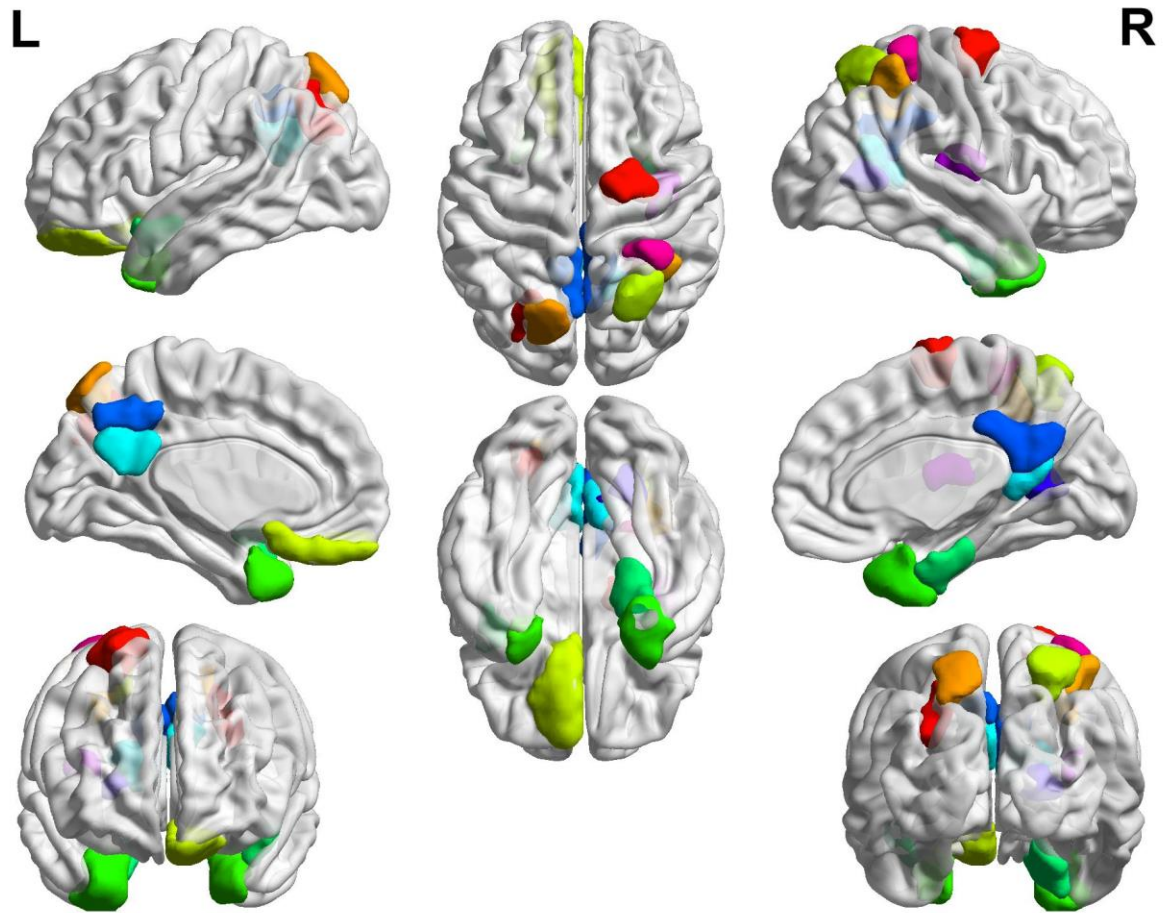


FIGURE III - SFC M1 (PCC) REGIONS OF SIGNIFICANCE

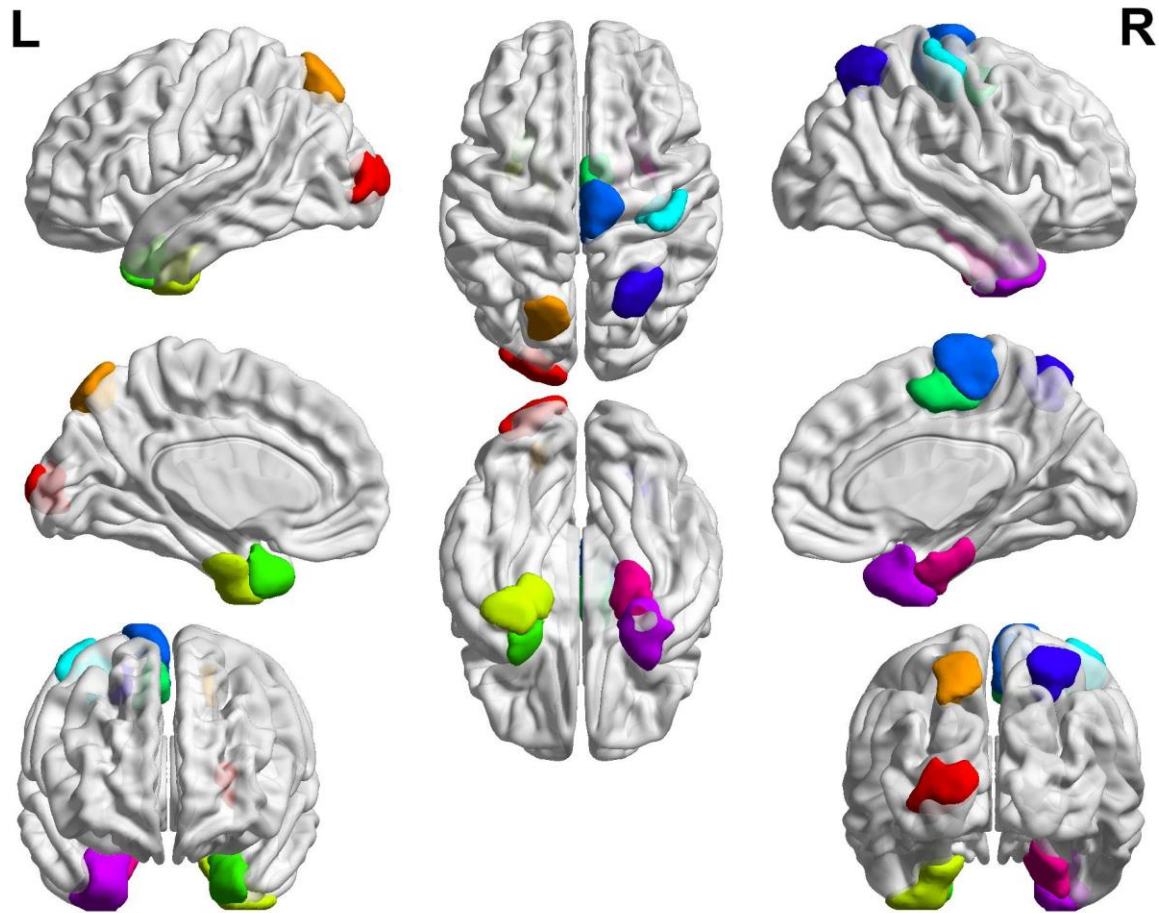


FIGURE IV - SFC M2 (MI) REGIONS OF SIGNIFICANCE

Metric	FC	DFC/SFC	Hemisphere	Coordinates	Region	#
EC	MI	DFC Integ	L	-12,18,-2	Nucleus accumbens, core	226
EC	PE	DFC Integ	R	26,-10,-32	Limbic Temporal Pole 3	164
DEG	PE	DFC Segr	L	-22,-96,6	Visual 9	9
BC	PE	DFC Segr	L	-22,-96,6	Visual 9	9
BC	PE	DFC Integ	L	-28,10,-34	Limbic Temporal Pole 3	59
DEG	PE	DFC Segr	R	26,-10,-32	Limbic Temporal Pole 3	164
DEG	PE	DFC Segr	L	-46,8,-32	DMN Temporal 1	74
BC	PE	SFC	L	-42,8,-18	Limbic Temporal Pole 4	60
DEG	PE	SFC	R	26,-10,-32	Limbic Temporal Pole 3	164
LE	PE	SFC	L	-28,10,-34	Limbic Temporal Pole 3	59

LE	PE	SFC	R	30,8,-38	Limbic Temporal Pole 1	162
DEG	PE	SFC	L	-28,10,-34	Limbic Temporal Pole 3	59
BC	PE	SFC	R	22,-8,68	Somatomotor 16	131
EC	PE	SFC	R	26,-10,-32	Limbic Temporal Pole 3	164
BC	MI	SFC	R	6,-10,52	Somatomotor 11	126
BC	MI	SFC	R	26,-10,-32	Limbic Temporal Pole 3	164
BC	MI	SFC	L	-28,10,-34	Limbic Temporal Pole 3	59
BC	MI	SFC	L	-30,-6,-40	Limbic Temporal Pole 1	57
EC	MI	SFC	L	-22,-96,6	Visual 9	9
BC	MI	SFC	R	30,8,-38	Limbic Temporal Pole 1	162

TABLE V – FM2 ALL SIGNIFICANT FEATURES – CONTROLS > MTBI

Metric	FC	DFC/SFC	Hemisphere	Coordinates	Region	#
SWP	MI	DFC Integ	-	-	Global	
SWP	MI	DFC Segr	-	-	Global	
GE	MI	DFC Integ	-	-	Global	
SWP	MI	SFC	-	-	Global	
LE	MI	DFC Segr	R	38,-62,48	Cont Par 3	167
LE	MI	DFC Integ	R	52,-32,2	DMN Temporal 5	189
LE	MI	DFC Integ	R	52,-22,52	Somatomotor 9	124
EC	MI	DFC Integ	L	-40,-36,48	DAN Posterior 5	35
LE	MI	DFC Segr	R	22,-48,70	DAN Posterior 10	144
LE	MI	DFC Segr	L	-16,-72,54	DAN Posterior 7	37
LE	MI	DFC Integ	R	42,-32,46	DAN Posterior 5	139
LE	PE	DFC Segr	R	58,-46,10	SalVentAttn TempOccPar	148
LE	PE	DFC Integ	R	14,-74,52	DAN Posterior 6	140
LE	PE	DFC Integ	L	-6,-54,42	DMN Precuneus PCC 4	99
LE	PE	DFC Segr	R	6,-48,30	DMN Precuneus PCC 2	199
DEG	PE	DFC Segr	R	22,-48,70	DAN Posterior 10	144
LE	PE	DFC Segr	L	-6,-54,28	DMN Precuneus PCC 2	97
LE	PE	DFC Segr	L	-56,-4,10	Somatomotor 4	18
LE	PE	DFC Segr	L	-26,-70,38	DAN Posterior 3	33
LE	PE	DFC Segr	L	-10,-56,12	DMN Precuneus PCC 1	96
DEG	PE	DFC Segr	L	-62,-26,28	SalVentAttn ParOper	45
LE	PE	DFC Segr	L	-10,36,-20	Limbic OFC	56

LE	PE	SFC	R	22,-60,8	Visual 10	110
LE	PE	SFC	R	34,-48,50	DAN Posterior 7	141
LE	PE	SFC	R	12,-54,14	DMN Precuneus PCC 1	198
LE	PE	SFC	L	-16,-72,54	DAN Posterior 7	37
LE	PE	SFC	R	26,-62,58	DAN Posterior 8	142
DEG	PE	SFC	R	6,-48,30	DMN Precuneus PCC 2	199
LE	PE	SFC	L	-6,-54,28	DMN Precuneus PCC 2	97
LE	PE	SFC	R	32,-40,64	Somatomotor 13	128
LE	PE	SFC	L	-6,-54,42	DMN Precuneus PCC 4	99
LE	PE	SFC	R	38,-14,14	Somatomotor 3	118
LE	PE	SFC	L	-26,-70,38	DAN Posterior 3	33
LE	PE	SFC	L	-10,36,-20	Limbic OFC 2	56
LE	MI	SFC	R	6,-22,68	Somatomotor 18	133
LE	MI	SFC	L	-16,-72,54	DAN Posterior 7	37
DEG	MI	SFC	R	26,-62,58	DAN Posterior 8	142
DEG	MI	SFC	R	40,-24,58	Somatomotor 12	127

TABLE VI – FM2 ALL SIGNIFICANT FEATURES – mTBI > CONTROLS

9. REFERENCES

- Allen, E. A., Damaraju, E., Plis, S. M., Erhardt, E. B., Eichele, T., & Calhoun, V. D. (2012). Tracking whole-brain connectivity dynamics in the resting state. *Cerebral Cortex*, 24(3), 663–676. <https://doi.org/10.1093/cercor/bhs352>
- Andrea I. Luppi and Emmanuel A. Stamatakis. (2020). Combining network topology and information theory to construct representative brain networks. *Network Neuroscience*. <https://doi.org/10.1162/NETN>
- Antonakakis, M., Dimitriadis, S. I., Zervakis, M., Micheloyannis, S., Rezaie, R., Babajani-Feremi, A., Zouridakis, G., & Papanicolaou, A. C. (2016). Altered cross-frequency coupling in resting-state MEG after mild traumatic brain injury. *International Journal of Psychophysiology*, 102, 1–11. <https://doi.org/10.1016/j.ijpsycho.2016.02.002>
- Antonakakis, M., Schrader, S., Wollbrink, A., Oostenveld, R., Rampp, S., Haueisen, J., & Wolters, C. H. (2019). The effect of stimulation type, head modeling, and combined EEG and MEG on the source reconstruction of the somatosensory P20/N20 component. *Human Brain Mapping*, 40(17), 5011–5028. <https://doi.org/10.1002/hbm.24754>
- Antonakakis, M., Dimitriadis, S. I., Zervakis, M., Papanicolaou, A. C., & Zouridakis, G. (2020). Aberrant Whole-Brain Transitions and Dynamics of Spontaneous Network Microstates in Mild Traumatic Brain Injury. *Frontiers in Computational Neuroscience*, 13(January), 1–19. <https://doi.org/10.3389/fncom.2019.00090>
- Antypa, D., Simos, N. J., Kavroulakis, E., Bertias, G., Fanouriakis, A., Sidiropoulos, P., Boumpas, D., & Papadaki, E. (2021). Anxiety and depression severity in neuropsychiatric SLE are associated with perfusion and functional connectivity changes of the frontolimbic neural circuit: A resting-state functional MRI study. *Lupus Science and Medicine*, 8(1). <https://doi.org/10.1136/lupus-2020-000473>
- Arbabshirani, M. R., Kiehl, K. A., Pearlson, G. D., & Calhoun, V. D. (2013). Classification of schizophrenia patients based on resting-state functional network connectivity. *Frontiers in Neuroscience*, 7(7 JUL), 1–16. <https://doi.org/10.3389/fnins.2013.00133>
- Bartfelda, P., Uhriga, L., Sitta, J. D., Sigmane, M., Jarraya, B., & Dehaene, S. (2015). Signature of consciousness in the dynamics of resting-state brain activity. *Proceedings of the National Academy of Sciences of the United States of America*, 112(3), 887–892. <https://doi.org/10.1073/pnas.1418031112>
- Basile, B., Castelli, M., Monteleone, F., Nocentini, U., Caltagirone, C., Centonze, D., Cercignani, M., & Bozzali, M. (2014). Functional connectivity changes within specific networks parallel the clinical evolution of multiple sclerosis. *Multiple Sclerosis Journal*, 20(8), 1050–1057. <https://doi.org/10.1177/1352458513515082>
- Bassett, D. S., & Bullmore, E. T. (2017). Small-World Brain Networks Revisited. *Neuroscientist*, 23(5), 499–516. <https://doi.org/10.1177/1073858416667720>
- Behzadi Y, Restom K, Liu J, & Liu TT. (2007). A component based noise correction method (CompCor) for BOLD and perfusion based fMRI. *NeuroImage*, 37(1), 90–101. <https://www.ncbi.nlm.nih.gov/pmc/articles/PMC2214855/pdf/nihms-27952.pdf>
- Benjamini, Y., & Hochberg, Y. (1995). Controlling The False Discovery Rate - A Practical And Powerful Approach To Multiple Testing. *Journal of the Royal Statistical Society*, 57(1), 289–300. <https://doi.org/10.2307/2346101>
- Bigdeli, B., Samadzadegan, F., & Reinartz, P. (2014). A decision fusion method based on multiple support vector machine system for fusion of hyperspectral and LIDAR data. *International Journal of Image and Data Fusion*, 5(3), 196–209. <https://doi.org/10.1080/19479832.2014.919964>
- Bijsterbosch, J., Smith, S., & Beckmann, C. (2017). *Introduction to Resting State fMRI Functional Connectivity*.
- Breiman, L. (2001). Random Forests. *Machine Learning*, 45, 5–32. https://doi.org/10.1007/978-3-030-62008-0_35

- Calhoun, V. D., Miller, R., Pearlson, G., & Adali, T. (2014). The Chronnectome: Time-Varying Connectivity Networks as the Next Frontier in fMRI Data Discovery. *Neuron*, 84(2), 262–274. <https://doi.org/10.1016/j.neuron.2014.10.015>
- Champagne, A. A., Coverdale, N. S., Ross, A., Chen, Y., Murray, C. I., Dubowitz, D., & Cook, D. J. (2020). Multi-modal normalization of resting-state using local physiology reduces changes in functional connectivity patterns observed in mTBI patients. *NeuroImage: Clinical*, 26(February), 102204. <https://doi.org/10.1016/j.nicl.2020.102204>
- Chao-Gan, Y., & Yu-Feng, Z. (2010). DPARSF: A MATLAB toolbox for “pipeline” data analysis of resting-state fMRI. *Frontiers in Systems Neuroscience*, 4(May), 1–7. <https://doi.org/10.3389/fnsys.2010.00013>
- Chen, T., & Guestrin, C. (2016). XGBoost: A Scalable Tree Boosting System. *22nd ACM SIGKDD International Conference on Knowledge Discovery and Data Mining*. <https://doi.org/http://dx.doi.org/10.1145/2939672.2939785>
- Damaraju, E., Allen, E. A., Belger, A., Ford, J. M., McEwen, S., Mathalon, D. H., Mueller, B. A., Pearlson, G. D., Potkin, S. G., Preda, A., Turner, J. A., Vaidya, J. G., Van Erp, T. G., & Calhoun, V. D. (2014). Dynamic functional connectivity analysis reveals transient states of dysconnectivity in schizophrenia. *NeuroImage: Clinical*, 5(July), 298–308. <https://doi.org/10.1016/j.nicl.2014.07.003>
- Dimitriadis, S. I., Antonakakis, M., Simos, P., Fletcher, J. M., & Papanicolaou, A. C. (2017). Data-Driven Topological Filtering Based on Orthogonal Minimal Spanning Trees: Application to Multigroup Magnetoencephalography Resting-State Connectivity. *Brain Connectivity*, 7(10), 661–670. <https://doi.org/10.1089/brain.2017.0512>
- Dimitriadis, S. I., Routley, B., Linden, D. E., & Singh, K. D. (2018). Reliability of static and dynamic network metrics in the resting-state: A MEG-beamformed connectivity analysis. *Frontiers in Neuroscience*, 12(AUG). <https://doi.org/10.3389/fnins.2018.00506>
- Dimitriadis, S. I., Salis, C., Tarnanas, I., & Linden, D. E. (2017). Topological filtering of dynamic functional brain networks unfolds informative chronnectomics: A novel data-driven thresholding scheme based on orthogonal minimal spanning trees (OMSTs). *Frontiers in Neuroinformatics*, 11(April). <https://doi.org/10.3389/fninf.2017.00028>
- Dos Santos Siqueira, A., Biazoli Junior, C. E., Comfort, W. E., Rohde, L. A., & Sato, J. R. (2014). Abnormal Functional Resting-State Networks in ADHD: Graph Theory and Pattern Recognition Analysis of fMRI Data. *BioMed Research International*, 2014. <https://doi.org/10.1155/2014/380531>
- Fox, M. D., & Raichle, M. E. (2007). Spontaneous fluctuations in brain activity observed with functional magnetic resonance imaging. *Nature Reviews Neuroscience*, 8(9), 700–711. <https://doi.org/10.1038/nrn2201>
- Fukushima, M., Betzel, R. F., He, Y., de Reus, M. A., van den Heuvel, M. P., Zuo, X. N., & Sporns, O. (2018). Fluctuations between high- and low-modularity topology in time-resolved functional connectivity. *NeuroImage*, 180(July), 406–416. <https://doi.org/10.1016/j.neuroimage.2017.08.044>
- Fukushima, M., Betzel, R. F., He, Y., van den Heuvel, M. P., Zuo, X. N., & Sporns, O. (2018). Structure–function relationships during segregated and integrated network states of human brain functional connectivity. *Brain Structure and Function*, 223(3), 1091–1106. <https://doi.org/10.1007/s00429-017-1539-3>
- Guyon, I., & Elisseeff, A. (2003). An Introduction to Variable and Feature Selection. *Journal Of Machine Learning Research*, 3, 1157–1182.
- Ho, T. kam, Hull, J. J., & Srihari, S. N. (1994). Decision Combination in Multiple Classifier Systems. *IEEE Transactions on Pattern Analysis and Machine Intelligence*, 16(1), 66–75. <https://doi.org/10.1109/34.273716>
- Hojjati, S. H., Ebrahimzadeh, A., Khazaei, A., & Babajani-Feremi, A. (2017). Predicting conversion from MCI to AD using resting-state fMRI, graph theoretical approach and SVM. *Journal of Neuroscience Methods*, 282, 69–80. <https://doi.org/10.1016/j.jneumeth.2017.03.006>
- Hou, W., Sours Rhodes, C., Jiang, L., Roys, S., Zhuo, J., Jaja, J., & Gullapalli, R. P. (2018). Dynamic Functional

- Network Analysis in Mild Traumatic Brain Injury. *Brain Connectivity*, 9(6), 475–487. <https://doi.org/10.1089/brain.2018.0629>
- Huang, D., Liu, Z., Cao, H., Yang, J., Wu, Z., & Long, Y. (2021). Childhood trauma is linked to decreased temporal stability of functional brain networks in young adults. *Journal of Affective Disorders*, 290(May), 23–30. <https://doi.org/10.1016/j.jad.2021.04.061>
- Iraji, A., Benson, R. R., Welch, R. D., O’Neil, B. J., Woodard, J. L., Ayaz, S. I., Kulek, A., Mika, V., Medado, P., Soltanian-Zadeh, H., Liu, T., Haacke, E. M., & Kou, Z. (2014). Resting State Functional Connectivity in Mild Traumatic Brain Injury at the Acute Stage: Independent Component and Seed Based Analyses. *Journal of Neurotrauma*. <https://doi.org/10.1089/neu.2014.3610>
- Jie, B., Liu, M., & Shen, D. (2018). Integration of Temporal and Spatial Properties of Dynamic Connectivity Networks for Automatic Diagnosis of Brain Disease. *Med Image Anal.*, 81–94. <https://doi.org/10.1016/j.media.2018.03.013>
- Johnson, B., Zhang, K., Gay, M., Horovitz, S., Hallett, M., Sebastianelli, W., & Slobounov, S. (2012). Alteration of brain default network in subacute phase of injury in concussed individuals: Resting-state fMRI study. *NeuroImage*, 59(1), 511–518. <https://doi.org/10.1016/j.neuroimage.2011.07.081>
- Kamarajan, C., Ardekani, B. A., Pandey, A. K., Chorlian, D. B., Kinreich, S., Pandey, G., Meyers, J. L., Zhang, J., Kuang, W., Stimus, A. T., & Porjesz, B. (2020). Random forest classification of alcohol use disorder using EEG source functional connectivity, neuropsychological functioning, and impulsivity measures. *Behavioral Sciences*, 10(3). <https://doi.org/10.3390/bs10030062>
- Kavroulakis, E., Simos, N. J., Maris, T. G., Zaganas, I., Panagiotakis, S., & Papadaki, E. (2021). Evidence of Age-Related Hemodynamic and Functional Connectivity Impairment: A Resting State fMRI Study. *Frontiers in Neurology*, 12(March), 1–13. <https://doi.org/10.3389/fneur.2021.633500>
- Khazae, A., Ebrahimzadeh, A., & Babajani-Feremi, A. (2017). Classification of patients with MCI and AD from healthy controls using directed graph measures of resting-state fMRI. *Behavioural Brain Research*, 322, 339–350. <https://doi.org/10.1016/j.bbr.2016.06.043>
- Len, T. K., & Neary, J. P. (2011). Cerebrovascular pathophysiology following mild traumatic brain injury. *Clinical Physiology and Functional Imaging*, 31(2), 85–93. <https://doi.org/10.1111/j.1475-097X.2010.00990.x>
- Levin, H. S., & Diaz-Arrastia, R. R. (2015). Diagnosis, prognosis, and clinical management of mild traumatic brain injury. *The Lancet Neurology*, 14(5), 506–517. [https://doi.org/10.1016/S1474-4422\(15\)00002-2](https://doi.org/10.1016/S1474-4422(15)00002-2)
- Liu, J., Liao, X., Xia, M., & He, Y. (2018). Chronnectome fingerprinting: Identifying individuals and predicting higher cognitive functions using dynamic brain connectivity patterns. *Human Brain Mapping*, 39(2), 902–915. <https://doi.org/10.1002/hbm.23890>
- Logothetis, N. K., Pauls, J., Augath, M., Trinath, T., & Oeltermann, A. (2001). Neurophysiological investigation of the basis of the fMRI signal. *NATURE*, 412, 150–157. <https://doi.org/10.1093/schbul/sbz045>
- Logothetis, N. K., & Wandell, B. A. (2004). Interpreting the BOLD signal. *Annual Review of Physiology*, 66, 735–769. <https://doi.org/10.1146/annurev.physiol.66.082602.092845>
- Long, Y., Chen, C., Deng, M., Huang, X., Tan, W., Zhang, L., Fan, Z., & Liu, Z. (2019). Psychological resilience negatively correlates with resting-state brain network flexibility in young healthy adults: a dynamic functional magnetic resonance imaging study. *Annals of Translational Medicine*, 7(24), 809–809. <https://doi.org/10.21037/atm.2019.12.45>
- Luppi, A. I., Carhart-Harris, R. L., Roseman, L., Pappas, I., Menon, D. K., & Stamatakis, E. A. (2021). LSD alters dynamic integration and segregation in the human brain. *NeuroImage*, 227(November 2020). <https://doi.org/10.1016/j.neuroimage.2020.117653>
- Luppi, A. I., Craig, M. M., Pappas, I., Finoia, P., Williams, G. B., Allanson, J., Pickard, J. D., Owen, A. M., Naci, L., Menon, D. K., & Stamatakis, E. A. (2019). Consciousness-specific dynamic interactions of brain integration

and functional diversity. *Nature Communications*, 10(1). <https://doi.org/10.1038/s41467-019-12658-9>

- Luppi, A. I., Gellersen, H. M., Peattie, A. R. D., Manktelow, A. E., Menon, D., Dimitriadis, S. I., & Stamatakis, E. A. (2021). Searching for Consistent Brain Network Topologies Across the Garden of (Shortest) Forking Paths. *BioRxiv*, 2021.07.13.452257. <https://www.biorxiv.org/content/10.1101/2021.07.13.452257v1%0Ahttps://www.biorxiv.org/content/10.1101/2021.07.13.452257v1.abstract>
- Madhavan, R., Joel, S. E., Mullick, R., Cogsil, T., Niogi, S. N., Tsiouris, A. J., Mukherjee, P., Masdeu, J. C., Marinelli, L., & Shetty, T. (2019). Longitudinal Resting State Functional Connectivity Predicts Clinical Outcome in Mild Traumatic Brain Injury. In *Journal of Neurotrauma* (Vol. 36, Issue 5). <https://doi.org/10.1089/neu.2018.5739>
- Martuzzi, R., Ramani, R., Qiu, M., Shen, X., Papademetris, X., & Constable, R. T. (2011). A whole-brain voxel based measure of intrinsic connectivity contrast reveals local changes in tissue connectivity with anesthetic without a priori assumptions on thresholds or regions of interest. *NeuroImage*, 58(4), 1044–1050. <https://doi.org/10.1016/j.neuroimage.2011.06.075>
- Mayer, A. R., Ling, J. M., Allen, E. A., Klimaj, S. D., Yeo, R. A., & Hanlon, F. M. (2014). Static and Dynamic Intrinsic Connectivity following Mild Traumatic Brain Injury. *Journal of Neurotrauma*, 23(859), 125–141.
- Mayer, A. R., Mannell, M. V., Ling, J., Gasparovic, C., & Yeo, R. A. (2011). Functional connectivity in mild traumatic brain injury. *Human Brain Mapping*, 32(11), 1825–1835. <https://doi.org/10.1002/hbm.21151>
- Mazoyer, B., Zago, L., Mellet, E., Bricogne, S., Etard, O., Houdé, O., Crivello, F., Joliot, M., Petit, L., & Tzourio-Mazoyer, N. (2001). Cortical networks for working memory and executive functions sustain the conscious resting state in man. *Brain Research Bulletin*, 54(3), 287–298. [https://doi.org/10.1016/S0361-9230\(00\)00437-8](https://doi.org/10.1016/S0361-9230(00)00437-8)
- Menon, S. S., & Krishnamurthy, K. (2019). A Comparison of Static and Dynamic Functional Connectivities for Identifying Subjects and Biological Sex Using Intrinsic Individual Brain Connectivity. *Scientific Reports*, 9(1), 1–11. <https://doi.org/10.1038/s41598-019-42090-4>
- Milo, R., Shen-Orr, S., Itzkovitz, S., Kashtan, N., Chklovskii, D., & Alon, U. (2002). Network motifs: Simple building blocks of complex networks. *Science*, 298(5594), 824–827. <https://doi.org/10.1126/science.298.5594.824>
- Moreno-López, L., Sahakian, B. J., Manktelow, A., Menon, D. K., & Stamatakis, E. A. (2016). Depression following traumatic brain injury: A functional connectivity perspective. *Brain Injury*, 30(11), 1319–1328. <https://doi.org/10.1080/02699052.2016.1186839>
- Muldoon, S. F., Bridgeford, E. W., & Bassett, D. S. (2016). Small-world propensity and weighted brain networks. *Scientific Reports*, 6(February), 1–13. <https://doi.org/10.1038/srep22057>
- Nathan, D. E., Oakes, T. R., Yeh, P. H., French, L. M., Harper, J. F., Liu, W., Wolfowitz, R. D., Wang, B. Q., Graner, J. L., & Riedy, G. (2014). Exploring variations in functional connectivity of the resting state default mode network in mild traumatic brain injury. *Brain Connectivity*, 2(10), 1–31. <https://doi.org/10.1089/brain.2014.0273>
- Newman, M. E. J. (2004). Fast algorithm for detecting community structure in networks. *Physical Review E - Statistical Physics, Plasmas, Fluids, and Related Interdisciplinary Topics*, 69(6), 5. <https://doi.org/10.1103/PhysRevE.69.066133>
- Onnela, J. P., Saramäki, J., Kertész, J., & Kaski, K. (2005). Intensity and coherence of motifs in weighted complex networks. *Physical Review E - Statistical, Nonlinear, and Soft Matter Physics*, 71(6). <https://doi.org/10.1103/PhysRevE.71.065103>
- Palacios, E. M., Yuh, E. L., Chang, Y. S., Yue, J. K., Schnyer, D. M., Okonkwo, D. O., Valadka, A. B., Gordon, W. A., Maas, A. I. R., Vassar, M., Manley, G. T., & Mukherjee, P. (2016). Resting-state functional connectivity alterations associated with six-month outcomes in mild traumatic brain injury. *Journal of Neurotrauma*, 34(8), 1546–1557. <https://doi.org/10.1089/neu.2016.4752>
- Papanicolaou, A. C. (2017). *The Oxford handbook of functional brain imaging in neuropsychology*. Oxford University Press.

https://books.google.com.br/books?hl=en&lr=lang_en&id=VtWdDgAAQBAJ&oi=fnd&pg=PA81&dq=positron+emission+tomography&ots=iwHt6KP6eN&sig=L50O1dDJe5Amvuf7ci-VEnPI2KE#v=onepage&q=positron+emission+tomography&f=false

- Pappas, I., Adapa, R. M., Menon, D. K., & Stamatakis, E. A. (2019). Brain network disintegration during sedation is mediated by the complexity of sparsely connected regions. *NeuroImage*, *186*(October 2018), 221–233. <https://doi.org/10.1016/j.neuroimage.2018.10.078>
- Parvande, S., Yeh, H. W., Paulus, M. P., & McKinney, B. A. (2020). Consensus features nested cross-validation. *Bioinformatics*, *36*(10), 3093–3098. <https://doi.org/10.1093/bioinformatics/btaa046>
- Pedersen, M., Zalesky, A., Omidvarnia, A., & Jackson, G. D. (2018). Multilayer network switching rate predicts brain performance. *Proceedings of the National Academy of Sciences of the United States of America*, *115*(52), 13376–13381. <https://doi.org/10.1073/pnas.1814785115>
- Pedregosa, F., Varoquaux, G., Gramfort, A., Michel, V., Thirion, B., Grisel, O., Blondel, M., Prettenhofer, P., Weiss, R., Dubourg, V., Vanderplas, J., Passos, A., Cournapeau, D., Brucher, M., Perrot, M., & Duchesnay, É. (2011). Scikit-learn: Machine Learning in Python. *Journal Of Machine Learning Research*, *85*(12), 2825–2830.
- Preti, M. G., Bolton, T. A., & Van De Ville, D. (2017). The dynamic functional connectome: State-of-the-art and perspectives. *NeuroImage*, *160*(December 2016), 41–54. <https://doi.org/10.1016/j.neuroimage.2016.12.061>
- Price, T., Wee, C. Y., Gao, W., & Shen, D. (2014). Multiple-network classification of childhood autism using functional connectivity dynamics. *Lecture Notes in Computer Science (Including Subseries Lecture Notes in Artificial Intelligence and Lecture Notes in Bioinformatics)*, *8675 LNCS*(PART 3), 177–184. https://doi.org/10.1007/978-3-319-10443-0_23
- Ramos-Nuñez, A. I., Fischer-Baum, S., Martin, R. C., Yue, Q., Ye, F., & Deem, M. W. (2017). Static and dynamic measures of human brain connectivity predict complementary aspects of human cognitive performance. *Frontiers in Human Neuroscience*, *11*(August), 1–13. <https://doi.org/10.3389/fnhum.2017.00420>
- Rashid, B., Arbabshirani, M. R., Damaraju, E., Cetin, M. S., Miller, R., Pearlson, G. D., & Calhoun, V. D. (2016). Classification of schizophrenia and bipolar patients using static and dynamic resting-state fMRI brain connectivity. *NeuroImage*, *134*, 645–657. <https://doi.org/10.1016/j.neuroimage.2016.04.051>
- Rashid, B., Damaraju, E., Pearlson, G. D., & Calhoun, V. D. (2014). Dynamic connectivity states estimated from resting fMRI Identify differences among Schizophrenia, bipolar disorder, and healthy control subjects. *Frontiers in Human Neuroscience*, *8*(November), 1–13. <https://doi.org/10.3389/fnhum.2014.00897>
- Rolls, E. T., Cheng, W., & Feng, J. (2021). Brain dynamics: the temporal variability of connectivity, and differences in schizophrenia and ADHD. *Translational Psychiatry*, *11*(1). <https://doi.org/10.1038/s41398-021-01197-x>
- Rubinov, M., & Sporns, O. (2010). Complex network measures of brain connectivity: Uses and interpretations. *NeuroImage*, *52*(3), 1059–1069. <https://doi.org/10.1016/j.neuroimage.2009.10.003>
- Rubinov, M., & Sporns, O. (2011). Weight-conserving characterization of complex functional brain networks. *NeuroImage*, *56*(4), 2068–2079. <https://doi.org/10.1016/j.neuroimage.2011.03.069>
- Ruff, R. M., Iverson, G. L., Barth, J. T., Bush, S. S., & Broshek, D. K. (2009). Recommendations for diagnosing a mild traumatic brain injury: A national academy of neuropsychology education paper. *Archives of Clinical Neuropsychology*, *24*(1), 3–10. <https://doi.org/10.1093/arclin/acp006>
- Saba, V., Premi, E., Cristillo, V., Gazzina, S., Palluzzi, F., Zanetti, O., Gasparotti, R., Padovani, A., Borroni, B., & Grassi, M. (2019). Brain connectivity and information-flow breakdown revealed by a minimum spanning tree-based analysis of mri data in behavioral variant frontotemporal dementia. *Frontiers in Neuroscience*, *13*(March), 1–16. <https://doi.org/10.3389/fnins.2019.00211>
- Saccà, V., Sarica, A., Novellino, F., Barone, S., Tallarico, T., Filippelli, E., Granata, A., Chiriaco, C., Bruno Bossio, R., Valentino, P., & Quattrone, A. (2019). Evaluation of machine learning algorithms performance for the prediction of early multiple sclerosis from resting-state FMRI connectivity data. *Brain Imaging and Behavior*,

13(4), 1103–1114. <https://doi.org/10.1007/s11682-018-9926-9>

- Saha, D. K., Damaraju, E., Rashid, B., Abrol, A., Plis, S. M., & Calhoun, V. D. (2021). A Classification-Based Approach to Estimate the Number of Resting Functional Magnetic Resonance Imaging Dynamic Functional Connectivity States. *Brain Connectivity*, *11*(2), 132–145. <https://doi.org/10.1089/brain.2020.0794>
- Sato, J. R., Fujita, A., Cardoso, E. F., Thomaz, C. E., Brammer, M. J., & Amaro, E. (2010). Analyzing the connectivity between regions of interest: An approach based on cluster Granger causality for fMRI data analysis. *NeuroImage*, *52*(4), 1444–1455. <https://doi.org/10.1016/j.neuroimage.2010.05.022>
- Schaefer, A., Kong, R., Gordon, E. M., Laumann, T. O., Zuo, X.-N., Holmes, A. J., Eickhoff, S. B., & Yeo, B. T. T. (2018). Local-Global Parcellation of the Human Cerebral Cortex from Intrinsic Functional Connectivity MRI. *Cerebral Cortex*, *28*(9), 3095–3114. <https://doi.org/10.1093/cercor/bhx179>
- Shine, J. M., Bissett, P. G., Bell, P. T., Koyejo, O., Balsters, J. H., Gorgolewski, K. J., Moodie, C. A., & Poldrack, R. A. (2016). The Dynamics of Functional Brain Networks: Integrated Network States during Cognitive Task Performance. *Neuron*, *92*(2), 544–554. <https://doi.org/10.1016/j.neuron.2016.09.018>
- Shine, J. M., Koyejo, O., Bell, P. T., Gorgolewski, K. J., Gilat, M., & Poldrack, R. A. (2015). Estimation of dynamic functional connectivity using Multiplication of Temporal Derivatives. *NeuroImage*, *122*(September 2019), 399–407. <https://doi.org/10.1016/j.neuroimage.2015.07.064>
- Simos, N. J., Kavroulakis, E., Manikis, G. C., Bertsias, G., Papadaki, E., & Marias, K. (2019). Machine learning classification of neuropsychiatric systemic lupus erythematosus patients using resting-state fmri functional connectivity. *IST 2019 - IEEE International Conference on Imaging Systems and Techniques, Proceedings, MI*, 8–13. <https://doi.org/10.1109/IST48021.2019.9010078>
- Simos, Nicholas J., Dimitriadis, S. I., Kavroulakis, E., Manikis, G. C., Bertsias, G., Simos, P., Maris, T. G., & Papadaki, E. (2020). Quantitative identification of functional connectivity disturbances in neuropsychiatric lupus based on resting-state fMRI: A robust machine learning approach. *Brain Sciences*, *10*(11), 1–18. <https://doi.org/10.3390/brainsci10110777>
- Sours, C., Zhuo, J., Roys, S., Shanmuganathan, K., & Gullapalli, R. P. (2015). Disruptions in resting state functional connectivity and cerebral blood flow in mild traumatic brain injury patients. *PLoS ONE*, *10*(8), 1–20. <https://doi.org/10.1371/journal.pone.0134019>
- Supekar, K., Menon, V., Rubin, D., Musen, M., & Greicius, M. D. (2008). Network analysis of intrinsic functional brain connectivity in Alzheimer’s disease. *PLoS Computational Biology*, *4*(6). <https://doi.org/10.1371/journal.pcbi.1000100>
- Tagliazucchi, E., von Wegner, F., Morzelewski, A., Brodbeck, V., & Laufs, H. (2012). Dynamic BOLD functional connectivity in humans and its electrophysiological correlates. *Frontiers in Human Neuroscience*, *6*(DEC), 1–22. <https://doi.org/10.3389/fnhum.2012.00339>
- Tang, L., Ge, Y., Sodickson, D. K., Miles, L., Zhou, Y., Reaume, J., & Grossman, R. I. (2011). Thalamic resting-state functional networks: Disruption in patients with mild traumatic brain injury. *Radiology*, *260*(3), 831–840. <https://doi.org/10.1148/radiol.11110014>
- Tian, Y., Margulies, D. S., Breakspear, M., & Zalesky, A. (2020). Topographic organization of the human subcortex unveiled with functional connectivity gradients. *Nature Neuroscience*, *23*(11), 1421–1432. <https://doi.org/10.1038/s41593-020-00711-6>
- Tong, Y., Hocke, L. M., & Frederick, B. B. (2019). Low frequency systemic hemodynamic “noise” in resting state BOLD fMRI: Characteristics, causes, implications, mitigation strategies, and applications. *Frontiers in Neuroscience*, *13*(JUL). <https://doi.org/10.3389/fnins.2019.00787>
- Torlay, L., Perrone-Bertolotti, M., Thomas, E., & Baciú, M. (2017). Machine learning–XGBoost analysis of language networks to classify patients with epilepsy. *Brain Informatics*, *4*(3), 159–169. <https://doi.org/10.1007/s40708-017-0065-7>

- Tulyakov, S., Jaeger, S., Govindaraju, V., & Doermann, D. (2008). Review of Classifier Combination Methods. *Studies in Computational Intelligence*, 361–386. [papers://5e3e5e59-48a2-47c1-b6b1-a778137d3ec1/Paper/p1978](https://doi.org/10.1007/978-1-4419-1798-1_17)
- Tzourio-Mazoyer, N., Landeau, B., Papathanassiou, D., Crivello, F., Etard, O., Delcroix, N., Mazoyer, B., & Joliot, M. (2002). Automated anatomical labeling of activations in SPM using a macroscopic anatomical parcellation of the MNI MRI single-subject brain. *NeuroImage*, 15(1), 273–289. <https://doi.org/10.1006/nimg.2001.0978>
- Van Der Horn, H. J., Kok, J. G., De Koning, M. E., Scheenen, M. E., Leemans, A., Spikman, J. M., & Van Der Naalt, J. (2017). Altered Wiring of the Human Structural Connectome in Adults with Mild Traumatic Brain Injury. *Journal of Neurotrauma*, 34(5), 1035–1044. <https://doi.org/10.1089/neu.2016.4659>
- Vatansever, D., Manktelow, A. E., Sahakian, B. J., Menon, D. K., & Stamatakis, E. A. (2016). Angular default mode network connectivity across working memory load. *Human Brain Mapping*, 38(1), 41–52. <https://doi.org/10.1002/hbm.23341>
- Vergara, V. M., Mayer, A. R., Damaraju, E., Kiehl, K. A., & Calhoun, V. (2016). Detection of Mild Traumatic Brain Injury by Machine Learning Classification Using Resting State Functional Network Connectivity and Fractional Anisotropy. *Journal of Neurotrauma*, 34(5), 1045–1053. <https://doi.org/10.1089/neu.2016.4526>
- Vergara, V. M., Mayer, A. R., Kiehl, K. A., & Calhoun, V. D. (2018). Dynamic functional network connectivity discriminates mild traumatic brain injury through machine learning. *NeuroImage: Clinical*, 19, 30–37. <https://doi.org/10.1016/j.nicl.2018.03.017>
- Wang, L., Zhu, C., He, Y., Zang, Y., Cao, Q., Zhang, H., Zhong, Q., & Wang, Y. (2009). Altered small-world brain functional networks in children with attention-deficit/hyperactivity disorder. *Human Brain Mapping*, 30(2), 638–649. <https://doi.org/10.1002/hbm.20530>
- Wang, X. H., Jiao, Y., & Li, L. (2018). Identifying individuals with attention deficit hyperactivity disorder based on temporal variability of dynamic functional connectivity. *Scientific Reports*, 8(1), 1–12. <https://doi.org/10.1038/s41598-018-30308-w>
- Waske, B., & Benediktsson, J. A. (2015). DECISION FUSION, CLASSIFICATION OF MULTISOURCE DATA. In *Encyclopedia of Remote Sensing. Encyclopedia of Earth Sciences Series*. (2014th ed., pp. 140–144). Springer, New York, NY. https://doi.org/10.1007/978-0-387-36699-9_34
- Watts, D. J., & Strogatz, S. H. (1998). Collective dynamics of ‘small-world’ networks. *NATURE*, 393, 440–442.
- Whitfield-Gabrieli, S., & Nieto-Castanon, A. (2012). Conn: A Functional Connectivity Toolbox for Correlated and Anticorrelated Brain Networks. *Brain Connectivity*, 2(3), 125–141. <https://doi.org/10.1089/brain.2012.0073>
- Xi Zhu, Du, X., Kerich, M., Lohoff, F. W., & Momenan, R. (2019). Random Forest Based Classification of Alcohol Dependence Patients and Healthy Controls Using Resting State MRI. *Neurosci Lett.*, 176(3), 139–148. <https://doi.org/10.1016/j.neulet.2018.04.007>
- Xia, M., Wang, J., & He, Y. (2013). BrainNet Viewer: A Network Visualization Tool for Human Brain Connectomics. *PLoS ONE*, 8(7). <https://doi.org/10.1371/journal.pone.0068910>
- Yang, J., Pu, W., Wu, G., Chen, E., Lee, E., Liu, Z., & Palaniyappan, L. (2020). Connectomic underpinnings of working memory deficits in schizophrenia: Evidence from a replication fMRI study. *Schizophrenia Bulletin*, 46(4), 916–926. <https://doi.org/10.1093/schbul/sbz137>
- Zhang, J., Cheng, W., Liu, Z., Zhang, K., Lei, X., Yao, Y., Becker, B., Liu, Y., Kendrick, K. M., Lu, G., & Feng, J. (2016). Neural, electrophysiological and anatomical basis of brain-network variability and its characteristic changes in mental disorders. *Brain*, 141(8), 2307–2321. <https://doi.org/10.1093/brain/awy169>
- Zhong, Y., Chalise, P., & He, J. (2020). Nested cross-validation with ensemble feature selection and classification model for high-dimensional biological data. *Communications in Statistics: Simulation and Computation*, 0(0), 1–18. <https://doi.org/10.1080/03610918.2020.1850790>
- Zhou, Y., Milham, M. P., Lui, Y. W., Miles, L., Reaume, J., Sodickson, D. K., Grossman, R. I., & Ge, Y. (2012).

Default-mode network disruption in mild traumatic brain injury. *Radiology*, 265(3), 882–892.
<https://doi.org/10.1148/radiol.12120748>

10. SCIENTIFIC CONTRIBUTIONS

PEER REVIEWED PROCEEDINGS

2nd best research project award in the 9th Panhellenic Conference on Biomedical Technology for:

Nicholas John Simas, Marios Antonakakis, Efrosini Papadaki, Michalis Zervakis (2021). Classification of Resting-State fMRI Functional Network Disturbances from Patients with Mild Traumatic Brain Injuries. Hellenic Society for Biomedical Technology, 9th Panhellenic Conference on Biomedical Technology, Proceedings, 116, ISBN: 978-960-243-727-8